UiO : University of Oslo

Rossana Rojas Molina

Membrane budding dynamics by diffusion and kinetic recruitment of proteins

Thesis submitted for the degree of Philosophiae Doctor

Department of Mathematics
Faculty of Mathematics and Natural Sciences

2020

Series of dissertations submitted to the
Faculty of Mathematics and Natural Sciences, University of Oslo
No. 2341

ISSN 1501-7710

Cover: Hanne Baadsgaard Utigard.
Print production: Reprosentralen, University of Oslo.

Preface

This thesis is submitted in partial fulfillment of the requirements for the degree of *Philosophiae Doctor* at the University of Oslo. The research presented here was conducted at the University of Oslo under the supervision of Associate Professor Andreas Carlson and Dr. Susanne Liese. The financial support for this work was provided by the Research Council of Norway, through the project "Mechanochemical interplay in Intraluminal Vesicle formation", project number 263056.

The thesis is a collection of three papers, presented in practical order. The main subject of these papers is the mathematical modelling of biological membranes, with a special focus on the effect of membrane-bound proteins in membrane shape transformation. The papers are preceded by four chapters, which serve to put in perspective the importance of membranes in living organisms and to describe the main foundations of the mathematical membrane models. The first paper studies the role of membrane morphology in the diffusion of proteins/molecules. The second paper incorporates both diffusion and recruitment of curvature-inducing proteins into a minimal model for membrane shape dynamics. The third paper introduces a theoretical model for the formation of Intraluminal Vesicles in the endosome.

Rossana Rojas Molina
Oslo,December 2020

Acknowledgements

First and foremost, I would like to extend my deepest thank you to my supervisors, Andreas Carlson and Susanne Liese. Their help and guidance, enriched by their knowledge and experience, were invaluable during these years. I specially extend my gratitude to Padmini Rangamani and Haleh Alimohamadi at the University of California for the fruitful discussions and suggestions which helped to improve my work. I thank Eva Maria Wenzel and Camilla Raiborg at the Institute for Cancer Research of Oslo University Hospital, for the stimulating discussions about biological membranes and proteins, which serve as an inspiration for this work. I also thank all my colleagues in the Mechanics section, which help to build a joyful work environment, but most specially to Reyna Ramirez for her invaluable friendship and support when I needed it most. I would also like to thank Silvia Lavagnini for the great and funny moments we spent during these years (running all over Venice to catch a train deserves a special mention), and for her generosity, friendship, and support from the beginning of this journey. My sincere gratitude also to Lorenzo Ciardo for his friendship and support. Finally, I thank my family for their love and support from the distance, which was the main motivation to go on. Most specially to my sister Grabiela, who was brave enough to take the task of reading my thesis without going mad in the attempt, and for giving me the extra push I always needed.

Rossana Rojas Molina
Oslo, December 2020

List of publications

Paper I

Rojas, R., Liese, S. and Carlson, A. "Diffusion on membrane domes, tubes and pearling structures". In: *bioRxiv*, currently in review. (2020), DOI: 10.1101/2020.10.08.331629.

Paper II

Rojas, R., Liese, S., Alimohamadi, H., Rangamani, P. and Carlson, A. "Diffuso-kinetic membrane budding dynamics". In: *Soft Matter* (2020) DOI: 10.1039/D0SM01028F

Paper III

Liese, S., Wenzel, E. M., Kjos, I., Rojas R., Schultz, S., Brech, A., Stenmark, H., Raiborg, C. and Carlson, A. "Protein crowding mediates membrane remodeling in upstream ESCRT-induced formation of intraluminal vesicles". In: *Proceedings of the National Academy of Sciences of the United States of America* (2020) DOI: 10.1101/834457

Contents

List of figures

Chapter 1

Introduction

As the building block of life for multi-cellular organisms, the cell is responsible for a myriad of processes. The cell's intrinsic complexity has fascinated researchers from all disciplines of natural sciences —from biology to physics and mathematics. The compartmentalization of the cell is one of the fundamental factors which make possible the physiological processes that produce and reproduce life [1]. Indeed, the cell's correct functioning, growth and proliferation hinges upon the concerted action of all its organelles. These organelles are encapsulated by membranes with diverse composition, and the cell as such is surrounded by its own plasma membrane. In consequence, membranes are directly involved in all fundamental processes taking place within each cell: on one hand, membranes protect both the organelles and the cell from the unrestricted flow of solutes and water [2] while acting as a selective permeable barrier that allows the entrance of solutes and ions [3]. On the other hand, membranes are composed by an array of proteins and lipid species distributed non-homogeneously [4], whose composition determines some of the membrane's primary functions. For instance, a membrane composed mostly by lipids will serve as a permeable barrier, whereas a membrane with a larger protein content (such as the plasma membrane and the internal membrane of the mitochondria), will additionally take on enzymatic and transport functions [5].

Crucial membrane properties are its fluidity and elasticity: the membrane behaves as a two-dimensional fluid with elastic properties. Both fluidity and elasticity allow the membrane to perform the lateral transport of its molecular components and undergo shape changes [6, 7]. Additionally, membrane elasticity plays a fundamental role in cellular events requiring the formation of vesicles and other highly deformed structures, all of which ultimately emanate from the membrane. A number of cellular processes of paramount importance depend on the membrane's capacity to successfully incorporate and release molecular substances: The process of exocytosis consists on the fusion of a vesicle and a target membrane in order to release its molecular content, *e.g.*, secretion of transmitters, peptides and hormones from the neurons [8] and secretion of vesicle from the endoplasmic reticulum to the plasma membrane [9]. Endocytosis is the process whereby —aided by the action of proteins such as clathrin and caveolin— trans-membrane proteins and lipids which are present in the plasma membrane and extracellular fluids, become internalized into the cell [10, 11, 12]. The formation of Intraluminal Vesicles (ILVs) on the endosome membrane is equally related to cell membranes. ILVs are required for the lysosomal degradation pathway of internalized receptors and other cargo, which are sorted and sequestered by the machinery of the Endosomal Sorting Complex Required for Transport (ESCRT) [13, 14]. Finally, the process of viral replication requires virus assembly in a

host-cell membrane to acquire its membranous envelope. The assembled virus is subsequently released as a small vesicle [15]. Within the biological processes mentioned above, the formation of a small spherical vesicle is a recurrent feature, regardless of the specific proteins and mechanisms participating in the membrane deformation. Fig. 1.1 illustrates the processes of endocytosis and formation of ILVs. Fig. 1.1a highlights different internalization pathways involving membrane deformation, which finally takes the form of a spherical vesicle or a tubular structure. Fig. 1.1b shows clathrin-coated vesicles formed on a giant liposome membrane, indicating that the clathrin polymerization alone leads to the formation of clathrin-coated spherical vesicles. After the endocytic event, the internalized cargo is trafficked into endosomes; at a later stage, the cargo is sorted into Multivisecular Bodies (MVBs) or lysosomes for degradation [11]. Fig. 1.1c is a representation of the ILVs formed in the endosome: a large membrane coat composed by several proteins leads to the formation of vesicles, yet these proteins neither cover the vesicle nor become part of its content.

The complex membrane composition poses a taxing challenge to the understanding of the specific roles played by the membrane's components. Depending on the membrane's varied make-up, it will take on an impressively wide range of functions and properties. The challenge is particularly evident if one attempts to understand such properties within the context of membrane deformation, which is the main subject of this thesis. As a way to overcome the challenge and enhance knowledge on the possible mechanisms inducing membrane deformation, biophysicists have resorted to the study of lipid monolayers or bilayers composed by a small number of lipid species and proteins. Monolayers and bilayers have revealed a multiplicity of mechanisms that are instrumental to processes of membrane shape transformation. Research has shown that a lipid bilayer can change its shape in response to different stimuli, such as osmotic conditions, lipid composition, or temperature [17]. Additionally, a lipid bilayer attached to an elastic surface changes its shape under compression, thus generating tubules. However, under dilation, the lipid bilayer will instead adsorb vesicles to preserve its area [18]. The role of different types of proteins bound to lipid bilayers has been assessed experimentally as well. Experiments have shown that the pressure generated by the mutual exclusion of proteins with different structures on membrane surfaces (known as protein crowding) induce tubulation whenever the membrane has a high protein density [19]. But tubulation is not the sole outcome of protein crowding. Additional experiments on protein crowding showed that this phenomenon is also correlated to vesicle fission, *i.e.*, the detachment of membrane-bound vesicles from the donor membrane [20]. The lipid composition of the bilayer is fundamental to the occurrence of the protein crowding mechanism. Experiments have shown that if a Giant Unilamellar Vesicle (GUV) is composed by lipid species which tend to strongly bind to a certain kind of proteins, these proteins will be confined to a limited region, thereby inducing protein crowding and membrane tubulation [21]. Another mechanism, consisting in the anchoring of amphiphilic molecules/polymers onto the membrane, *via* the insertion of one or more hydrophobic groups into the

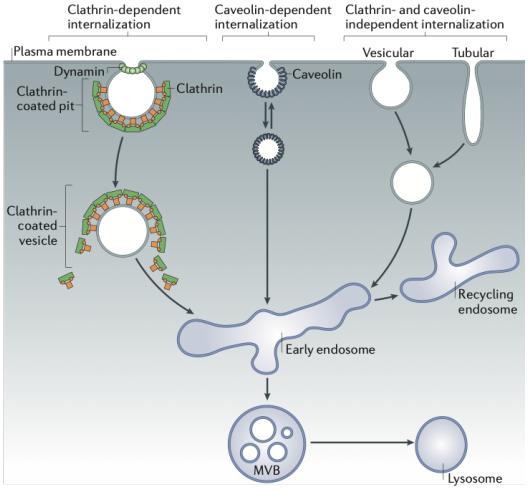

(a) Different endocytic pathways in a membrane [11].

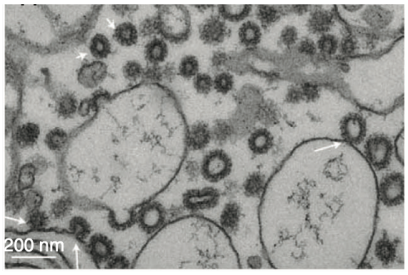

(b) Clathrin-coated vesicles [16].

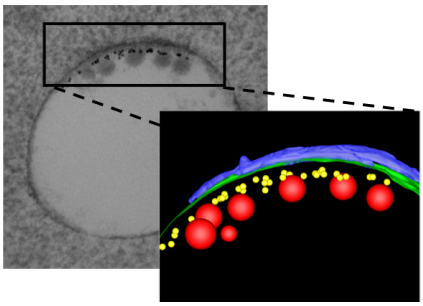

(c) Formation of ILVs [13].

Figure 1.1: Processes in the cell leading to formation of membrane vesicles. (a) Schematic representation of different endocytic processes leading to internalization of cargo proteins into the cell. Clathrin mediated endocytosis is the best characterized endocytic pathway, but endocytosis can also be clathrin-independent. The cargo is then trafficked into the endosome, for its later degradation in Multivesiclar Bodies (MVBs) and in the lysosome. Figure reprinted by permission from Springer Nature: [11], ©2011. (b) Vesicles formed on a liposome after the incubation with clathrin, a fundamental protein of the endocytic pathway and which is capable, by polimerization on the membrane, of forming clathrin-coated vesicles which at the final stage of the deformation detach themselves from the liposome. Figure reprinted by permission from Springer Nature: [16], ©2012. (c) Formation of Intraluminal Vesicles (ILVs) in the endosome membrane. The inlet represents an electron tomography of the endosome, showing that a large protein complex or coat (blue) composed by clathrin and proteins of the Endosomal Sorting Complex Required for Transport (ESCRT) machinery is formed on the endosome membrane (green). Several ILVs (red) are detached from the membrane and are not covered by the coat proteins. The yellow dots are gold particles marking newly internalized activated Epidermal Growth Factor Receptors (EGFRs) into the ILVs. Figure modified from [13], which is licensed under CC BY 4.0.

lipid bilayer, induces changes in membrane morphology [22]. Experiments with proteins which are the main component of the envelope of viruses have revealed

that, once these proteins had self-assembled on the membrane, ILVs became visible on a liposome, mimicking in this way the formation of viral particles [23]. Such experimental findings in synthetic membranes suggest that both the lipid bilayer and the membrane-bound proteins are key to membrane remodeling, and that proteins exploit different mechanisms to deform the membrane.

Over the last decades, scientists have proposed mathematical models to describe the membrane. Such abstraction-driven models aim at presenting the membrane's most important attributes in a mathematical way. These models proceed by assigning generic properties such as elasticity, tension and curvature to membranes. Mathematical models rightfully consider that the membrane's thickness and the individual size of the lipid molecules it contains are so much smaller than the membrane's surface, that the membrane can be consequently regarded as a two-dimensional continuous surface [24]. It then becomes possible to correlate the membrane's shape with its elastic properties, given that, as Helfrich proposed [25], the energy stored in the membrane depends on its curvature and possibly on the asymmetries between the membrane monolayers (also called spontaneous curvature). The rationale behind this correlation has illuminated a fundamental quality of the membrane: the membrane adopts a shape whereby it will minimize the total membrane energy. Helfrich's model has been extensively used. The model has predicted the biconcave discoid shape of red blood cells [26] and other shapes found in experiments with purified lipid bilayers [17], thereby suggesting that the bending energy is a determining factor of the membrane's shape. Fig. 1.2 presents a comparison between the shapes exhibited by giant liposomes under changes of temperature and their predicted theoretical shapes. The prediction is the result of the minimization of the bending energy, as long as each of the membrane's monolayers has a slightly different thermal expansivity. These experiments reveal the importance of the bending energy in the modelling of biological membranes.

Similarities between membrane shapes calculated by mathematical models and observed in experiments have encouraged further development and use of mathematical models to predict shape transformation of membranes, including additional biophysical mechanisms to describe the membrane energy. For example, past research established that certain proteins are capable of inducing curvature. The full mechanism by which these proteins deform the membrane is multi-faceted and complex [27] (more than one protein species is often involved in the membrane's shape transformation [28]). Nevertheless, it is possible to describe proteins as a continuous patch or coat, the size of which is considerably larger than the proteins' individual size. Such a patch or coat has also macroscopic properties, of which bending rigidity and spontaneous curvature are the most significant. A coat-like description of proteins is suitable for cellular processes such as clathrin mediated endocytosis, whereby a complex assembly of proteins is formed on the cell membrane [29]. The theoretical models referred above have demonstrated that whenever the model's parameters —the coat's spontaneous curvature, bending rigidity and membrane

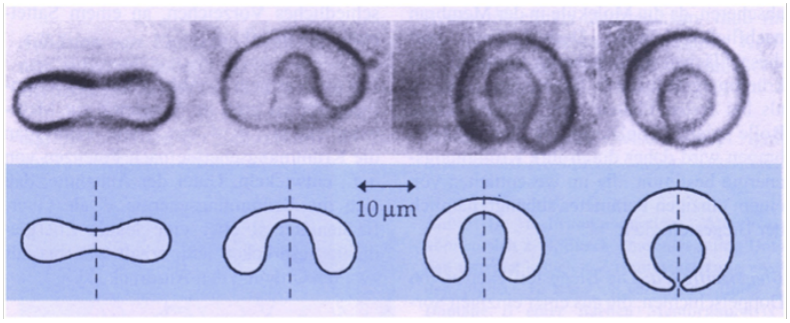

Figure 1.2: Comparison between the shapes of giant liposomes under changes of temperature and the predicted theoretical shapes resulting from minimizing the bending energy of the membrane, assuming that each of the monolayers have a different thermal expansivity. The experiments were performed by Berndl *et. al.* in 1990 [17] and highlight the importance of the bending energy in the theoretical modelling of membranes. Figure reprinted from [24], ©2014, with permission from Elsevier.

tension— fall into the range of values measured experimentally, the membrane shapes obtained theoretically closely coincide with experimental results [30]. In the context of ILV formation, a theoretical model which incorporated the bending energy and additional energy contributions arising from protein crowding [31] predicted the experimentally observed membrane shapes [13]. This theoretical model and its experimental verification unraveled the biophysical mechanism leading to the formation of these uncoated vesicles. As part of the present thesis, the results of this theoretical work is summarized in Chapter 5.

In addition to the models in which the membrane is a continuous surface with macroscopic properties, there are also discrete membrane models. In the latter case, the membrane is studied at the molecular level, which means that it becomes a three-dimensional structure constituted by lipids and proteins of different shape and properties [32]. Both Molecular Dynamics and Monte Carlo methods delivered a fully atomistic description of the membrane's molecular properties, and allowed the study of processes such as the transport of molecules across the lipid bilayer and the self-diffusion of lipid molecules within the membrane [33]. Unfortunately, these methods are computationally costly and limited to small membrane patches and short time scales. Coarse-grained models partly overcame these limitations by providing simplified descriptions which omitted some of the atomistic details. Rather than considering each individual atom on the membrane, the latter model proposed that effective particles are constituted by several atoms which experience effective forces and interactions [33]. Coarse-grained models helped to reveal mechanisms by which proteins and colloidal particles can drive vesiculation, as it is the case with curvature-mediated interaction between either colloidal particles or proteins [34].

This thesis is built upon the assumption that the mathematical modelling of membranes is a heuristic tool which facilitates the understanding of the biophysical mechanisms underlying shape changes observed in biological membranes. In particular, the present study builds upon the development of generic membrane models based on the Helfrich energy while adding additional biophysical effects. In consequence, Chapter 2 outlines the fundamental assumptions that lead to a theoretical description of the membrane. Additionally, it describes the formalism by which one can obtain the mathematical equations which predict membrane shape by minimizing the membrane energy. Chapter 3 is devoted to show a second formalism used to obtain the membrane shape, which consists in balancing the forces acting on a membrane. This chapter also includes a comparison between the formalism based on the energy minimization and on the balance of membrane forces. For the purpose of incorporating the gradual shape transformation of the membrane into the mathematical model, Chapter 4 outlines the processes which can influence membrane dynamics and the manner by which they can be described mathematically. Finally, Chapter 5 presents a summary of this study's findings, and offers an outlook on the future of membrane modelling.

References

[1] Dobereiner, H., Kas, J., Noppl, D., Sprenger, I., and Sackmann, E. "Budding and fission of vesicles". In: *Biophysical Journal* vol. 65, no. 4 (1993), pp. 1396–1403.

[2] Janmey, P. and Kinnunen, P. "Biophysical properties of lipids and dynamic membranes". In: *Trends in Cell Biology* vol. 16, no. 10 (2006), pp. 538–546.

[3] Sha'afi, R. I., Gary-Bobo, C. M., and Solomon, A. K. "Permeability of red cell membranes to small hydrophilic and lipophilic solutes". In: *The Journal of General Physiology* vol. 58, no. 3 (1971), pp. 238–258.

[4] Engelman, D. "Membranes are more mosaic than fluid". In: *Nature* vol. 438, no. 7068 (2005), pp. 578–580.

[5] Guidotti, G. "The composition of biological membranes". In: *Archives of Internal Medicine* vol. 2, no. 129 (1972), pp. 194–201.

[6] "Physics of Biological Membranes". In: Springer, Cham, 2018. Chap. I.

[7] Dimova, R. "Recent developments in the field of bending rigidity measurements on membranes". In: *Advances in Colloid and Interface Science* vol. 208 (2014), pp. 225–234.

[8] Wu, L.-G., Hamid, E., Shin, W., and Chiang, H.-C. "Exocytosis and endocytosis: Modes, functions, and coupling mechanisms". In: *Annual Review of Physiology* vol. 76, no. 1 (2014), pp. 301–331.

[9] Battey, N., James, N., Greenland, A., and Brownlee, C. "Exocytosis and endocytosis". In: *Plant Cell* vol. 11, no. 4 (1999), pp. 643–660.

[10] Doherty, G. J. and McMahon, H. T. “Mechanisms of endocytosis”. In: *Annual Review of Biochemistry* vol. 78, no. 1 (2009), pp. 857–902.

[11] McMahon, H. T. and Boucrot, E. “Molecular mechanism and physiological functions of clathrin-mediated endocytosis”. In: *Nature Reviews Molecular Cell Biology* vol. 12, no. 8 (2011), pp. 517–533.

[12] Robinson, M. S. “Forty years of clathrin-coated vesicles”. In: *Traffic* vol. 16, no. 12 (2015), pp. 1210–1238.

[13] Wenzel, E. M., Schultz, S. W., Schink, K. O., Pedersen, N. M., Nahse, V., Carlson, A., Brech, A., Stenmark, H., and Raiborg, C. “Concerted ESCRT and clathrin recruitment waves define the timing and morphology of intraluminal vesicle formation”. In: *Nature Communications* vol. 9, no. 1 (2018), pp. 2932–2950.

[14] Wollert, T. and Hurley, J. H. “Molecular mechanism of multivesicular body biogenesis by ESCRT complexes”. In: *Nature* vol. 464, no. 7290 (2010), pp. 864–869.

[15] Weissenhorn, W., Poudevigne, E., Effantin, G., and Bassereau, P. “How to get out: ssRNA enveloped viruses and membrane fission”. In: *Current Opinion in Virology* vol. 3, no. 2 (2013), pp. 159–167.

[16] Dannhauser, P. N. and Ungewickell, E. J. “Reconstitution of clathrin-coated bud and vesicle formation with minimal components”. In: *Nature Cell Biology* vol. 14, no. 6 (2012), pp. 634–639.

[17] Berndl, K., Käs, J., Lipowsky, R., Sackmann, E., and Seifert, U. “Shape transformations of giant vesicles: Extreme sensitivity to bilayer asymmetry”. In: *Europhysics Letters* vol. 13, no. 7 (1990), pp. 659–664.

[18] Staykova, M., Holmes, D. P., Read, C., and Stone, H. A. “Mechanics of surface area regulation in cells examined with confined lipid membranes”. In: *Proceedings of the National Academy of Sciences* vol. 108, no. 22 (2011), pp. 9084–9088.

[19] Stachowiak, J. C., Schmid, E. M., Ryan, C. J., Ann, H. S., Sasaki, D. Y., Sherman, M. B., Geissler, P. L., Fletcher, D. A., and Hayden, C. C. “Membrane bending by protein-protein crowding”. In: *Nature Cell Biology* vol. 14, no. 9 (2012), pp. 944–949.

[20] Snead, W. T., Hayden, C. C., Gadok, A. K., Zhao, C., Lafer, E. M., Rangamani, P., and Stachowiak, J. C. “Membrane fission by protein crowding”. In: *Proceedings of the National Academy of Sciences of the United States of America* vol. 114, no. 16 (2017), pp. E3258–E3267.

[21] Stachowiak, J. C., Hayden, C. C., and Sasaki, D. Y. “Steric confinement of proteins on lipid membranes can drive curvature and tubulation”. In: *Proceedings of the National Academy of Sciences of the United States of America* vol. 107, no. 17 (2010), pp. 7781–7786.

[22] Tsafrir, I., Caspi, Y., Guedeau-Boudeville, M.-A., Arzi, T., and Stavans, J. "Budding and tubulation in highly oblate vesicles by anchored amphiphilic molecules". In: *Physical Review Letters* vol. 91, no. 13 (2003), pp. 138102–138106.

[23] Shnyrova, A. V., Ayllon, J., Mikhalyov, I. I., Villar, E., Zimmerberg, J., and Frolov, V. A. "Vesicle formation by self-assembly of membrane-bound matrix proteins into a fluidlike budding domain". In: *Journal of Cell Biology* vol. 179, no. 4 (2007), pp. 627–633.

[24] Lipowsky, R. "Coupling of bending and stretching deformations in vesicle membranes". In: *Advances in Colloid and Interface Science* vol. 208 (2014), pp. 14–24.

[25] Helfrich, W. "Elastic properties of lipid bilayers: Theory and possible experiments". In: *Zeitschrift für Naturforschung C* vol. 28, no. 11-12 (1973), pp. 693–703.

[26] Deuling, H. and Helfrich, W. "The curvature elasticity of fluid membranes : A catalogue of vesicle shapes". In: *Journal de Physique* vol. 37, no. 11 (1976), pp. 1335–1345.

[27] Zimmerberg, J. and Kozlov, M. "How proteins produce cellular membrane curvature". In: *Nature Reviews Molecular Cell Biology* vol. 7, no. 1 (2006), pp. 9–19.

[28] Kaksonen, M. and Roux, A. "Mechanisms of clathrin-mediated endocytosis". In: *Nature Reviews Molecular Cell Biology* vol. 19, no. 5 (2018), pp. 313–326.

[29] Hassinger, J. E., Oster, G., Drubin, D. G., and Rangamani, P. "Design principles for robust vesiculation in clathrin-mediated endocytosis". In: *Proceedings of the National Academy of Sciences* vol. 114, no. 7 (2017), pp. E1118–E1127.

[30] Dmitrieff, S. and Nédélec, F. "Membrane mechanics of endocytosis in cells with turgor". In: *PLOS Computational Biology* vol. 11, no. 10 (2015), pp. 1–15.

[31] Liese, S., Wenzel, E. M., Kjos, I., Rojas Molina, R., Schultz, S. W., Brech, A., Stenmark, H., Raiborg, C., and Carlson, A. "Protein crowding mediates membrane remodeling in upstream ESCRT-induced formation of intraluminal vesicles". In: *Proceedings of the National Academy of Sciences* vol. 117, no. 46 (2020), pp. 28614–28624.

[32] Venturoli, M., Sperotto, M. M., Kranenburg, M., and Smit, B. "Mesoscopic models of biological membranes". In: *Physics Reports* vol. 437, no. 1 (2006), pp. 1–54.

[33] Müller, M., Katsov, K., and Schick, M. "Biological and synthetic membranes: What can be learned from a coarse-grained description?" In: *Physics Reports* vol. 434, no. 5 (2006), pp. 113–176.

[34] Reynwar, B. J., Illya, G., Harmandaris, V. A., Mueller, M. M., Kremer, K., and Deserno, M. “Aggregation and vesiculation of membrane proteins by curvature-mediated interactions”. In: *Nature* vol. 447, no. 7143 (2007), pp. 461–464.

Chapter 2

Membrane energy and shape equations

Helfrich's seminal work [1] proposed that the energy associated to membrane elasticity —the bending energy— depends on two factors: the bending rigidity measuring the membrane's resistance to deformations, and the membrane curvature. The curvature is a mathematical concept that helps to describe the shape of a smooth surface [2]. Although a biological membrane is far from being a smooth surface on short length scales, as the molecular thermal fluctuations roughen the membrane [3], membrane elastic models are suitable for length scales much larger than the typical lipid size and therefore such models allow to conceive the membrane as a continuous and smooth surface described by its curvature.

In this chapter, I will present two mathematical formalisms leading to the so-called *shape equations*, *i.e.*, equations predicting membrane shape. These formalisms are the explicit formulation (which prescribes a coordinate system and the mathematical parametrization of the membrane), and the covariant formulation (which is independent from the coordinate system used to describe the membrane and is based on the general expression of the curvature). Although these two formalisms are equivalent, relying on one rather than on the other might simplify the mathematical equations describing the membrane shape.

2.1 Membrane energy

The energy per unit area of the membrane is written as [1, 4, 5]:

$$w = B(H - C)^2 + \lambda \tag{2.1}$$

where B is the membrane bending rigidity, $H = \frac{1}{2}(\kappa_1 + \kappa_2)$ is the membrane mean curvature given by the sum of its two principal curvatures κ_1 and κ_2, and C is the *spontaneous curvature* that measures any asymmetry between the two membrane monolayers, *e.g.*, different lipid composition [4] or the presence of membrane-bound proteins or polymers on the membrane [6]. In general, the spontaneous curvature imposed by proteins, for example, is the result of the combined effect of different mechanisms exploited by the proteins to produce membrane deformation [7]. In this model, the spontaneous curvature is an effective parameter or function that does not consider the exact molecular mechanism producing the curvature on the membrane. Additionally, the model includes a surface tension λ acting on the entire membrane. The tension is associated with the membrane stretching and has a complex physical and

biological origin [8]. Again, λ represents an effective parameter or function that does not detail all the possible mechanisms which produce it.

To better understand the concept of principal curvatures, Fig. 2.1 shows their schematic representation. At any point $\mathbf{X}$ of a surface, one can define a normal vector $\mathbf{N}$ and a tangent vector $\mathbf{df}(\mathbf{X})$. The plane that contains these two vectors intersects the surface and allows to define the normal curvature κ_n, as shown in Fig. 2.1a. However, in general the normal curvature κ_n is not the same for all the tangent directions to the surface. The principal directions $\mathbf{X_1}$ and $\mathbf{X_2}$ are such that the normal curvature becomes extremal. The corresponding curvatures are denoted as first and second principal curvatures κ_1 and κ_2, as shown in Fig. 2.1b.

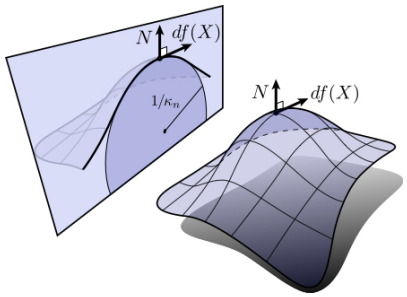

(a) The normal curvature κ_n

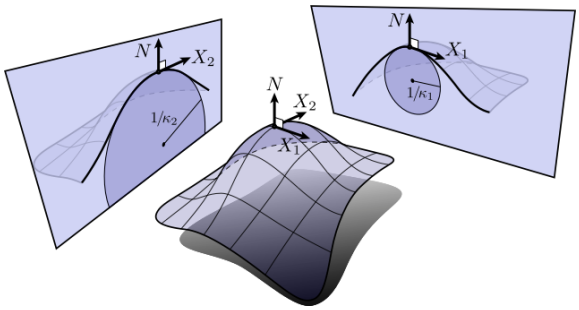

(b) The principal curvatures κ_1 and κ_2.

Figure 2.1: Illustration of the principal curvatures describing a membrane surface, adopted from [9]. (a) At each point $\mathbf{X}$ of the surface, one can define a normal vector $\mathbf{N}$ and a tangent vector $\mathbf{df}(\mathbf{X})$. These two vectors form a plane that intersect the surface and defines the normal curvature κ_n. (b) The normal curvature is maximal and minimal along the principal directions $\mathbf{X_1}$ and $\mathbf{X_2}$, respectively, and their values are κ_1 and κ_2. These are the principal curvatures that define the membrane mean curvature.

The membrane shape will be given by the minimization of the total energy of the membrane with respect to its curvature. The total energy is given by the

integral over the entire membrane area A of Eq. 2.1:

$$W = \int [B(H - C)^2 + \lambda] dA \tag{2.2}$$

If the membrane forms a closed surface with a fixed area, some constraints need to be added, in the form of Lagrange multipliers that enforce a given fixed area and volume [4]. However, in many cases it is convenient to assume that the membrane is an infinite surface. For example, in processes such as clathirn mediated endocytosis or virus budding, the membrane deforms to generate a vesicle of radius $\sim$ 100nm [10, 11], much smaller than the cell radius, which is $\sim 10\mu$m [11], in which case the membrane can be approximated as an infinite surface. As consequence, there is no constraint on either the membrane area or volume. This assumption helps to simplify the membrane description.

An additional term can be added to Eq. 2.2, which is proportional to the Gaussian curvature, and written as $k_G \kappa_1 \kappa_2$, where k_G is the Gaussian bending rigidity [1]. However, if there are no topological changes on the membrane (associated, for example, to the vesicle scission) and if k_G is constant, the integral of the Gaussian curvature energy is a constant which can be omitted [4].

2.2 Shape equations

The term *shape equations* refers to a set of differential equations that allow to find the shape of a membrane that minimizes the energy in Eq. 2.2, for any given spontaneous curvature C and tension λ. These equations can be found by two different means: by prescribing *a priori* a suitable coordinate system and membrane parametrization to write explicitly the bending energy, or by using the general expression of the curvature, in a coordinate-independent manner, giving the covariant shape equations. The section below presents key details regarding the derivation of the shape equations based on these two formalisms.

2.2.1 Euler-Lagrange formalism

In order to determine the shape equations, one needs to establish a suitable parametrization of the membrane. In this regard, experiments on membrane shape deformation induced by proteins indicate that many membrane vesicles closely resemble axially symmetric shapes [12, 13]. The assumption of axial symmetry significantly simplifies the equation describing the membrane curvature and, as consequence, the shape equations will be simpler as well.

The Euler-Lagrange (EL) formalism's main purpose consists in finding the equations satisfied by the functions of a given Lagrangian functional, so that this functional is extremal. In a general way, the Lagrangian functional $\mathcal{L}$, parametrized by an arbitrary variable t, depends on a set of functions

$f_i(t)$, its derivatives $f_i'(t) \equiv \frac{df_i}{dt}$, and one or more functions $\Gamma(t)$ introduced to impose constraints. The Lagrangian is written in a general form as $\mathcal{L} \equiv \mathcal{L}(f_i(t), f_i'(t), \Gamma(t))$ [14, 15]. The Euler-Lagrange (EL) equation, satisfied by each of the functions f_i, reads:

$$\frac{\partial \mathcal{L}}{\partial f_i} - \frac{d}{dt}\left(\frac{\partial \mathcal{L}}{\partial f_i'}\right) = 0 \tag{2.3}$$

In the present case, the Lagrangian $\mathcal{L}$ will be associated with the membrane energy, while the functions f_i will describe the membrane curvature. The exact form of the EL equations depends on the parametrization used to describe the surface coordinates, given that the expression for the curvature will depend on this choice. In the context of membranes, it is usual to use cylindrical coordinates $\{r, \theta, z\}$ to describe the membrane. The position vector in cylindrical coordinates is given by:

$$\mathbf{X} = \hat{\mathbf{x}} r\cos\theta + \hat{\mathbf{y}} r\sin\theta + \hat{\mathbf{z}} z \tag{2.4}$$

where $\{\hat{\mathbf{x}}, \hat{\mathbf{y}}, \hat{\mathbf{z}}\}$ are the unit basis vectors in cartesian coordinates. The functions r, θ, and z can be parametrized in different ways, the most common of which are the *arc-length* and the *radial* parametrization.

2.2.1.1 Arc-length parametrization

The arc-length is the distance measured along a curve. A schematic representation of an axially symmetric budded membrane parametrized by the arc-length s is shown in Fig. 2.2. There, the radial coordinate r and the height z are functions of s, and the tangent angle $\phi(s)$ relates the change of r and z along the curve with the arc-length, that is:

$$r' = \cos\phi \tag{2.5}$$
$$z' = \sin\phi \tag{2.6}$$
$$A' = 2\pi r \tag{2.7}$$

where $()' \equiv \frac{d}{ds}$. Fig. 2.2 also shows the polar angle θ, but the membrane surface will be symmetric with respect to the z-axis due to the axial symmetry. In such cases, the membrane shape will not depend on the polar angle.

In order to write the energy in Eq. 2.2 explicitly as a function of the membrane curvature, one needs to find the expressions for the tangent vectors and the mean and Gaussian curvature in the arc-length parametrization. The tangent vectors define the tangent plane on the surface, and are given in terms of the position vector in Eq. 2.4 as:

$$\mathbf{e}_s = \frac{d\mathbf{X}}{ds} = \hat{\mathbf{x}} r'\cos\theta + \hat{\mathbf{y}} r'\sin\theta + \hat{\mathbf{z}} z' \tag{2.8}$$

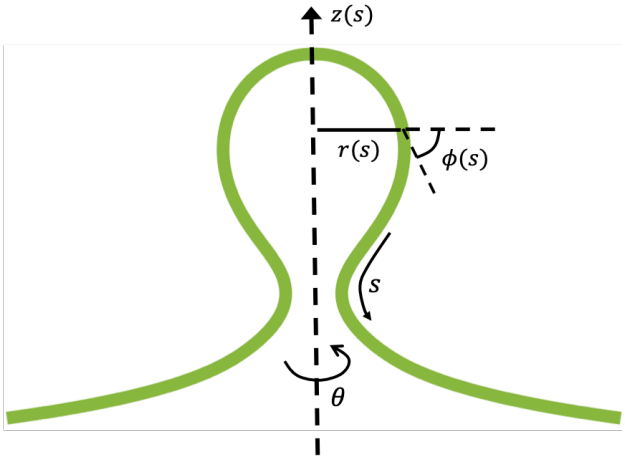

Figure 2.2: Schematic representation of the coordinates used to describe an axially symmetric budded membrane with the arc-length parametrization. The radial distance r and the membrane height z are functions of the arc-length s, and the change of r and z along the curve is given in terms of the tangent angle ϕ. Due to the axial symmetry, the membrane shape will not depend on the polar angle θ, and the membrane surface will be a surface of revolution around the z-axis.

$$\mathbf{e}_\theta = \frac{d\mathbf{X}}{d\theta} = -\hat{\mathbf{x}} r \sin\theta + \hat{\mathbf{y}} r \cos\theta \tag{2.9}$$

The basis vectors define the metric. Intuitively, the metric measures "the infinitesimal squared distance associated to an infinitesimal displacement in the surface" [16]. As the basis vectors are orthogonal, the metric is a diagonal matrix, and its coefficients are [17]:

$$\begin{aligned} g_{ss} = \mathbf{e}_s \cdot \mathbf{e}_s = r'^2 + z'^2 = 1, \qquad g^{ss} = 1 \\ g_{\theta\theta} = \mathbf{e}_\theta \cdot \mathbf{e}_\theta = r^2, \qquad g^{\theta\theta} = 1/r^2 \end{aligned} \tag{2.10}$$

The determinant of the metric is then given by $|g_{ij}| = g_{ss} g_{\theta\theta} = r^2$. The outward normal vector $\mathbf{N}$ is:

$$\mathbf{N} = \frac{\mathbf{e}_s \times \mathbf{e}_\theta}{r} = -\hat{\mathbf{x}} z' \cos\theta - \hat{\mathbf{y}} z' \sin\theta + \hat{\mathbf{z}} r' \tag{2.11}$$

With the expressions of the tangent vectors in Eqs. 2.8 and 2.9 and the normal vector in Eq. 2.11, one can calculate the membrane curvature. Ultimately, the curvature is defined in terms of the *second fundamental form*, denoted as b_{ij}, which is an intrinsic property of the surface, and is defined as:

$$b_{ij} = \mathbf{e}_{i,j} \cdot \mathbf{N} \tag{2.12}$$

where $\mathbf{e}_{i,j} \equiv \frac{\partial \mathbf{e}_i}{\partial x^j}$ is the derivative of the basis vectors with respect to the coordinates. The non-vanishing components of b_{ij} are:

$$b_{ss} = -z'r'' + r'z'' = \phi'$$
$$b_{\theta\theta} = rz' = r\sin\phi$$

where Eqs. 2.5 and 2.6 were used. Consequently, b_{ij} is a diagonal matrix and its determinant is $|b_{ij}| = \phi' r \sin\phi$. The mean and Gaussian curvature of the membrane are [17]:

$$2H = b^i_i = g^{ij}b_{ij} = \kappa_1 + \kappa_2 = \phi' + \frac{\sin\phi}{r} \tag{2.13}$$

$$K = \frac{|b_{ij}|}{|g_{ij}|} = \frac{\phi' r \sin\phi}{r^2} = \kappa_1\kappa_2 = \phi'\frac{\sin\phi}{r} \tag{2.14}$$

where I have introduced the expressions of inverse metric components in Eq. 2.10. Having established both the expression of the mean curvature H and the area differential given by $dA = 2\pi r ds$, the membrane energy is:

$$W = 2\pi \int \left\{ B\left[\frac{1}{2}\left(\phi' + \frac{\sin\phi}{r}\right) - C\right]^2 + \lambda \right\} r ds \tag{2.15}$$

Minimizing the energy in Eq. 2.15 with respect to the curvature means to minimize W with respect to the functions $r(s)$ and $\phi(s)$, for any given spontaneous curvature C and surface tension λ. The Lagrange functional will have as parameter the arc-length s. Additionally, one must take into account that the function r satisfies Eq. 2.5, which means that one needs to include a constraint, or Lagrange parameter function, which is called $\Gamma(s)$. Therefore, the Lagrangian $\mathcal{L}$ is:

$$\mathcal{L}(r, r', \phi, \phi', \Gamma) = \left\{ B\left[\frac{1}{2}\left(\phi' + \frac{\sin\phi}{r}\right) - C\right]^2 + \lambda \right\} r + \Gamma(r' - \cos\phi) \tag{2.16}$$

The EL equations satisfied by $r(s)$ and $\phi(s)$, given in generic form in Eq. 2.3, are:

$$\frac{\partial \mathcal{L}}{\partial r} - \frac{d}{ds}\left(\frac{\partial \mathcal{L}}{\partial r'}\right) = 0 \rightarrow \Gamma' = \lambda + \frac{M^2}{B} - \frac{M\sin\phi}{r} \tag{2.17}$$

$$\frac{\partial \mathcal{L}}{\partial \phi} - \frac{d}{ds}\left(\frac{\partial \mathcal{L}}{\partial \phi'}\right) = 0 \rightarrow M' = \frac{\Gamma\sin\phi}{r} \tag{2.18}$$

where M is the bending moment of the membrane and describes the response of a deformable surface to the bending stresses. M is proportional to the membrane curvature and the bending rigidity [11, 18]:

$$M = B\left[\frac{1}{2}\left(\phi' + \frac{\sin\phi}{r}\right) - C\right] \tag{2.19}$$

The Lagrangian has an associated functional called Hamiltonian, denoted as $\mathcal{H}$ and defined as [14]:

$$\mathcal{H} = -\mathcal{L} + r' \frac{\partial \mathcal{L}}{\partial r'} + \phi' \frac{\partial \mathcal{L}}{\partial \phi'}$$

The Hamiltonian $\mathcal{H}$ satisfies $\frac{d\mathcal{H}}{ds} = -\frac{\partial \mathcal{L}}{\partial s}$. The Lagrangian $\mathcal{L}$ does not depend explicitly on the coordinate s, *i.e.*, $\frac{\partial \mathcal{L}}{\partial s} = 0$. As consequence, the Hamiltonian $\mathcal{H}$ is a conserved quantity, given that $\frac{d\mathcal{H}}{ds} = 0$. Since the membrane surface is infinite, the edge of the arc-length s_{max} is not constrained. This implies that the Hamiltonian fulfills $\mathcal{H}(s_{max}) = 0 \rightarrow \mathcal{H}(s) = 0$ [14]. The Hamiltonian $\mathcal{H}$ is given by:

$$\begin{aligned} \mathcal{H} &= r\left[\frac{\Gamma\cos\phi}{r} - \frac{M^2}{B} - \lambda + M\phi'\right] = 0 \\ &\rightarrow \frac{\Gamma\cos\phi}{r} - \frac{M^2}{B} - \lambda + M\phi' = 0 \end{aligned} \tag{2.20}$$

It now becomes possible to write Eqs. 2.17 and 2.18 as a single equation, by writing $\Gamma = \frac{M'r}{\sin\phi}$, taking the derivative of this expression and writing the result so that it equals Eq. 2.17. Therefore one obtains, after multiplying by $\frac{\sin\phi}{r}$:

$$M'' + \frac{M'\cos\phi}{r} - \frac{M'\phi'\cos\phi}{\sin\phi} = M\left[\frac{M}{B}\frac{\sin\phi}{r} - \frac{\sin^2\phi}{r^2}\right] + \frac{\lambda\sin\phi}{r} \tag{2.21}$$

The Laplace-Beltrami operator is the Laplacian in generalized coordinates, defined as $\nabla^2 \equiv \frac{1}{\sqrt{|g_{ij}|}}\frac{d}{dx^i}(g^{ij}\frac{d}{dx^j})$. The Laplace-Beltrami operator in the arc-length parametrization, applied to M, is given by:

$$\nabla^2 M = \frac{1}{r}\frac{d}{ds}\left(r\frac{dM}{ds}\right) = M'' + \frac{M'\cos\phi}{r}$$

From this expression, it is evident that the two first terms in Eq. 2.21 correspond to $\nabla^2 M$. From the mean curvature given in Eq. 2.13, one can write $\frac{\sin\phi}{r} = 2H - \phi'$, and using the expression for the Gaussian curvature in Eq. 2.14, Eq. 2.21 becomes:

$$\nabla^2 M - \frac{M'\phi'\cos\phi}{\sin\phi} = M[-2H(H+C) + K + \phi'(H+C)] + \lambda(2H - \phi') \tag{2.22}$$

For convenience, I wrote $K = 2K - K$ in the previous expression, and placed all the terms proportional to ϕ' on the right hand side. Thus, one now obtains:

$$\begin{aligned} &\nabla^2 M + 2M[H^2 - K + HC] - 2H\lambda \\ &= \phi'\left(\frac{M'\cos\phi}{\sin\phi} + M(H+C) - \lambda - \frac{M\sin\phi}{r}\right) \end{aligned} \tag{2.23}$$

With the expression for the bending moment in Eq. 2.19 and the mean curvature H in Eq. 2.13, one writes $H + C = 2H - \frac{M}{B} = \frac{\sin\phi}{r} + \phi' - \frac{M}{B}$. Also, using Eq. 2.18 to write M' as a function of Γ, one finds that:

$$\begin{aligned} &\nabla^2 M + 2M[H^2 - K + HC] - 2H\lambda \\ &= \phi' \left(\frac{\Gamma \cos\phi}{r} - \frac{M^2}{B} - \lambda + M\phi' \right) \end{aligned} \tag{2.24}$$

According to the condition for the Hamiltonian to vanish (Eq. 2.20), the right hand side of the expression above is identically zero. The left hand side, upon writing $M = B(H - C)$, is:

$$B\nabla^2(H - C) + 2B(H - C)[H^2 - K + HC] - 2H\lambda = 0 \tag{2.25}$$

This equation has the form of the *covariant* shape equation which will be derived from a more general point of view further below. The EL formalism using the arc-length parametrization specifically has been used to determine the phase space of stationary membrane shapes. The phase space is spanned by the spontaneous curvature and the area-to-volume ratio of closed vesicles [14]. The EL formalism was also the theoretical base for the study of membrane shape deformations induced by protein coats, whereby an assembly of proteins in the membrane surface induces a constant spontaneous curvature over a certain area [19, 20]. Furthermore, it was used to determine theoretically the influence of such coats in the shape of the neck regions joining together the vesicle and the surrounding membrane [21]. Below, I will describe the process of writing the shape equations as a coupled system of linear, ordinary differential equations.

First, one eliminates the Lagrange function Γ, redefining Eq. 2.18 in terms of a new function that is called Q. This means that now Eq. 2.18 is written as:

$$M' = \frac{\Gamma \sin\phi}{r} \equiv -Q \tag{2.26}$$

Then, one writes the EL equation for the radial coordinate r using the expression for the Hamiltonian in Eq. 2.20. By expressing $\lambda + \frac{M^2}{B} = \frac{\Gamma\cos\phi}{r} + \phi' M$ and inserting this expression into Eq. 2.17 one obtains:

$$\Gamma' = \frac{\Gamma\cos\phi}{r} - \frac{2M\sin\phi}{r} + M\left(\frac{2M}{B} + 2C\right) \tag{2.27}$$

From the definition of Q in Eq. 2.26, one finds its derivative and substitutes the expression for Γ' given in Eq. 2.27 to obtain:

$$\begin{aligned} Q' &= -\frac{M\sin\phi}{r}\left(\frac{2M}{B} + 2C - \frac{2\sin\phi}{r}\right) - \frac{\Gamma\cos\phi}{r}\phi' \\ &\equiv -\frac{M\sin\phi}{r}\left(\frac{2M}{B} + 2C - \frac{2\sin\phi}{r}\right) - T\phi' \end{aligned} \tag{2.28}$$

where a new function $T \equiv \frac{\Gamma \cos\phi}{r}$ was introduced. Again, one finds its corresponding differential equation using the expression for Γ' in Eq. 2.27 and the definition of Q in Eq. 2.26:

$$T' = \frac{M\cos\phi}{r}\left(\frac{2M}{B} + 2C - \frac{2\sin\phi}{r}\right) + Q\phi' \tag{2.29}$$

It now becomes possible to find expressions for Q and T that satisfy Eq. 2.28 and 2.29. These expressions are:

$$Q = -U\sin\phi$$
$$T = U\cos\phi$$

where the function U satisfies the following differential equation:

$$U' = \frac{M}{r}\left(\frac{2M}{B} + 2C - \frac{2\sin\phi}{r}\right)$$

To summarize, one arrives at the following set of coupled, first order, ordinary differential equations, derived from the minimization of the energy functional in Eq. 2.2. In the differential equations, I have used the definition of the bending moment in Eq. 2.19 to express ϕ' as a function of M, r and C:

$$\phi' = \frac{2M}{B} - \frac{\sin\phi}{r} + 2C \tag{2.30}$$
$$r' = \cos\phi \tag{2.31}$$
$$z' = \sin\phi \tag{2.32}$$
$$A' = 2\pi r \tag{2.33}$$
$$M' = U\sin\phi \tag{2.34}$$
$$U' = \frac{M}{r}\left(\frac{2M}{B} + 2C - \frac{2\sin\phi}{r}\right) \tag{2.35}$$

Next, I will use this set of equations to illustrate membrane shapes obtained from a simple choice of the spontaneous curvature C. I will also present another commonly used membrane parametrization where, instead of the arc-length, the parameter of the Lagrangian functional is the radial distance r.

2.2.1.2 Radial distance r as a parameter

If one chooses to describe the membrane using the radial coordinate r as parameter, there will be only one Euler-Lagrange equation, associated with the tangent angle ϕ. The expressions for $\frac{dz}{ds}$ and $\frac{dA}{ds}$ in Eqs. 2.6 and 2.7, respectively, need to be rewritten as functions of r. These expression are given by:

$$\frac{dz}{ds} = \frac{dz}{dr}\frac{dr}{ds} \rightarrow \frac{dz}{dr} \equiv z_r = \frac{\sin\phi}{\cos\phi} \tag{2.36}$$
$$\frac{dA}{ds} = \frac{dA}{dr}\frac{dr}{ds} \rightarrow \frac{dA}{dr} \equiv A_r = \frac{2\pi r}{\cos\phi} \tag{2.37}$$

where, to ease notation, $()_r \equiv \frac{d()}{dr}$. Additionally, the mean and Gaussian curvature given in Eqs. 2.13 and 2.14, respectively, are expressed as:

$$\frac{d\phi}{ds} = \frac{d\phi}{dr}\frac{dr}{ds} \equiv \phi_r \cos\phi \tag{2.38}$$

$$H = \frac{1}{2}\left(\phi_r \cos\phi + \frac{\sin\phi}{r}\right) \tag{2.39}$$

$$K = \frac{\phi_r \cos\phi \sin\phi}{r} \tag{2.40}$$

As before, one needs to find the basis vectors and the metric coefficients in this parametrization. The basis vectors are given by:

$$\mathbf{e}_r = \frac{d\mathbf{X}}{dr} = \hat{\mathbf{x}}\cos\theta + \hat{\mathbf{y}}\sin\theta + \hat{\mathbf{z}}z_r$$
$$\mathbf{e}_\theta = \frac{d\mathbf{X}}{d\theta} = -\hat{\mathbf{x}}r\sin\theta + \hat{\mathbf{y}}r\cos\theta$$

where $\mathbf{X}$ is the position vector in cylindrical coordinates, given in Eq. 2.4. The corresponding non-vanishing metric coefficients are given by:

$$g_{rr} = \mathbf{e}_r \cdot \mathbf{e}_r = 1 + z_r^2 = \frac{1}{\cos^2\phi} \qquad g^{rr} = \cos^2\phi \tag{2.41}$$

$$g_{\theta\theta} = \mathbf{e}_\theta \cdot \mathbf{e}_\theta = r^2 \qquad g^{\theta\theta} = 1/r^2 \tag{2.42}$$

Above, I have used the expression for z_r in Eq. 2.36. The Lagrangian functional is given as:

$$\mathcal{L}(r,\phi,\phi_r) = \left[B\left[\frac{1}{2}\left(\frac{\sin\phi}{r} + \phi_r\cos\phi\right) - C\right]^2 + \lambda\right]\frac{r}{\cos\phi} \tag{2.43}$$

where one notes that, as the radial distance r is the parameter, there is no Lagrange parameter function associated to r. Moreover, $\mathcal{L}$ depends explicitly on the parameter r, and hence the Hamiltonian is not conserved, because $\frac{\partial\mathcal{L}}{\partial r} \neq 0$. There will be only one EL equation, which is given by:

$$\frac{\partial\mathcal{L}}{\partial\phi} - \frac{d}{dr}\left(\frac{\partial\mathcal{L}}{\partial\phi'}\right) = 0 \rightarrow M\sin\phi\left[\frac{\sin\phi}{r} - \frac{M}{B} - 2C\right] + \lambda\sin\phi - M_r\cos^2\phi = 0 \tag{2.44}$$

The Laplace-Beltrami operator applied to the bending moment M is given as:

$$\nabla^2 M = \frac{1}{\sqrt{|g_{ij}|}}\frac{d}{dr}\left(g^{rr}\sqrt{|g_{ij}|}\frac{dM}{dr}\right) = \frac{M_r\cos^2\phi}{r} - M_r\phi'\cos\phi\sin\phi + M_{rr}\cos^2\phi \tag{2.45}$$

where $M_{rr} \equiv \frac{d^2M}{dr^2}$, and where I have used the metric coefficients in Eq. 2.41 in order to find that the determinant of the metric is $|g_{ij}| = g_{rr}g_{\theta\theta} = \frac{r^2}{\cos^2\phi}$.

It is now possible to take the derivative $\frac{d}{dr}$ of the Eq. 2.44 and use Eq. 2.45 to express $M'' \cos^2\phi$ in terms of the Laplacian $\nabla^2 M$. Additionally, with the expression for the Gaussian curvature in Eq. 2.40, one writes:

$$\begin{aligned} &B\nabla^2(H-C) + 2B(H-C)(H^2+HC-K) - 2H\lambda \\ &+\frac{1}{r}\left[M\sin\phi\left(\frac{\sin\phi}{r} - \frac{M}{B} - 2C\right) + \lambda\sin\phi - M_r\cos^2\phi\right] \\ &\qquad -2C_r M\sin\phi + \lambda_r\sin\phi = 0 \end{aligned} \tag{2.46}$$

In the second line of Eq. 2.46 it is possible to recognize the EL equation of the angle ϕ in Eq. 2.44, which vanishes identically. The third line provides a relation between the spontaneous curvature and the surface tension λ that reads $\lambda_r = 2MC_r$, which indicates that the surface tension accommodates the possible dependence of the spontaneous curvature with the surface coordinates. If this condition is satisfied, one obtains:

$$B\nabla^2(H-C) + 2B(H-C)(H^2+HC-K) - 2H\lambda = 0 \tag{2.47}$$

In the seminal work by Helfrich [1], this parametrization has been used to study the deformation of spherical vesicles.

2.2.2 Covariant formulation

The term *covariant* refers to the way of writing physical quantities in a coordinate-independent manner, that is to say, without specifying *a priori* how to describe the membrane surface. The equations derived in this way will then be valid regardless of the coordinate system and surface parametrization used. To derive the covariant shape equation for the shape that minimizes the energy given in Eq. 2.2, one needs to write the area differential dA and the curvatures in a coordinate-independent way. In covariant form, $dA = \sqrt{|g_{ij}|}dx_1 dx_2$, where $|g_{ij}|$ is the determinant of the metric, the indexes i, j refer to the coordinates used to describe the membrane surface, and dx_1 and dx_2 are the infinitesimal displacement in the coordinate x_1 and x_2, respectively. The metric is defined as:

$$g_{ij} = \mathbf{e}_i \cdot \mathbf{e}_j \tag{2.48}$$

where $\{\mathbf{e}_i\}$ are the basis vectors defining the tangent plane on the surface, that is:

$$\mathbf{e}_i = \frac{\partial \mathbf{X}}{\partial x^i} \tag{2.49}$$

where $\mathbf{X}$ is the position vector on the surface.

The total energy is given, in a covariant form, as:

$$W = \int \sqrt{|g_{ij}|}[B(H-C)^2 + \lambda]dx_1 dx_2 \tag{2.50}$$

Minimizing the energy W means to perform an infinitesimal deformation of the surface, which will induce a variation of the position vector denoted as $\delta\mathbf{X}$. The resulting expression should vanish for any arbitrary $\delta\mathbf{X}$. That is, $\delta W = 0$. In general, $\delta\mathbf{X}$ has two components: one along the tangent plane on the surface and one along the normal direction. However, in order to find the shape equation, it suffices to assume that the variation of $\mathbf{X}$ has only one component, lying along the normal direction [22], *i.e*, $\delta\mathbf{X} = \epsilon(x_1, x_2)\mathbf{N}$, where ϵ is a function of the coordinates and $\mathbf{N}$ is the unit normal vector to the surface, defined as:

$$\mathbf{N} = \frac{\mathbf{e}_1 \times \mathbf{e}_2}{\sqrt{|g_{ij}|}} \tag{2.51}$$

The tangential variations of the surface energy are associated with boundary terms. If the surface has no boundary or edges, these terms will vanish and will not contribute to the energy [23]. In such case, it is enough to consider the normal variations of the surface energy. As consequence, the variation of the energy can be written in a general form, as [17, 23]:

$$\delta W = \int \{\delta\sqrt{|g_{ij}|}[B(H-C)^2 + \lambda] + 2B\sqrt{|g_{ij}|}(H-C)\delta H\} dx_1 dx_2 = 0 \tag{2.52}$$

Obtaining the variation $\delta\sqrt{|g_{ij}|}$ and δH involves many intermediate calculations whose details can be found in [22, 23, 24]. Although my purpose is not to present an exhaustive derivation of the covariant shape equation, it is worth mentioning that the expression of $\delta\sqrt{|g_{ij}|}$ and δH are functions of the mean and Gaussian curvature, which are given in terms of the *second fundamental form*, denoted as b_{ij} and which was first introduced in Eq. 2.12. From the second fundamental form, the mean and Gaussian curvature are defined as:

$$H = \frac{g^{ij}b_{ij}}{2} = \frac{b^j_j}{2} = \frac{(\kappa_1 + \kappa_2)}{2} \tag{2.53}$$

$$K = \frac{|b_{ij}|}{|g_{ij}|} = \kappa_1\kappa_2 \tag{2.54}$$

where g^{ij} is the inverse metric. The mean curvature is the trace of the second fundamental form and the Gaussian curvature is the ratio between the determinants of b_{ij} and the metric g_{ij}. The expressions for $\delta\sqrt{|g_{ij}|}$ and δH are given by [17, 23]:

$$\delta^{(1)}\sqrt{|g_{ij}|} = \sqrt{|g_{ij}|}\,[-2\epsilon H] \tag{2.55}$$

$$\delta^{(1)}H = \epsilon(2H^2 - K) + \frac{1}{2}\nabla^2\epsilon \tag{2.56}$$

where the symbol $\delta^{(1)}$ denotes the variation up to the first order with respect to the perturbation ϵ. By substituting Eqs. 2.55 and 2.56 into Eq. 2.52 one obtains:

$$\delta^{(1)}W = \int \sqrt{|g_{ij}|}\{2B(H-C)[\epsilon(H^2 - K + HC) + 1/2\nabla^2\epsilon] - 2\epsilon H\lambda\} dx_1 dx_2$$

And integrating by parts the term $(H-C)\nabla^2\epsilon$ twice, one obtains [17, 23]:

$$\delta^{(1)}W = \int \sqrt{|g_{ij}|}\epsilon\{B\nabla^2(H-C) + 2B(H-C)(H^2-K+HC) - 2H\lambda\}dx_1dx_2$$

Finally, the condition $\delta^{(1)}W = 0$ should hold for any arbitrary ϵ, and the expression inside the curly brackets must vanish. That is:

$$B\nabla^2(H-C) + 2B(H-C)(H^2-K+HC) - 2H\lambda = 0 \qquad (2.57)$$

where the operator $\nabla^2 \equiv \frac{1}{\sqrt{|g_{ij}|}}\frac{d}{dx^i}(g^{ij}\frac{d}{dx^j})$ is called Lapace-Beltrami operator. The Eq. 2.57 is the shape equation in covariant form and it is identical to Eqs. 2.25 and 2.47. This means that, as expected, the Euler-Lagrange equations lead to the covariant shape equation, regardless of the membrane parametrization used. The covariant shape equation, which poses considerable challenges for it to be solved, is a non-linear, second order partial differential equation. However, if one assumes that the equilibrium shapes have axial symmetry, Eq. 2.57 becomes an ordinary differential equation of higher order [25]. Theoretical studies of membranes have used the covariant shape equation, primarily for axially symmetric shapes [26, 27, 28].

References

[1] Helfrich, W. "Elastic properties of lipid bilayers: Theory and possible experiments". In: *Zeitschrift für Naturforschung C* vol. 28, no. 11-12 (1973), pp. 693–703.

[2] Lipowsky, R. "Coupling of bending and stretching deformations in vesicle membranes". In: *Advances in Colloid and Interface Science* vol. 208 (2014), pp. 14–24.

[3] Brannigan, G. and Brown, F. L. "A consistent model for thermal fluctuations and protein-induced deformations in lipid bilayers". In: *Biophysical Journal* vol. 90, no. 5 (2006), pp. 1501–1520.

[4] Deuling, H. and Helfrich, W. "The curvature elasticity of fluid membranes : A catalogue of vesicle shapes". In: *Journal de Physique* vol. 37, no. 11 (1976), pp. 1335–1345.

[5] Bassereau, P., Sorre, B., and Levy, A. "Bending lipid membranes: Experiments after W. Helfrich's model". In: *Advances in Colloid and Interface Science* vol. 208, no. SI (2014), pp. 47–57.

[6] Tsafrir, I., Caspi, Y., Guedeau-Boudeville, M.-A., Arzi, T., and Stavans, J. "Budding and tubulation in highly oblate vesicles by anchored amphiphilic molecules". In: *Physical Review Letters* vol. 91, no. 13 (2003), pp. 138102–138106.

[7] McMahon, H. and Gallop, J. "Membrane curvature and mechanisms of dynamic cell membrane remodelling". In: *Nature* vol. 438, no. 7068 (2005), pp. 590–596.

[8] Kozlov, M. M. and Chernomordik, L. V. "Membrane tension and membrane fusion". In: *Current Opinion in Structural Biology* vol. 33 (2015), pp. 61–67.

[9] Crane, K. *A Quick and Dirty Introduction to the Curvature of Surfaces*. URL: http://wordpress.discretization.de/geometryprocessingandapplicationsws19/a-quick-and-dirty-introduction-to-the-curvature-of-surfaces/.

[10] Scott, B. L., Sochacki, K. A., Low-Nam, S. T., Bailey, E. M., Luu, Q., Hor, A., Dickey, A. M., Smith, S., Kerkvliet, J. G., Taraska, J. W., and Hoppe, A. D. "Membrane bending occurs at all stages of clathrin-coat assembly and defines endocytic dynamics". In: *Nature Communications* vol. 9, no. 1 (2018), pp. 419–428.

[11] Schley, D., Whittaker, R. J., and Neuman, B. W. "Arenavirus budding resulting from viral-protein-associated cell membrane curvature". In: *Journal of the Royal Society Interface* vol. 10, no. 86 (2013), pp. 20130403–20130416.

[12] Avinoam, O., Schorb, M., Beese, C. J., Briggs, J. A. G., and Kaksonen, M. "Endocytic sites mature by continuous bending and remodeling of the clathrin coat". In: *Science* vol. 348, no. 6241 (2015), pp. 1369–1372.

[13] Wenzel, E. M., Schultz, S. W., Schink, K. O., Pedersen, N. M., Nahse, V., Carlson, A., Brech, A., Stenmark, H., and Raiborg, C. "Concerted ESCRT and clathrin recruitment waves define the timing and morphology of intraluminal vesicle formation". In: *Nature Communications* vol. 9, no. 1 (2018), pp. 2932–2950.

[14] Seifert, U., Berndl, K., and Lipowsky, R. "Shape transformations of vesicles: Phase diagram for spontaneous- curvature and bilayer-coupling models". In: *Physical Review A* vol. 44, no. 2 (1991), pp. 1182–1202.

[15] Jülicher, F. and Seifert, U. "Shape equations for axisymmetric vesicles: A clarification". In: *Phys. Rev. E* vol. 49, no. 5 (1994), pp. 4728–4731.

[16] Wald, R. M. *General relativity*. Chicago, IL: Chicago Univ. Press, 1984.

[17] Deserno, M. "Fluid lipid membranes: From differential geometry to curvature stresses". In: *Chemistry and Physics of Lipids* vol. 185 (2015), pp. 11–45.

[18] Preston, S. P., Jensen, O. E., and Richardson, G. "Buckling of an axisymmetric vesicle under compression: The effects of resistance to shear". In: *Quarterly Journal of Mechanics and Applied Mathematics* vol. 61, no. 1 (2008), pp. 1–24.

[19] Dmitrieff, S. and Nédélec, F. "Membrane mechanics of endocytosis in cells with turgor". In: *PLOS Computational Biology* vol. 11, no. 10 (2015), pp. 1–15.

[20] Foret, L. "Shape and energy of a membrane bud induced by protein coats or viral protein assembly". In: *European Physical Journal E* vol. 37, no. 5 (2014), pp. 42–55.

[21] Kumar, G. and Sain, A. “Shape transitions during clathrin-induced endocytosis”. In: *Physical Review E* vol. 92, no. 6 (2016), pp. 062404–062411.

[22] Zhong-can, O.-Y. and Helfrich, W. “Bending energy of vesicle membranes: General expressions for the first, second, and third variation of the shape energy and applications to spheres and cylinders”. In: *Physical Review A* vol. 39, no. 10 (1989), pp. 5280–5288.

[23] Capovilla, R., Guven, J., and Santiago, J. A. “Deformations of the geometry of lipid vesicles”. In: *Journal of Physics A: Mathematical and General* vol. 36, no. 23 (2003), pp. 6281–6295.

[24] Steigmann, D. “Fluid films with curvature elasticity”. In: *Archive for Rational Mechanics and Analysis* vol. 150, no. 2 (1999), pp. 127–152.

[25] Jian-Guo, H. and Zhong-Can, O.-Y. “Shape equations of the axisymmetric vesicles”. In: *Physical Review E* vol. 47, no. 1 (1993), pp. 461–467.

[26] Agrawal, A. and Steigmann, D. J. “Boundary-value problems in the theory of lipid membranes”. In: *Continuum Mechanics and Thermodynamics* vol. 21, no. 1 (2009), pp. 57–82.

[27] Hassinger, J. E., Oster, G., Drubin, D. G., and Rangamani, P. “Design principles for robust vesiculation in clathrin-mediated endocytosis”. In: *Proceedings of the National Academy of Sciences* vol. 114, no. 7 (2017), pp. E1118–E1127.

[28] Chabanon, M. and Rangamani, P. “Gaussian curvature directs the distribution of spontaneous curvature on bilayer membrane necks”. In: *Soft Matter* vol. 14, no. 12 (2018), pp. 2281–2294.

Chapter 3

Forces on a membrane

Aside from the mathematical formalism described in the previous chapter, a second formalism —the force balance based on the thin shell theory—, also serves to describe the membrane. This alternative formalism deals with the elastic deformations experienced by a solid, closed surface, whose thickness is significantly smaller than the length scale associated to its area. The assumption of negligible thickness was also adopted in the energy formulation of the membrane, discussed in Chapter 2.

A biological membrane has a solid-fluid duality: on one hand, it can be both stretched and compressed as if it were a thin shell [1, 2], due to the slightly elastic nature of the lipid molecules [3]. On the other hand, the membrane shows a fluid structure at physiological temperatures [4], and the lipid molecules and proteins can laterally diffuse. Due to the elastic nature of the biological membrane, a bent lipid membrane is bound to experience forces and torques. The physical condition for the mechanical equilibrium of the bent membrane is the balance of the net force along the normal and tangent directions. The forces acting on a small patch of a fluid membrane and the equations resulting from their balance are equal to the ones found on a solid thin shell. Researchers have derived these equations in detail [5] and summarized them in several publications [3, 6, 7].

Within lipid membranes, which are the object of this study, the force balance formalism illustrated the modeling of budding induced by viral proteins embedded in the cell membrane [8]. Additionally, the formalism was used in the modeling of lipid membranes containing coexisting fluid domains, that is to say, a liquid-ordered and liquid-disordered phase. The boundary between these two phases generates a line tension [9], which is related to the matching conditions satisfied by the transverse shear and lateral stresses across the boundary created between the two fluids phases [7].

The force balance formalism establishes several intrinsically dissimilar constitutive relations between the membrane tension and the bending moments [3, 10]; depending on the chosen relation, the predicted membrane shapes may differ. The section below presents the force balance equations. While describing them, I will set forth and analyze some of the implications that such different constitutive relations pose for the predicted membrane shapes.

3.1 Forces balance equations

As in Chapter 2, this chapter will consider an axially symmetric membrane described with cylindrical coordinates $\{r, \theta, z\}$, involving r and z (parametrized using the arc-length s), together with the angle between the axis of revolution and the normal to the meridian, ϕ. Fig. 2.2 shows a representation of the membrane parametrization with these characteristics. The coordinates r and z, together with the membrane area A, satisfy Eqs. 2.5, 2.6 and 2.7, respectively. The deformed membrane describes two radii of curvature, r_θ, along the azimuthal direction, and r_ϕ along the meridional direction. These two radii of curvature will define the principal curvatures of the membrane, κ_θ and κ_ϕ, which are given by [11]:

$$\kappa_\theta = \frac{1}{r_\theta} = \frac{\sin\phi}{r} \tag{3.1}$$

$$\kappa_\phi = \frac{1}{r_\phi} = \phi' \tag{3.2}$$

Once the mathematical description of the membrane has been established, it is possible to determine the forces acting on it. In order to do this, one envisions a small membrane patch, as shown in Fig. 3.1. Membrane forces act on the membrane patch. Specifically, $\mathbf{Q}$ (transverse shear) and p (pressure) act perpendicularly to the membrane. The tensile stresses, $\mathbf{T}_\theta$ and $\mathbf{T}_\phi$, act in the tangential direction of the membrane. These forces generate bending moments (denoted by $\mathbf{M}_\theta$ and $\mathbf{M}_\phi$) which adopt the direction of the axis around which they are applied, following a right-handed sense. The bending moments depend on the membrane curvature and on a prescribed spontaneous curvature C, as it is shown further below. As a consequence of axial symmetry, none of the forces depend on the angle θ. The forces act on the membrane patch edges whose lengths are given in terms radius of curvatures r_θ and r_ϕ and the differential angles $d\theta$ and $d\phi$. Fig. 3.1 illustrates these lengths, together with the forces acting on the membrane patch. To ease the visualization of such forces, each force is represented with a different color.

The balance of the forces and bending moments in Fig. 3.1 results in the following equations [5, 6]:

$$\begin{aligned} M_\phi' &= (M_\theta - M_\phi)\frac{\cos\phi}{r} - Q \\ T_\phi' &= (T_\theta - T_\phi)\frac{\cos\phi}{r} + Q\phi' \\ Q' &= p - \frac{T_\theta \sin\phi}{r} - T_\phi\phi' - \frac{1}{r}Q\cos\phi \end{aligned}$$

Within the general theory of thin shells, the bending moments M_ϕ and M_θ are defined in terms of the bending strains [6, 10]. Within lipid bilayers, these

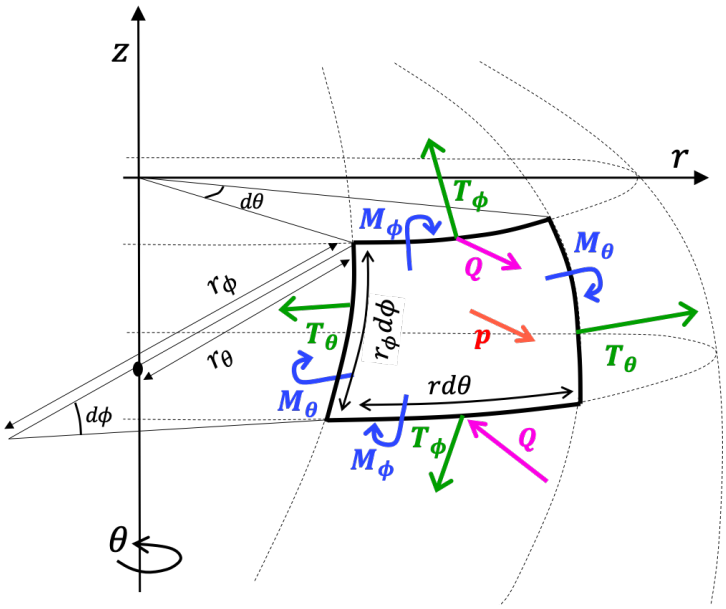

Figure 3.1: Schematic representation of the forces acting on a small membrane patch, subtended by a small azimuthal angle $d\theta$ and a small meridional angle $d\phi$. On the patch, tensile stresses $\mathbf{T}_\theta$ and $\mathbf{T}_\phi$ (depicted in green) act on the membrane; they are located on the plane of the membrane and directed on the $\mathbf{e}_\theta$ and $\mathbf{e}_\phi$ directions, respectively. These tensile forces generate bending moments (depicted in blue), that act around the membrane edges and are directed on a right-handed sense: $\mathbf{M}_\theta$ is directed on the $-\mathbf{e}_\phi$ direction and $\mathbf{M}_\phi$ follows the $\mathbf{e}_\theta$ direction. The transverse shear $\mathbf{Q}$ (depicted in magenta) is directed along the normal direction $\mathbf{n}$ respect to the membrane patch. The net pressure p is depicted in orange. The forces act over different lengths depending on the edge where they are applied. Each length is given in terms of the principal radii of curvature r_θ and r_ϕ and the differential angles $d\theta$ and $d\phi$. These lengths are also shown in the figure.

bending strains are the membrane curvatures, and the bending moments are [6]:

$$M_\theta = M_\phi \equiv M = B\left[\frac{1}{2}\left(\frac{\sin\phi}{r} + \phi'\right) - C\right] \tag{3.3}$$

where B is the bending rigidity and C is the spontaneous or preferred curvature. The equation for the balance of moments adopts the following simplified form:

$$M' = -Q$$

To summarize, the differential equations to be solved in the force balance formalism are:

$$\phi' = \frac{2M}{B} - \frac{\sin\phi}{r} + 2C \tag{3.4}$$

$$r' = \cos\phi \tag{3.5}$$

$$z' = \sin\phi \tag{3.6}$$

$$A' = 2\pi r \tag{3.7}$$

$$M' = -Q \tag{3.8}$$

$$Q' = p - \frac{T_\theta \sin\phi}{r} - T_\phi \phi' - \frac{1}{r} Q \cos\phi \tag{3.9}$$

$$T'_\phi = (T_\theta - T_\phi)\frac{\cos\phi}{r} + Q\phi' \tag{3.10}$$

Eqs. 3.4-3.8 are equivalent to Eqs. 2.30-2.34. The following section discusses the conditions which allow that the equation for the transverse shear Q (Eq. 3.9) and the tension (Eq. 3.10) are equivalent to Eq. 2.28 and Eq. 2.29, respectively. In order to examine this possible equivalence, one needs to establish the description of membrane tension. Theoretical research [12, 13] proposed that membrane tension and bending moments are related to each other by a constitutive relation. The physical origin of such relation lies in the stratified nature of the membrane, where the tangential stresses and moments accumulate across the material and can be defined with respect to a "neutral" or equivalent surface. The tension T_ϕ and T_θ, which are defined in this neutral mid-surface, are [3, 12, 13]:

$$T_\phi = \tau + \kappa_\theta M = \tau + \frac{M \sin\phi}{r} \tag{3.11}$$

$$T_\theta = \tau + \kappa_\phi M = \tau + M\phi' \tag{3.12}$$

where τ is a tension that is common to both T_ϕ and T_θ. Regarding the particular case of vanishing spontaneous curvature ($C = 0$) [3], the constitutive relations in Eqs. 3.11 and 3.12 demonstrated that the force balance equations lead to the covariant shape equation, Eq. 2.57. I intend to illustrate whether the force balance equations are equivalent to the equations derived from the energy minimization with the constitutive relations described above (Eqs. 3.11 and 3.12) for the membrane tension. In consequence, Eqs. 3.11 and 3.12 are introduced into Eq. 3.10 to obtain:

$$T'_\phi = \frac{M\cos\phi}{r}\left(\phi' - \frac{\sin\phi}{r}\right) + Q\phi' = \frac{M\cos\phi}{r}\left(\frac{2M}{B} + 2C - \frac{2\sin\phi}{r}\right) + Q\phi' \tag{3.13}$$

where the expression for the bending moment M in Eq. 3.3 was used to write ϕ' as a function of M, ϕ, and r. The derivative of T_ϕ, following Eq. 3.11, is:

$$T'_\phi = \tau' + \frac{M'\sin\phi}{r} + \frac{M\cos\phi}{r}\left(\frac{2M}{B} + 2C - \frac{2\sin\phi}{r}\right) \tag{3.14}$$

In consequence, Eq. 3.13 becomes:

$$\tau' = Q\left(\frac{\sin\phi}{r} + \phi'\right) \tag{3.15}$$

Previously, the first order differential equations of the functions T and Q, Eqs. 2.29 and 2.28 were obtained from the EL formalism. The equation for T was:

$$T' = \frac{M\cos\phi}{r}\left(\frac{2M}{B} + 2C - \frac{2\sin\phi}{r}\right) + Q\phi' \tag{3.16}$$

The right hand side of Eqs. 3.13 and 3.16 are identical. Yet it remains to be seen whether their left hand sides are also identical. To answer this, the expression of the Hamiltonian in Eq. 2.20 is used, together with the definition of T, $T \equiv \frac{\Gamma\cos\phi}{r}$. From the expression of $\mathcal{H}$, it then follows that:

$$\frac{\Gamma\cos\phi}{r} \equiv T = \frac{M^2}{B} + \lambda - M\phi' = \lambda - \frac{M^2}{B} - 2MC + \frac{M\sin\phi}{r} \tag{3.17}$$

where Eq. 2.26 was used to write $M' = -Q$. Hence, the left hand side of Eqs. 3.13 (force balance formalism) and 3.16 (EL formalism) are equal as long as $T = T_\phi$. This condition is fulfilled if $T = \tau + \frac{M\sin\phi}{r}$, where τ is:

$$\tau = \lambda - \frac{M^2}{B} - 2MC \rightarrow \tau' = -M'\left(\frac{2M}{B} + 2C\right) = Q\left(\frac{\sin\phi}{r} + \phi'\right) \tag{3.18}$$

From this point onwards, λ and C are constants. As the equations fulfilled by τ' in Eqs. 3.15 and 3.18 are consistent, I have been able to show that the function T defined in the EL formalism conveys the physical interpretation of the tension along the meridional direction, $T = T_\phi$.

It is possible to perform a similar analysis for the equations corresponding to the transverse shear Q. The equation for Q, Eq. 3.9, with the definition of the tension T_ϕ and T_θ in Eqs. 3.11 and 3.12, respectively, is written as:

$$Q' = p - \tau\left(\frac{\sin\phi}{r} + \phi'\right) - \frac{2M\phi'\sin\phi}{r} - \frac{Q\cos\phi}{r} \tag{3.19}$$

Previously, the function Q from the EL formalism appeared as the following expression:

$$Q' = -\frac{M\sin\phi}{r}\left(\frac{2M}{B} + 2C - \frac{2\sin\phi}{r}\right) - \left(\tau + M\frac{\sin\phi}{r}\right)\phi' \tag{3.20}$$

where I used $T = T_\phi = \tau + \frac{M\sin\phi}{r}$. By comparing the expression for Q' in both Eqs. 3.9 (force balance formalism) and 3.20 (EL formalism), it is possible to notice that they are equal if:

$$p - \frac{\tau\sin\phi}{r} - \frac{Q\cos\phi}{r} = \frac{M\sin^2\phi}{r^2} \rightarrow p - \frac{T\sin\phi}{r} - \frac{Q\cos\phi}{r} = 0 \tag{3.21}$$

where I have also used $T = T_\phi = \tau + \frac{M\sin\phi}{r}$. The functions T and Q in the EL formalism admitted as solution:

$$Q = -U\sin\phi$$
$$T = U\cos\phi$$

By inserting these expressions into Eq. 3.21, this equation is fulfilled as long as $p = 0$. In the derivation of the EL equations, it was assumed that the membrane is infinite. As a result, there was no constraint on the volume it enclosed. In consequence, the pressure $p = 0$. On the other hand, when analyzing the forces, it is now justifiable to assume that the pressure is negligible as long as the radius of the bud formed on the vesicle is significantly smaller than the vesicle size, as it will be shown further below. Therefore, if $T = T_\phi$ and if $p = 0$, Eqs. 3.9 and 3.10 are equivalent to Eqs. 2.28 and 2.29, respectively.

Consequently, I have shown that the functions T and Q derived from the EL formalism can have a clear interpretation of membrane tension and transverse shear stress, respectively, provided that the tension and bending moments are coupled according to the constitutive relations Eqs. 3.11 and 3.12.

Previous literature on this topic indicates that there is another way of describing membrane tension: the tensions are decoupled from the bending moments, that is, $T_\theta = T_\phi = \tau$ [8, 10]. This assumption simplifies the equations derived from the force balance formalism which, together with the geometric equations derived from the membrane parametrization, form the following set of coupled first order, ordinary differential equations:

$$\phi' = \frac{2M}{B} - \frac{\sin\phi}{r} + 2C \tag{3.22}$$

$$r' = \cos\phi \tag{3.23}$$

$$z' = \sin\phi \tag{3.24}$$

$$A' = 2\pi r \tag{3.25}$$

$$M' = -Q \tag{3.26}$$

$$\tau' = Q\phi' \tag{3.27}$$

$$Q' = p - \frac{\tau\sin\phi}{r} - \tau\phi' - \frac{Q\cos\phi}{r} \tag{3.28}$$

However, Eq. 3.27 does not allow to establish an equivalence with the equations derived from the EL formalism. Therefore, the solution of the equations derived from these two formalisms will be, in general, different. In the following section, I will compare the shapes obtained by solving Eqs. 3.22-3.28 (when decoupled tension and bending moments are chosen) with the shapes obtained through the EL formalism, Eqs. 2.30-2.35, for a given spontaneous curvature C.

3.1.1 Boundary conditions in the force balance equations

To illustrate the predictions from both the EL formalism (Eqs. 2.30-2.35) and the force balance equations (Eqs. 3.22-3.28), it is assumed that a small bud of radius L is formed on a closed vesicle of radius r_c, which is significantly larger than L. The formation of the bud is driven by the spontaneous curvature C

defined on a certain region of the membrane. Such region has an area equal to A_p. The spontaneous curvature C is a piecewise constant function, given by [8]:

$$C = \left\{ \begin{array}{ll} 1/L & \text{if } A < A_p \\ 1/r_c & \text{if } A \geq A_p \end{array} \right\} \tag{3.29}$$

The boundary conditions for the tangential angle ϕ, the radial coordinate r, the membrane height z, and the membrane area A are:

$$\phi(s=0) = 0, \qquad r(s=0) = 0, \qquad z(s=0) = 0, \qquad A(s=0) = 0$$

which defined the origin of the coordinate z to be set at $s = 0$. The bending moment M in Eq. 3.3 satisfies the following boundary condition at $s = 0$:

$$M(s=0) = \frac{B}{2}\left(\lim_{s\to 0}\frac{\sin\phi}{r} + \phi'(0) - 2C(0)\right) = B(\phi'(0) - C(0))$$

given that the L'hopital rule allowed to approximate the limit of $\frac{\sin\phi}{r}$ as $s \to 0$. Additionally, the transverse shear Q at $s = 0$ vanishes. Away from the budding region, the membrane has a mean curvature given by the inverse of the vesicle radius r_c. Both the mean curvature and the spontaneous curvature (defined in Eq. 3.29) at the far boundary s_{max} are given by $1/r_c$, whereby the bending moment M vanishes. Subsequently, from Eq. 3.26 it is found that $M' = 0 = -Q$ at $s = s_{max}$. From the equation for the transverse shear Q (Eq. 3.28), it results that $Q = Q' = 0$ at $s = s_{max}$, and that the boundary condition for the tensile stress is:

$$0 = p - 2\tau(s_{max})r_c \rightarrow \tau(s_{max}) = \frac{pr_c}{2} \tag{3.30}$$

Hence, the far field tension is related to the net pressure difference acting on the membrane. Lastly, at the far boundary s_{max}, the tangential angle ϕ satisfy $\phi(s_{max}) = 0$, if $r_c \gg L$.

3.1.2 Non-dimensional analysis

A usual step of analysis consists in finding the dimensionless form of both the shape equations and the boundary conditions. The forces are scaled with the bud radius L and the bending rigidity B. The lengths in the system are scaled with L. The dimensionless forces and lengths are:

$$\begin{gathered} \bar{s} = \frac{s}{L}, \qquad \bar{r} = \frac{r}{L}, \qquad \bar{z} = \frac{z}{L}, \qquad \bar{A} = \frac{A}{L^2}, \qquad \bar{C} = CL \\ \bar{M} = \frac{ML}{B}, \qquad \bar{Q} = \frac{QL^2}{B}, \qquad \bar{\tau} = \frac{\tau L^2}{B}, \qquad \bar{p} = \frac{pL^3}{B} \end{gathered} \tag{3.31}$$

The spontaneous curvature C in Eq. 3.29 in dimensionless form is:

$$\bar{C} = \left\{ \begin{array}{ll} 1 & \text{if } \bar{A} < \bar{A}_p \\ L/r_c \equiv 1/R \approx 0 & \text{if } \bar{A} \geq \bar{A}_p \end{array} \right\} \tag{3.32}$$

where it was defined that $R \equiv \frac{r_c}{L}$. If the vesicle radius is significantly larger than the bud radius ($r_c \gg L$), then $R \gg 1$. In this limit, the spontaneous curvature outside the budding region $C \to 0$. The dimensionless boundary condition in Eq. 3.30 is given by:

$$\bar{\tau}(s_{max}) = \frac{\bar{p}R}{2} \equiv T_0 \tag{3.33}$$

As consequence, $\bar{p} = \frac{2\bar{\tau}(\bar{s}_{max})}{R} \to 0$ in the limit $R \gg 1$, and the equation for the transverse shear Q (Eq. 3.28) is simplified, given that the dimensionless pressure is small. As result, $\bar{Q}'$ is:

$$\bar{Q}' = -\frac{\bar{\tau}\sin\phi}{\bar{r}} - \bar{\tau}\left(2\bar{M} - \frac{\sin\phi}{\bar{r}} + 2\bar{C}\right) - \frac{\bar{Q}\cos\phi}{\bar{r}} \tag{3.34}$$

However, the far field tension $\bar{\tau}(\bar{s}_{max})$ will generally have a finite value, unless $p = 0$. To ease notation, all bars from the dimensionless quantities and variables from the non-dimensional equations will be omitted. The simplified equation for the transverse shear shown in Eq. 3.34 allows the finding of exact solutions for Q and τ which satisfy the boundary conditions summarized before. These solutions are [8]:

$$\tau = T_0 \cos\phi \tag{3.35}$$

$$Q = -T_0 \sin\phi \tag{3.36}$$

and satisfy identically Eq. 3.27 and Eq. 3.34. As consequence, the governing ordinary differential equations are reduced to:

$$\phi' = 2M - \frac{\sin\phi}{r} + 2C \tag{3.37}$$

$$r' = \cos\phi \tag{3.38}$$

$$z' = \sin\phi \tag{3.39}$$

$$A' = 2\pi r \tag{3.40}$$

$$M' = T_0 \sin\phi \tag{3.41}$$

Noticing that the equations will become singular if the boundary conditions at $s = 0$ are not properly regularized, the boundary conditions are defined with respect to a small value $\epsilon \ll 1$, instead of defining them at $s = 0$. By performing a Taylor expansion of the boundary conditions around $s = 0$, the result is:

$$\phi(s=0) = 0 \to \phi(\epsilon) \approx \epsilon\phi'(0) \equiv \epsilon c_1 \tag{3.42}$$

$$r(s=0) = 0 \to r(\epsilon) \approx \epsilon \tag{3.43}$$

$$z(s=0) = 0 \to z(\epsilon) \approx \frac{\epsilon^2 c_1}{2} \tag{3.44}$$

$$A(s=0) = 0 \to A(\epsilon) \approx \pi\epsilon^2 \tag{3.45}$$

$$M(s=0) = \phi'(0) - C(0) \to M(\epsilon) = c_1 - C \tag{3.46}$$

$$\phi(s = s_{max}) = 0 \tag{3.47}$$

In these regularizations, one free parameter (c_1) was introduced. The system of five ordinary differential equations (ODEs) given in Eqs. 3.37-3.41, the parameter c_1, and the six boundary conditions in Eqs. 3.42-3.47 all close the systems of unknowns and equations.

3.1.3 Boundary conditions in the Euler-Lagrange formalism

The shape equations derived from the EL formalism are given in Eqs. 2.30-2.35. The surface tension λ and the function U are non-dimensionalized as:

$$\bar{\lambda} = \frac{\lambda L^2}{B}, \qquad \bar{U} = \frac{U L^2}{B} \tag{3.48}$$

and the variables s, r, z, A, M and C are written in dimensionless form as in Eq. 3.31. Again, to ease notation, the bars from the dimensionless variables were omitted.

The boundary conditions in the EL formalism are given by Eq. 3.42-3.47. Additionally, a boundary condition for the function U is obtained from the Hamiltonian, Eq. 2.20. As $r(s = 0) = 0$, the condition $\mathcal{H} = 0$ is satisfied automatically. However, there is a non-trivial boundary condition at $s = s_{max}$ related to the surface tension λ. If at $s = s_{max}$ the bending moment and the tangential angle ϕ vanish, the boundary condition for U is written as:

$$\mathcal{H}(s_{max}) = r(s_{max}) \left[-\lambda - M^2 + U \cos\phi + \phi' M \right] = 0 \rightarrow U(s_{max}) = \lambda \tag{3.49}$$

3.1.4 Comparing force balance and Euler-Lagrange formalisms

By comparing the set of differential equations derived from the energy minimization (EL formalism), Eqs. 2.30-2.35 with the ones obtained using the force balance formalism, Eqs. 3.37-3.41, one notices that both formalisms are equivalent only under very particular situations. If the bending moment M is zero everywhere, the equations obtained from the force balance formalism reduces to $U' = U = 0$, which is satisfied only if the surface tension λ vanishes. On the other hand, the bending moment vanishes in Eq. 3.41 if $T_0 = 0$. This means that both formalisms are equivalent only if the far field tension vanishes. In such case, $M = 0$, implying that $H = C$, that is, the membrane shape adopts the form imposed by its spontaneous curvature. Intuitively, one can notice that, given the form of the energy functional in Eq. 2.2, the energy will be minimal if indeed the bending moment vanishes, as long as the surface tension λ vanishes. In general, the inclusion of surface tension in the system will lead to non-vanishing bending moments on the membrane.

In Fig. 3.2, I obtained the membrane shapes corresponding to different values of the far field tension and protein area coverage A_p. This was achieved by solving numerically the shape equations derived from the balance of forces (Eqs. 3.37-3.41 with the boundary conditions in Eqs. 3.42-3.47) and the equations

derived from the energy formalism (Eqs. 2.30-2.35 with the boundary conditions in Eqs. 3.42-3.47 and Eq. 3.49). Both sets of equations contain the spontaneous curvature C given by Eq. 3.32. To facilitate the comparison between the two formalisms, I will assume that the far field tension is the same, which I will designate as T_0. I also select the area coverage $A_p = 8$ and $T_0 \in [0, 0.4]$. Fig. 3.2 illustrates the shapes obtained from the two formalisms discussed previously, which are equivalent whenever $T_0 = 0$. As T_0 increases, the solutions are no longer the same. Furthermore, I observed that a larger value of T_0 prevents the formation of a bud and flattens the membrane.

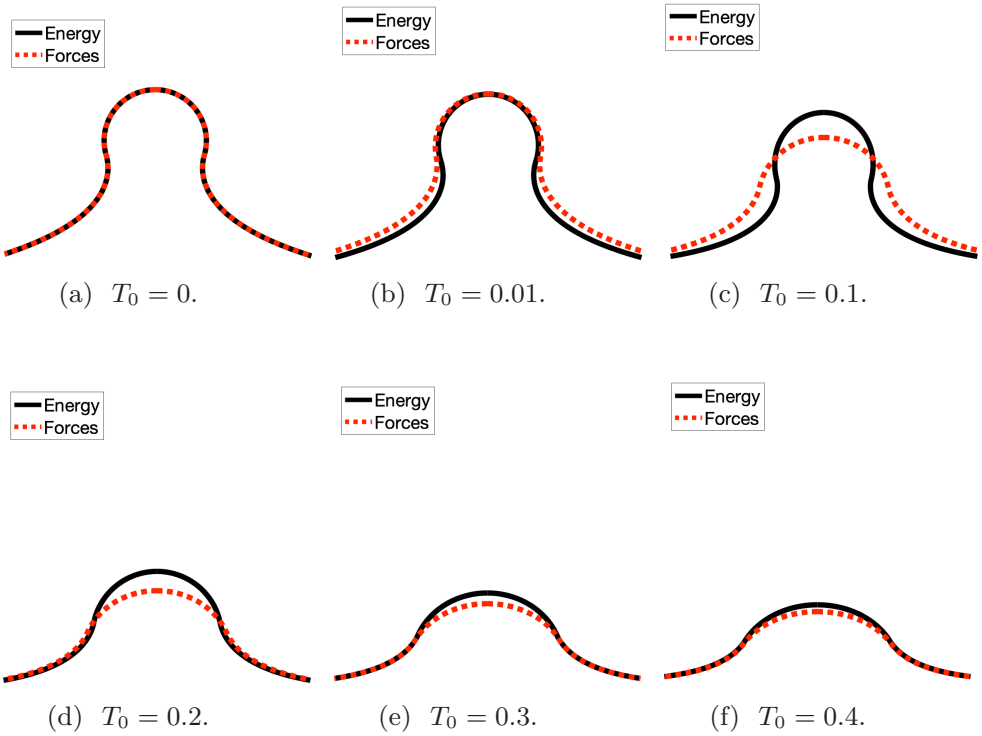

(a) $T_0 = 0.$ (b) $T_0 = 0.01.$ (c) $T_0 = 0.1.$

(d) $T_0 = 0.2.$ (e) $T_0 = 0.3.$ (f) $T_0 = 0.4.$

Figure 3.2: Comparison between the predicted membrane shapes obtained with the force balance (red curves) and EL (black curves) formalisms. When the far field tension vanishes, $T_0 = 0$ (a) the shapes are identical, but as T_0 increases ((b)-(f)), the shapes are no longer the same. A larger T_0 brings about a closer similitude between the shapes, whereas a smaller T_0 makes the extent of their difference more noticeable, as a lower far field tension allows more complex shapes. Additionally, the far field tension prevents membrane budding, which results in a flattened membrane.

The examples above demonstrates that the force balance formalism and the EL formalism are equivalent as long as specific conditions are met. Yet in theoretical studies of biological membranes, energy minimization is the prevalent formalism. The reason for such preference resides in the fact that it acknowledges

that a typical membrane is not only an elastic surface with bending energy: the membrane energy can include many other biophysical effects, such as mixing entropy between its components and protein-protein interactions [14]. Protein flux, which is a fundamental concept behind protein movement, is defined in terms of membrane energy [15, 16]. Furthermore, given that I am also concerned with the movement of curvature-inducing proteins on the membrane (which also plays a role on membrane shape evolution [17]), it is then more convenient to rely on the EL formalism (and not on the force balance formalism). The latter does not allow to define the flux of proteins, given that the membrane energy cannot be readily found purely from the balance of forces. For this reason, I will employ the EL formalism to describe the membranes which the present study examines.

References

[1] Torres-Sánchez, A., Millán, D., and Arroyo, M. "Modelling fluid deformable surfaces with an emphasis on biological interfaces". In: *Journal of Fluid Mechanics* vol. 872 (2019), pp. 218–271.

[2] Lipowsky, R. "The conformation of membranes". In: *Nature* vol. 349, no. 6309 (1991), pp. 475–481.

[3] Powers, T., Huber, G., and Goldstein, R. "Fluid-membrane tethers: Minimal surfaces and elastic boundary layers". In: *Physical Review E* vol. 65, no. 4 (2002), pp. 041901–041912.

[4] Dimova, R., Aranda, S., Bezlyepkina, N., Nikolov, V., Riske, K. A., and Lipowsky, R. "A practical guide to giant vesicles. Probing the membrane nanoregime via optical microscopy". In: *Journal of Physics-Condensed Matter* vol. 18, no. 28 (2006), pp. S1151–S1176.

[5] Preston, S. P., Jensen, O. E., and Richardson, G. "Buckling of an axisymmetric vesicle under compression: The effects of resistance to shear". In: *Quarterly Journal of Mechanics and Applied Mathematics* vol. 61, no. 1 (2008), pp. 1–24.

[6] Knoche, S. and Kierfeld, J. "Buckling of spherical capsules". In: *Physical Review E* vol. 84 (2011), pp. 046608–046621.

[7] Baumgart, T., Das, S., Webb, W., and Jenkins, J. "Membrane elasticity in giant vesicles with fluid phase coexistence". In: *Biophysical Journal* vol. 89, no. 2 (2005), pp. 1067–1080.

[8] Schley, D., Whittaker, R. J., and Neuman, B. W. "Arenavirus budding resulting from viral-protein-associated cell membrane curvature". In: *Journal of the Royal Society Interface* vol. 10, no. 86 (2013), pp. 20130403–20130416.

[9] Jülicher, F. and Lipowsky, R. "Shape transformations of vesicles with intramembrane domains". In: *Physical Review E* vol. 53, no. 3 (1996), pp. 2670–2683.

[10] Pozrikidis, C. “Deformed shapes of axisymmetric capsules enclosed by elastic membranes”. In: *Journal of Engineering Mathematics* vol. 45, no. 2 (2003), pp. 169–182.

[11] Deserno, M. “Fluid lipid membranes: From differential geometry to curvature stresses”. In: *Chemistry and Physics of Lipids* vol. 185 (2015), pp. 11–45.

[12] Evans, E. and Yeung, A. “Hidden dynamics in rapid changes of bilayer shape”. In: *Chemistry and Physics of Lipids* vol. 73, no. 1 (1994), pp. 39–56.

[13] Blyth, M. and Pozrikidis, C. “Solution space of axisymmetric capsules enclosed by elastic membranes”. In: *European Journal of Mechanics A-Solids* vol. 23, no. 5 (2004), pp. 877–892.

[14] Gov, N. S. “Guided by curvature: shaping cells by coupling curved membrane proteins and cytoskeletal forces”. In: *Philosophical Transactions of the Royal Society B: Biological Sciences* vol. 373, no. 1747 (2018), pp. 20170115–20170128.

[15] Arroyo, M., Walani, N., Torres-Sanchez, A., and Kaurin, D. “Onsager’s variational principle in soft matter: introduction and application to the dynamics of adsorption of proteins onto fluid membranes”. In: *Role of Mechanics in the Study of Lipid Bilayers*. Vol. 577. 2018, pp. 287–332.

[16] Chaikin, P. M. and Lubensky, T. C. *Principles of condensed matter physics*. Cambridge University Press, 1995.

[17] Tozzi, C., Walani, N., and Arroyo, M. “Out-of-equilibrium mechanochemistry and self-organization of fluid membranes interacting with curved proteins”. In: *New Journal of Physics* vol. 21, no. 9 (2019), pp. 093004–093026.

Chapter 4

Membrane dynamics

The fluid nature of biological membranes has significant implications: lipids and proteins —key membrane components— are mobile on the membrane surface [1, 2], they reorganize themselves, and migrate from one place of the membrane to another. Proteins and lipids play a crucial role in membrane deformation, which exhibits a gradual and progressive behavior. In clathrin-mediated endocytosis, a fundamental process on the cell membrane, a nascent invagination or pit grows depth-wise and evolves into a well-defined vesicle, joined to the membrane by a narrow neck. In the last stage of the membrane deformation, the vesicle is separated from the donor membrane through a scission process [3, 4]. Fig. 4.1 shows the gradual membrane deformation during clathrin-mediated endocytosis, where the membrane evolves from being a shallow pit to become a fully formed vesicle. Progressive membrane deformation is observed in other processes as well. For example, in ILV formation, the endosome membrane is deformed into budding profiles characterized by a larger invagination depth and narrower necks as the deformation process evolves in time [5].

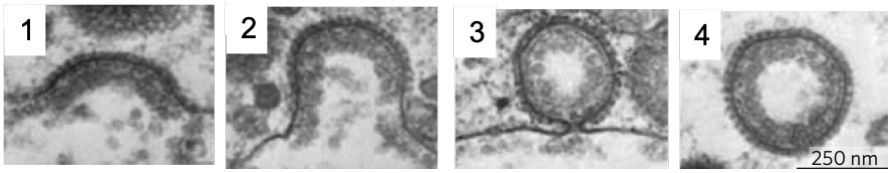

Figure 4.1: Clathrin-coated vesicle budding where yolk protein is being incorporated into vesicles in oocytes. The process involves a series of shapes: (1) shallow pit, (2) U-shape, (3) spherical vesicle attached to the membrane by a narrow neck, and (4) a vesicle completely detached after neck scission. The image is adapted from [6].

Membrane deformation requires the cooperative action of a large number of proteins. Research has been able to identify several protein modules involved in clathrin-mediated endocytosis. The protein modules function and recruitment dynamics into the endocytic site has been also identified [7, 8, 9]. The proteins required for membrane deformation are hardly static: proteins in the cytosol such as clathrin are in constant exchange with the membrane [4]. Such constant exchange between membrane-bound and free clathrin proteins is a fundamental property of clathrin coats assembled on the membrane; this exchange contributes to clathrin structural rearrangement as the membrane deformation evolves [10]. Additionally, the evolution of protein accumulation required for vesicle formation is also correlated with the progression of mem-

brane deformation: the initiation of the pulling forces produced by the actin protein in the endocytic site is correlated with an increase in its density [8]. A cooperative and concerted action between different proteins is also observed in the formation of Intraluminal Vesicles: the ESCRT machinery exhibits a well-defined recruitment dynamics in time, where the accumulation of some of these proteins is slower, and other proteins exhibit faster dynamic recruitment [5].

In an attempt to broaden the theoretical models based on membranes energy minimization (reviewed in Chapter 2), I will discuss some of the details of the theoretical modelling of dynamic shape deformation, *i.e.*, the time evolution of the membrane shape. I take into account the role of two primary factors on the membrane dynamics: the diffusion of proteins on the membrane (owed to its fluid properties), and the recruitment of these proteins onto the membrane through a kinetic model. I will discuss the implications of these mechanisms in membrane budding dynamics.

4.1 Diffusion in membranes

Diffusion is one of the mechanisms which facilitates the migration of solutes and molecules [11, 12]. The transport of proteins and other molecules occurs on cell membranes with complex shapes, and these shapes can be the result of biological processes that require membrane deformation, such as endo/exocytosis [13]. In the early stages of endocytosis, membranes form pits, while at later stages of the process membranes form nearly spherical vesicles joined with their surrounding membrane by a narrow neck [4, 14]. Another example of complex shape formation is exhibited by the communication pathways for material transport between the Golgi apparatus and the endoplasmic reticulum, which requires the formation of tube networks [15]. More complex shapes, such as concatenated buds joined together by narrow bridges or necks (pearled structures) are observed in experiments where amphiphilic molecules anchor themselves onto a lipid bilayer [16]. These pearled structures were also observed as the result of adsorption of nanoparticles into the inner leaflet of Giant Unilamellar Vesicles (GUVs) [17].

Experiments designed to establish the influence of membrane geometry in the sorting of trans-membrane proteins demonstrated that the radii of tubular structures have a strong effect in the enrichment of proteins in the tubes [18]. Subsequently, theoretical studies were developed to account for these experimental findings. For example, the solution of the diffusion equation in tubular membranes employing numerical methods established a dependence between time and protein density on the tube [19]. This dependence was confirmed by experiments [18], where protein density was measured over time through the Fluorescence Recovery After Photobleaching (FRAP) experimental technique. The FRAP technique consists in labeling a population of molecules within a certain region with a fluorescent tag. The molecules then undergo

photobleaching, which allows the observer to follow the fluorescence recovery resulting from the exchange between bleached and unbleached molecules located in the surroundings of that region [20, 21]. The tight correspondence between theoretical and experimental findings pointing to the link between protein density and time, provides a validation of the theoretical foundations of diffusion on surfaces.

The mathematical treatment of diffusion often involves numerical methods for solving the diffusion equation on an arbitrary surface, given that analytical solutions are found for simple geometrical surfaces only, such as the surface corresponding to spheres and cylinders [22]. In contrast, numerical solutions do account for arbitrary surfaces. For example, numerical studies of diffusion were performed on surfaces mimicking dendritic spines, which range from elongated to mushroom-like protrusions [23], with the random walk simulation technique. This technique was also used to simulate diffusion in the mitochondrial inner membrane, which possess numerous invaginations or cristae of different shapes [24]. Additionally, random walk simulations were performed on periodical, nodal surfaces [22].

The numerical solutions of the diffusion equation on such arbitrary shapes determine how protein density evolves over time, and enable the exploration of possible relations between membrane shape and protein density.

4.1.1 Diffusion on axially symmetric surfaces

The axially symmetric surfaces I will consider are structures that constitute a more complex object of study than the surface of a sphere or cylinder. The surface of axially symmetric membranes where protein diffusion takes place can be parametrized by the arc-length, as described in Fig. 2.2. The diffusion equation satisfied by the protein density $\tilde{\sigma}$ is [25]:

$$\frac{\partial \tilde{\sigma}}{\partial t} - \frac{D}{r}(r\tilde{\sigma}')' = 0 \tag{4.1}$$

where D is the diffusion coefficient (considered here as a constant), which measures the rate of molecule movement in the absence of active transport or flow [26]. The dimensionless protein density $\tilde{\sigma}$ is a continuous field that depends on time and on the arc-length, $\tilde{\sigma} = \tilde{\sigma}(s,t)$. The radial coordinate r, the membrane height z, and the area A satisfy Eqs. 2.5, 2.6 and 2.7, respectively. The diffusion equation, Eq. 4.1, on a flat surface is written as $\frac{\partial \tilde{\sigma}}{\partial t} - D\tilde{\sigma}'' - \frac{D}{s}\tilde{\sigma}' = 0$ in polar coordinates, while on a curved surface is contains an additional term $D\tilde{\sigma}'\left(\frac{1}{s} - \frac{\cos\phi}{r}\right)$. As consequence, diffusion dynamics on a flat surface is clearly different from diffusion on a flat surface.

Diffusion is a process by which an initial protein density is distributed over the available membrane surface. The protein density tends to acquire an

homogeneous profile as time proceeds, as observed in Fig. 4.2. There, a pearled structure with two buds is depicted with its corresponding protein density at different points in time. The initial density spreads over the entire membrane and, as consequence, the density in the pearled structure decreases over time.

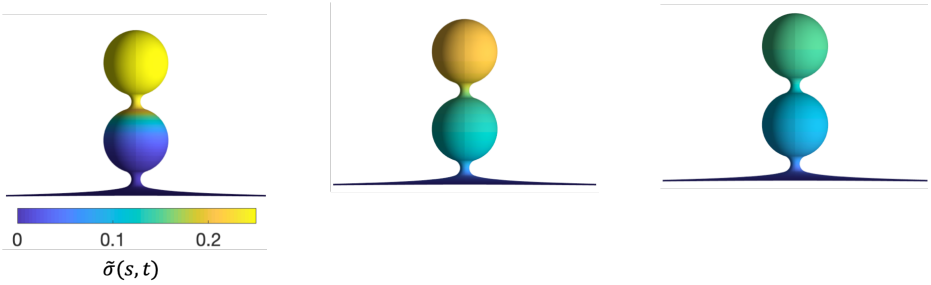

(a) $\tilde{\sigma}(s, t = 0)$. (b) $\tilde{\sigma}(s, t = 150dt)$. (c) $\tilde{\sigma}(s, t = 250dt)$.

Figure 4.2: Time evolution of protein density on a pearled structure with two buds, *via* diffusive dynamics. (a) At $t = 0$, the proteins are mostly concentrated in the upper bud. As time proceeds ((b) and (c)) the density becomes smaller and more uniform over the pearled structure because proteins leave the budded region. The color bar represents the protein density. The dimensionless time interval (employed to solve the diffusion equation numerically) is $dt = 5 \times 10^{-3}$.

By considering diffusion of protein density on fixed, generic shapes (mimicking the ones observed in biological membranes, such as tubes, domes, and pearled structures with different number of concatenated buds), it was possible to find a quadratic relation between the membrane curvature and the exit time of proteins from tubes [27]. In some cases, these shapes can be reproduced experimentally, as it is the case with tubular structures [18]. The FRAP technique is a powerful tool to measure the half-time, that is to say, the time required to recover half of the initial fluorescence of the proteins after photobleaching in a certain membrane region [21]. These measurements provide insights on protein mobility and have corroborated the recovery time predicted theoretically by means of the diffusion equation on tubular membranes [19]. Once again, such fine congruity between experiments and theory encourages the further use of mathematical models for diffusion of molecules in membranes with diverse shapes. In consequence, the mathematical models for diffusion can be applied to the biological membrane, even if one takes into account that the biological membrane is not a static, fixed surface.

Additionally, experiments have shown that the shape transformation of a single-component phospholipid vesicle is correlated with diffusion of adsorbed polymers on the membrane. These polymers induce a spontaneous curvature whose primary determinant is the polymers' density on the membrane [16]. Experiments have also revealed that a typical membrane remodeling process goes on as proteins are locally recruited on the membrane surface, inducing

curvature [5, 7, 28]. Indeed, experiments revealed that membrane deformation is driven by a gradual recruitment and accumulation of membrane-bound proteins. This suggests that, in order to derive a more complete theoretical description of the evolution of the membrane shape, it becomes necessary to include the recruitment of curvature-inducing proteins into the theoretical model.

Experimental findings on diffusion-driven shape transformation [16] inspired a modification in the membrane energy defined in Eq. 2.2. The modification consisted in the inclusion of a spontaneous curvature which depends on the protein/polymer density, and which evolves over time according to the diffusion equation (Eq. 4.1). This modified membrane energy served as basis for the theoretical study of the influence of macromolecules diffusion on the shape of closed vesicles [29]. Another theoretical model for diffusion-mediated shape transformation of an initially flat membrane containing trans-membrane proteins established the dynamics of the protein density from the *protein flux*, defined in terms of the chemical potential of the proteins [30].

4.2 Protein recruitment and diffusion

The starting point to build a theoretical model for membrane shape transformation induced by protein diffusion and kinetic recruitment is to define the membrane energy. This step is accomplished by defining an energy having a spontaneous curvature that depends on the membrane-bound density of proteins $\tilde{\sigma}$. The second step towards the model necessitates that the membrane energy includes the *mixing entropy* of the proteins. This term (mixing entropy) was not included in the Eq. 2.2 (defined in Chapter 2). The rationale and motivation for including an entropic contribution in the energy derives from the fact that entropic free energy minimization *is* the physical driving mechanism of diffusion [31]. Yet, other theoretical models for protein diffusion did not include mixing entropy in the energy [29, 30]. In its most general mathematical form, the mixing entropy considers that the binding sites on the membrane are bounded [32]. For simplicity's sake, it can be rather assumed that the binding sites are unbound, in which case the mixing entropy of the proteins is that of the ideal gases [31, 33]. Taking into account these considerations, the membrane energy can be formulated as:

$$W = \int \left[B(H - C_0\tilde{\sigma})^2 + \lambda + \frac{k_b T}{a_p}\tilde{\sigma}(\log\tilde{\sigma} - 1) \right] dA \tag{4.2}$$

The first term is the Helfrich energy [30, 34]. The induced spontaneous curvature $C = C_0\tilde{\sigma}$ depends linearly on the protein density [30, 35], where C_0 is the spontaneous curvature induced by one protein and $\tilde{\sigma}$ is the non-dimensional protein density on the membrane. The proteins are mobile on the membrane, hence the density $\tilde{\sigma}$ varies in time and space. The second term in Eq. 4.2 is the surface tension. The third term is the mixing entropy of the proteins, where k_b is the Boltzmann constant, T is the temperature, and a_p is the area occupied by

one protein.

The membrane geometry is described according to the arc-length parametrization described in Fig. 2.2. Additionally, the entropic term in the energy described in Eq. 4.2 does not depend on the membrane curvature —it only depends on the protein density $\tilde{\sigma}$. Hence, the shape equations associated to the total energy in Eq. 4.2 are the same as those which were derived from the Euler-Lagrange formalism, Eqs. 2.31-2.35. This implies that the membrane is at mechanical equilibrium at all times, supported by the fast mechanical relaxation dynamics of the membrane if compared to the larger time scale associated to protein diffusion [36].

In order to couple the diffusive dynamics of proteins with their kinetic recruitment, the first defined term is the protein flux, which is given in terms of the chemical potential derived from the energy functional in Eq. 4.2, $J = -\Lambda\tilde{\sigma}\nabla\left(\frac{\delta W}{\delta\tilde{\sigma}}\right)$, [31, 37]. Λ is the protein mobility and $\frac{\delta W}{\delta\tilde{\sigma}}$ is the functional derivative of the energy functional W with respect to the protein density. As the energy does not depend on protein gradients, the functional derivative is $\frac{\delta W}{\delta\tilde{\sigma}} = \frac{\partial W}{\partial\tilde{\sigma}}$ [38]. Hence, the non-vanishing component of the flux J is given by:

$$J = -\Lambda\left(\frac{k_bT}{a_p}\tilde{\sigma}' + 2C_0\tilde{\sigma}Q\right) \equiv -D\tilde{\sigma}' - 2\Lambda C_0\tilde{\sigma}Q \tag{4.3}$$

$\mathcal{E}_{diff}$ is the diffusive contribution of the evolution equation of the protein density $\tilde{\sigma}$, and is given by:

$$\mathcal{E}_{diff} = \frac{\partial\tilde{\sigma}}{\partial t} + \frac{1}{r}(rJ)' = \frac{\partial\tilde{\sigma}}{\partial t} - \frac{1}{r}(r(D\tilde{\sigma}' + 2\Lambda\tilde{\sigma}C_0Q))' \tag{4.4}$$

The recruitment dynamics is included in the model *via* a combination of a source (protein attachment to the membrane) and a sink (detachment from the membrane). The source term has the following property: protein attachment is triggered when the membrane mean curvature exceeds a threshold value H_0. This assumption is suggested by experimental observations, which found that certain proteins are enriched in curved regions of the membrane [39, 40]; some of these proteins can induce curvature [41]. Theoretical studies based on molecular dynamics simulations [42] and Monte Carlo simulations [43] have shown that protein adsorption on the membrane can have a step-like behaviour with respect to the membrane mean curvature. These key characteristics are included in a phenomenological recruitment model, where the on-rate is multiplied by a Heaviside function $\Theta(H - H_0)$. In contrast, protein detachment is curvature-independent. The mathematical form of $\mathcal{E}_{source}$, which includes the recruitment and detachment term, is:

$$\mathcal{E}_{source} = c_p k_{on}\Theta(H - H_0) - k_{off}\tilde{\sigma} \tag{4.5}$$

where c_p is the constant bulk density of proteins, k_{on} measures the recruitment rate of proteins, Θ is the Heaviside function, H_0 is the curvature above which

the recruitment is triggered, and k_{off} is the turnover rate.

The equation governing the time evolution of $\tilde{\sigma}$, $\mathcal{E}_{diff} = \mathcal{E}_{source}$, in non-dimensional form is written as:

$$\frac{\partial \tilde{\sigma}}{\partial \bar{t}} - \frac{1}{r}\left(r\left(\tilde{\sigma}' + 2\bar{\Lambda}\bar{C}_0\tilde{\sigma}\bar{Q}\right)\right)' = K_1\Theta(\bar{H} - \bar{H}_0) - K_2\tilde{\sigma} \tag{4.6}$$

where, in order to obtain the dimensionless variables, I have used Eq. 3.31. The model reveals a characteristic length $L = 1/(C_0\bar{\sigma}_{eq})$, *i.e*, the length scale given by the spontaneous curvature C_0 induced by one protein and the equilibrium density of proteins, $\bar{\sigma}_{eq} = K_1/K_2$, obtained when all gradients vanish in Eq. 4.6. The ratio was fixed to $K_1/K_2 = 1/5$, to keep the number of parameters minimal. Time has been scaled with $\tau_D = L^2/D$. Additionally, the dimensionless numbers $\bar{\Lambda}, K_1$ and K_2 are defined as $\bar{\Lambda} = \frac{B}{k_bT}\frac{a_p}{L^2}$, $K_1 = c_p k_{on} L^2/D$ and $K_2 = k_{off}L^2/D$. To ease notation, all the bars from Eq. 4.6 are omitted.

The exploration of the phase space spanned by the parameters K_1 and H_0 made possible the finding of diverse shapes, ranging from single vesicles to pearled structures [44]. The diffuso-kinetic protein dynamics induces a progressive shape transformation, as shown in Fig. 4.3. A membrane with a small deformation induced by a low protein density evolves into a pearled structure, which has a high protein density in its most curved region. The time intervals are defined with respect to the time at which the neck width equals the membrane thickness, which is called t_{cut}.

It is important to emphasize that, for the present study, I focused on the implications of the phenomenological recruitment model described above. This model offers an intuitive formulation for the process of recruitment that experimental research also observes: recruitment depends on membrane curvature. A different formalism, the Onsager's variational principle, lead to the coupling between diffusion and recruitment kinetics, based on the competition between dissipation and energy release rate [31]. When applied to a curvature-induced recruitment of proteins that also diffuse on the membrane, the Onsager formalism lead to yet another recruitment model where the off-rate was also multiplied by the step function. But given that them main predictions of both recruitment models proved to be very similar (additional simulations not presented here), I focused on the implications of the phenomenological model due to its already-mentioned intuitive formulation. Additionally, researchers have proposed other theoretical models for the recruitment of proteins. For example, one study implemented a spatio-temporal coordination between the recruitment of different proteins without the effect of protein diffusion, thereby proposing a more complex dependence between protein recruitment and membrane curvature [8].

The simplified continuous model of the membrane I have described is a minimal model for protein recruitment induced by membrane curvature, coupled with protein diffusive dynamics. As a phenomenon which takes place on

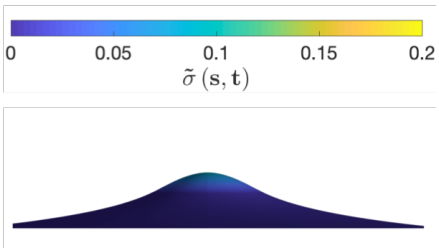

(a) $t = 0.2t_{cut} = 0.02$.

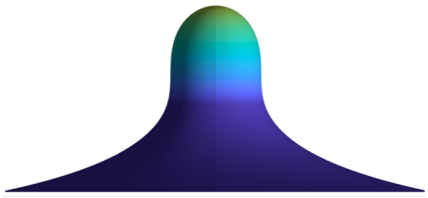

(b) $t = 0.5t_{cut} = 0.05$.

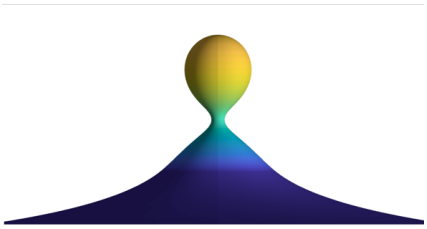

(c) $t = 0.8t_{cut} = 0.08$

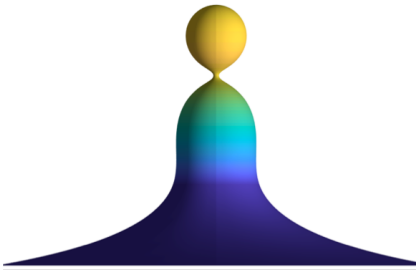

(d) $t = t_{cut} = 0.1$.

Figure 4.3: Shape evolution of the membrane, driven by the diffuso-kinetic dynamics of curvature-inducing proteins, for $K_1 = 4.5$ and $H_0 = 0.0015$. (a) At an early stage, the membrane has a pit shape with low protein density. As time evolves, the membrane turns to a (b) U-shape, (c) an Ω-shape, and (d) a pearled structure, with high protein density in its most curved region. The time points are defined respect to t_{cut}, at which the membrane neck width equals the typical membrane thickness. The scale bar represent the protein density on the membrane.

membrane cells, recruitment is often overlooked in theoretical models. Yet this study's contribution does not intend to offer an exhaustive explanation of the detailed binding/recruitment mechanism. A number of biophysical processes can contribute to membrane dynamics, which were purposefully left aside. I however hope that protein recruitment will be taken into account on further theoretical descriptions of dynamic membrane remodeling.

References

[1] Cicuta, P., Keller, S. L., and Veatch, S. L. "Diffusion of liquid domains in lipid bilayer membranes". In: *The Journal of Physical Chemistry B* vol. 111, no. 13 (2007), pp. 3328–3331.

[2] Kenworthy, A., Nichols, B., Remmert, C., Hendrix, G., Kumar, M., Zimmerberg, J., and Lippincott-Schwartz, J. “Dynamics of putative raft-associated proteins at the cell surface”. In: *Journal of Cell Biology* vol. 165, no. 5 (2004), pp. 735–746.

[3] McMahon, H. and Gallop, J. “Membrane curvature and mechanisms of dynamic cell membrane remodelling”. In: *Nature* vol. 438, no. 7068 (2005), pp. 590–596.

[4] Avinoam, O., Schorb, M., Beese, C. J., Briggs, J. A. G., and Kaksonen, M. “Endocytic sites mature by continuous bending and remodeling of the clathrin coat”. In: *Science* vol. 348, no. 6241 (2015), pp. 1369–1372.

[5] Wenzel, E. M., Schultz, S. W., Schink, K. O., Pedersen, N. M., Nahse, V., Carlson, A., Brech, A., Stenmark, H., and Raiborg, C. “Concerted ESCRT and clathrin recruitment waves define the timing and morphology of intraluminal vesicle formation”. In: *Nature Communications* vol. 9, no. 1 (2018), pp. 2932–2950.

[6] Gallop, J. L. and McMahon, H. T. “BAR domains and membrane curvature: bringing your curves to the BAR”. In: *Biochemical Society symposium*, no. 72 (2005), pp. 223–231.

[7] Kaksonen, M., Toret, C. P., and Drubin, D. G. “A modular design for the clathrin- and actin-Mediated endocytosis machinery”. In: *Cell* vol. 123, no. 2 (2005), pp. 305–320.

[8] Liu, J., Sun, Y., Drubin, D. G., and Oster, G. F. “The mechanochemistry of endocytosis”. In: *PLOS Biology* vol. 7, no. 9 (2009), pp. 1–16.

[9] Liu, J., Sun, Y., Oster, G. F., and Drubin, D. G. “Mechanochemical crosstalk during endocytic vesicle formation”. In: *Current Opinion in Cell Biology* vol. 22, no. 1 (2010), pp. 36–43.

[10] Wu, X., Zhao, X., Baylor, L., Kaushal, S., Eisenberg, E., and Greene, L. “Clathrin exchange during clathrin-mediated endocytosis”. In: *Journal of Cell Biology* vol. 155, no. 2 (2001), pp. 291–300.

[11] Dix, J. A. and Verkman, A. S. “Crowding effects on diffusion in solutions and cells”. In: *Annual Review of Biophysics* vol. 37, no. 1 (2008), pp. 247–263.

[12] Crank, J. *The mathematics of diffusion*. 2nd. Edition. Clarendon Press, 1975.

[13] Wu, L.-G., Hamid, E., Shin, W., and Chiang, H.-C. “Exocytosis and endocytosis: modes, functions and coupling mechanisms”. In: *Annual Review of Physiology* vol. 76, no. 1 (2014), pp. 301–331.

[14] Lampe, M., Vassilopoulos, S., and Merrifield, C. “Clathrin coated pits, plaques and adhesion”. In: *Journal of Structural Biology* vol. 196, no. 1 (2016), pp. 48–56.

[15] Waterman-Storer, C. and Salmon, E. “Endoplasmic reticulum membrane tubules are distributed by microtubules in living cells using three distinct mechanisms”. In: *Current Biology* vol. 8, no. 14 (1998), pp. 798–806.

[16] Tsafrir, I., Caspi, Y., Guedeau-Boudeville, M.-A., Arzi, T., and Stavans, J. “Budding and tubulation in highly oblate vesicles by anchored amphiphilic molecules”. In: *Physical Review Letters* vol. 91, no. 13 (2003), pp. 138102–138106.

[17] Yu, Y. and Granick, S. “Pearling of lipid vesicles induced by nanoparticles”. In: *Journal of the American Chemical Society* vol. 131, no. 40 (2009), pp. 14158–14159.

[18] Aimon, S., Callan-Jones, A., Berthaud, A., Pinot, M., Toombes, G. E. S., and Bassereau, P. “Membrane shape modulates transmembrane protein distribution”. In: *Developmental Cell* vol. 28, no. 2 (2014), pp. 212–218.

[19] Klaus, C. J. S., Raghunathan, K., DiBenedetto, E., and Kenworthy, A. K. “Analysis of diffusion in curved surfaces and its application to tubular membranes”. In: *Molecular Biology of the Cell* vol. 27, no. 24 (2016), pp. 3937–3946.

[20] Yguerabide, J., Schmidt, J., and Yguerabide, E. “Lateral mobility in membranes as detected by fluorescence recovery after photobleaching”. In: *Biophysical Journal* vol. 40, no. 1 (1982), pp. 69–75.

[21] Kang, M., Day, C. A., Kenworthy, A. K., and DiBenedetto, E. “Simplified equation to extract diffusion coefficients from confocal FRAP data”. In: *Traffic* vol. 13, no. 12 (2012), pp. 1589–1600.

[22] Hołyst, R., Plewczyski, D., Aksimentiev, A., and Burdzy, K. “Diffusion on curved, periodic surfaces”. In: *Physical Review E* vol. 60, no. 1 (1999), pp. 302–307.

[23] Kusters, R., Kapitein, L. C., Hoogenraad, C. C., and Storm, C. “Shape-induced asymmetric diffusion in dendritic spines allows efficient synaptic AMPA receptor trapping”. In: *Biophysical Journal* vol. 105, no. 12 (2013), pp. 2743–2750.

[24] Sukhorukov, V. M. and Bereiter-Hahn, J. “Anomalous diffusion induced by cristae geometry in the inner mitochondrial membrane”. In: *PLOS One* vol. 4, no. 2 (2009), pp. 1–14.

[25] Faraudo, J. “Diffusion equation on curved surfaces. I. Theory and application to biological membranes”. In: *Journal of Chemical Physics* vol. 116, no. 13 (2002), pp. 5831–5841.

[26] Lippincott-Schwartz, J., Snapp, E., and Kenworthy, A. “Studying protein dynamics in living cells”. In: *Nature Reviews Molecular Cell Biology* vol. 2, no. 6 (2001), pp. 444–456.

[27] Rojas, R., Liese, S., and Carlson, A. “Protein diffusion on membrane domes, tubes and pearling structures”. In: *bioRxiv* (2020).

[28] Rosendale, M. and Perrais, D. “Imaging in focus: Imaging the dynamics of endocytosis”. In: *International Journal of Biochemistry & Cell Biology* vol. 93 (2017), pp. 41–45.

[29] Góźdź, W. T. “Diffusion of macromolecules on lipid vesicles”. In: *Langmuir* vol. 24, no. 21 (2008), pp. 12458–12468.

[30] Agrawal, A. and Steigmann, D. J. “A model for surface diffusion of trans-membrane proteins on lipid bilayers”. In: *Zeitschrift fur Angewandte Mathematik und Physik* vol. 62, no. 3 (2011), pp. 549–563.

[31] Arroyo, M., Walani, N., Torres-Sanchez, A., and Kaurin, D. “Onsager’s variational principle in soft matter: introduction and application to the dynamics of adsorption of proteins onto fluid membranes”. In: *Role of Mechanics in the Study of Lipid Bilayers*. Vol. 577. 2018, pp. 287–332.

[32] Flory, P. J. “Thermodynamics of high polymer solutions”. In: *The Journal of Chemical Physics* vol. 10, no. 1 (1942), pp. 51–61.

[33] Peletier, M. A. *Variational modelling: Energies, gradient flows, and large deviations*. 2014. arXiv: 1402.1990 [math-ph].

[34] Helfrich, W. “Elastic properties of lipid bilayers: Theory and possible experiments”. In: *Zeitschrift für Naturforschung C* vol. 28, no. 11-12 (1973), pp. 693–703.

[35] Gov, N. S. “Guided by curvature: shaping cells by coupling curved membrane proteins and cytoskeletal forces”. In: *Philosophical Transactions of the Royal Society B: Biological Sciences* vol. 373, no. 1747 (2018), pp. 20170115–20170128.

[36] Tozzi, C., Walani, N., and Arroyo, M. “Out-of-equilibrium mechanochemistry and self-organization of fluid membranes interacting with curved proteins”. In: *New Journal of Physics* vol. 21, no. 9 (2019), pp. 093004–093026.

[37] Chaikin, P. M. and Lubensky, T. C. *Principles of condensed matter physics*. Cambridge University Press, 1995.

[38] George B. Arfken and Hans J. Weber and Frank E. Harris. *Mathematical methods for physicists*. Seventh Edition. Academic Press, 2013.

[39] Masuda, T., Hirose, H., Baba, K., Walrant, A., Sagan, S., Inagaki, N., Fujimoto, T., and Futaki, S. “An artificial amphiphilic peptide promotes endocytic uptake by inducing membrane curvature”. In: *Bioconjugate Chemistry* vol. 31, no. 6 (2020), pp. 1611–1615.

[40] Larsen, J. B., Jensen, M. B., Bhatia, V. K., Pedersen, S. L., Bjornholm, T., Iversen, L., Uline, M. J., Szleifer, I., Jensen, K. J., Hatzakis, N. S., and Stamou, D. “Membrane curvature enables N-Ras lipid anchor sorting to liquid-ordered membrane phases”. In: *Nature Chemical Biology* vol. 11, no. 3 (2015), pp. 192–U176.

[41] Zhao, W., Hanson, L., Lou, H.-Y., Akamatsu, M., Chowdary, P. D., Santoro, F., Marks, J. R., Grassart, A., Drubin, D. G., Cui, Y., and Cui, B. "Nanoscale manipulation of membrane curvature for probing endocytosis in live cells". In: *Nature Nanotechnology* vol. 12, no. 8 (2017), pp. 750–756.

[42] Florentsen, C., Kamp-Sonne, A., Moreno-Pescador, G., Pezeshkian, W., Zanjani, A. A. H., Khandelia, H., Nylandsted, J., and Bendix, P. M. "Annexin A4 trimers are recruited by high membrane curvatures in giant plasma membrane vesicles". In: *accepted in Soft Matter* (2020).

[43] Krishnan, T. V. S., Das, S. L., and Kumar, P. B. S. "Transition from curvature sensing to generation in a vesicle driven by protein binding strength and membrane tension". In: *Soft Matter* vol. 15, no. 9 (2019), pp. 2071–2080.

[44] Rojas, R., Liese, S., Alimohamadi, H., Rangamani, P., and Carlson, A. "Diffuso-kinetic membrane budding dynamics". In: *Soft Matter* (2020).

Chapter 5

Summary of papers and future outlook

5.1 Summary of papers

Paper I: Diffusion on membrane domes, tubes and pearling structures.

The fluid nature of biological membranes allows the migration of their components (lipid molecules, trans-membrane and membrane-bound proteins) from one place to another on the membrane. Biological membranes often exhibit complex shapes, such as concatenated buds joined by narrow necks, and tubes.

In this work, we solved numerically the diffusion equation on several complex surfaces with axial symmetry (dome, pearled structures with different number of buds, and tubes), where we prescribed an initial protein density. In order to find a relation between the membrane curvature and the exit time of proteins away from these budded structures, we defined the average mean and Gaussian curvature (the integral of the mean and Gaussian curvature over the budded region) and $\tilde{t}$, which is the time required for the total protein content in the budded region to reach half of its initial value. Our results suggest that the exit time $\tilde{t}$ is not clearly correlated to the average Gaussian curvature $\tilde{K}$ of the budded region of the membrane (Fig. 5.1a), but is shows a clear quadratic dependence with respect to the average mean curvature $\tilde{H}$ for the tubes (Fig. 5.1). The relations between the exit time and the membrane curvature can help to estimate relevant time scales associated to diffusion of proteins and molecules in complex surfaces.

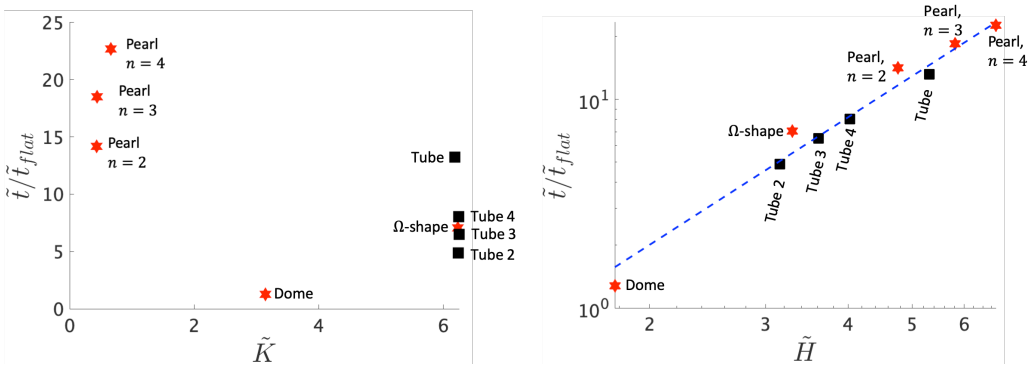

(a) (b)

Figure 5.1: (a) The ratio $\tilde{t}/\tilde{t}_{flat}$ is depicted as a function of the averaged Gaussian curvature $\tilde{K} = \int_0^1 K da$. There is not a clear dependence between $\tilde{t}$ and $\tilde{K}$ across all the shapes considered. (b) The ratio $\tilde{t}/\tilde{t}_{flat}$ is presented as a function of the average mean curvature $\tilde{H}$ for each of the shapes considered, in logarithmic scale. The blue dashed line represents a fit $\tilde{t} \sim H^m$, where $m = 2.03$ is the average of the slopes of the logarithmic relations between $\tilde{H}$ and $\tilde{t}$ for the tubes and the pearled structures, indicating that the exit time follows approximately a quadratic relation with respect to $\tilde{H}$.

Paper II: Diffuso-kinetic membrane budding dynamics.

Many biological processes, such as endocytosis, exocytosis and virus budding, require gradual membrane shape transformation. Experiments have shown that membrane shape transformation involves the concerted recruitment of proteins, some of which are able to induce curvature. Additionally, these proteins are able to diffuse on the membrane, due to the membrane's fluid structure.

In this work, we focused on protein diffusion and recruitment. The protein density evolves in time following a diffuso-kinetic equation, describing the protein distribution driven by diffusion and a phenomenological recruitment model where proteins attach to curved regions of the membrane surface. The proteins induce a spontaneous curvature on the membrane, which is proportional to the protein density. The membrane shape is the solution of the shape equations obtained from the energy minimization formalism. The budding structures obtained range from single vesicles joined to the surrounding membrane by a narrow neck to pearled structures. We defined the scission time t_{cut} as the time at which the neck width is equal to the membrane thickness. This theoretical model revealed that t_{cut} is related to the kinetic recruitment parameter K_1, defined as the ratio between the diffusive and the recruitment time scale. The relation between t_{cut} and K_1 is shown in Fig. 5.2a and has the form of a scaling law, $t_{cut} \sim K_1^{-2/3}$. The scaling law is found for all the values of H_0, which measures the membrane curvature above which proteins are recruited. Additionally, the values of K_1

and H_0 had an influence on the final membrane shape, which can be a pearled structure for small H_0 (protein recruitment occurs in a larger, less curved region) or a single vesicle for larger H_0 (protein recruitment occurs in a smaller, more curved region). Additionally, by rescaling the membrane shapes at $t = t_{cut}$ with the length given by the average protein density on the bud region and the spontaneous curvature induced by one protein C_0, self-similar shapes were obtained, as shown in Fig. 5.2b.

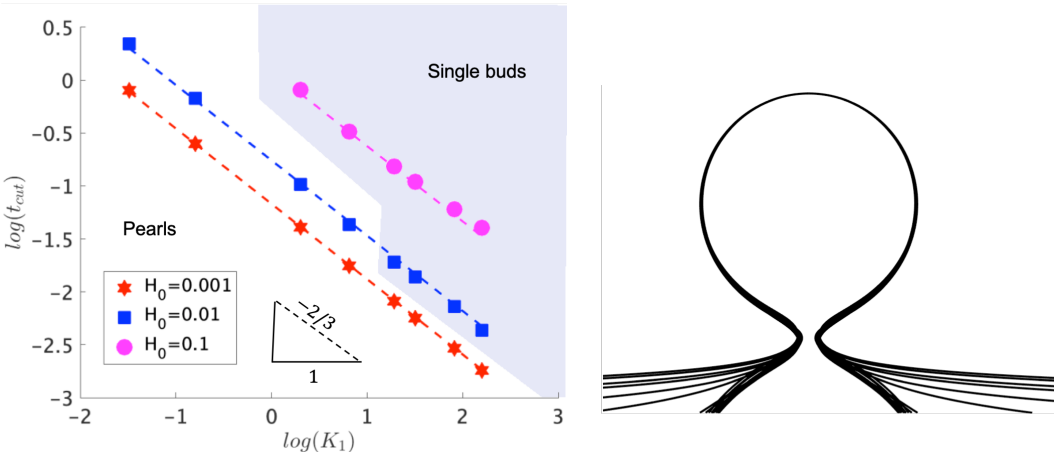

(a) t_{cut} as a function of K_1 for in logarithmic axis.

(b) Rescaled shapes for $K_1 \in [0.2 - 9]$ and $H_0 \in [0.0015 - 0.15]$.

Figure 5.2: (a) Scission time t_{cut} as a function of K_1 for different values of H_0 in logarithmic axis. The scission time follows a power law $t_{cut} \sim K_1^{\alpha}$, with $\alpha \approx -2/3$ for all values of H_0. The blue and white regions represent the part of the phase space where single buds or pearls are formed, respectively. When H_0 is small, the formation of pearls is observed across all the values of K_1. When $H_0 = 0.015$, the formation of pearls is observed only for small values of K_1 and as K_1 increases pearls are no longer observed. When $H_0 = 0.15$ pearl formation is prevented and only single buds are formed. (b) Rescaled shapes obtained for all the values of K_1 and H_0. The model predicts self-similar shapes, where both the vesicle and neck regions coincide.

Paper III: Protein crowding mediates membrane remodeling in upstream ESCRT-induced formation of Intraluminal vesicles

The formation in Intraluminal Vesicles (ILVs) from the endosome membrane is a fundamental requirement in the lysosomal degradation pathway, where the Endosomal Sorting Complexes Required for Transport (ESCRTs) sequester cargo and deform the membrane. The ESCRT proteins form a large patch on the endosome membrane, but do not become part of the ILV. As consequence, the mechanism involved in the formation of ILV is different from other internalization pathways, such as clathrin-mediated endocytosis, where diverse proteins deform the membrane *via* an scaffold mechanism, creating a protein-coated vesicle.

Theoretical models for the formation of uncoated vesicles emphasized the importance of the Gaussian bending energy, an energy contribution that is often omitted, as long as the Gaussian rigidity is constant. However, in this work, a protein density-dependent Gaussian rigidity was proposed, and also included an effective steric repulsion due to protein crowding in the membrane energy. This theoretical model predicted that no energy consumption was needed to form ILVs, and also predicted the membrane shapes observed in the experiments, as shown in Fig. 5.3. The theoretical shapes are such that they minimize the total membrane energy. Additionally, the theoretical model predicts that the proteins have a high density in the neck region joining the vesicle with the surrounding membrane.

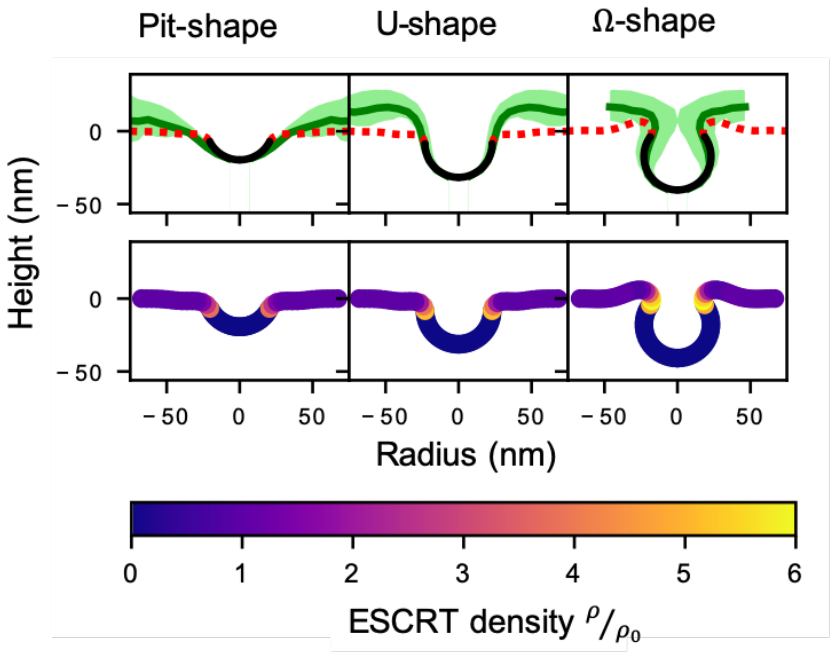

Figure 5.3: *Top row*: Comparison between the experimentally measured endosome shapes and the shapes obtained with the theoretical model, by minimizing the membrane energy. The shapes are grouped into three categories: Pit, U-shape and Ω-shape. The average shapes obtained from the experiments are shown as solid green lines. The shaded green regions are the standard deviations from the experimental data. The theoretical shapes of the uncoated vesicles are shown as solid black lines. The red dashed lines represent the protein-coated membrane region. *Bottom row*: the ESCRT density ρ/ρ_0, where ρ_0 is the equilibrium density of ESCRT on a flat membrane. The protein density is higher in the neck regions.

5.2 Future outlook

Biological membranes are highly complex structures with distinctive physical properties such as fluidity, elasticity, and viscosity. In consequence, future comprehensive mathematical models of a membrane should account for these properties as well.

This thesis might be a starting point for further analysis and model refinement. One of the possible extensions of the models proposed in this study would be to include the effect of the dissipative dynamics induced by the in-plane shear experienced by the lipid molecules constituting the membrane. Additionally, future research could also take into account energy terms as a result of protein-protein interactions. To facilitate a minimal formulation, the mixing entropy was that of an ideal gas, valid in the limit of low protein densities. More complex studies could also engage with a more general mixing entropy, accounted by bounded (rather than unbounded) binding sites.

This study proposed that the driving mechanism for protein recruitment was membrane curvature, through a simple switch-like model. Experiments have suggested that certain proteins are enriched in curved regions and, consequently, a curvature-driven recruitment became a plausible assumption. Although I incorporated an element overlooked is some models for membrane dynamics, a complete understanding of the mechanisms driving protein recruitment is still lacking. Deeper knowledge of these molecular mechanisms would help to model protein recruitment more accurately, as there is no universal way to describe protein kinetics driven by curvature.

A description of the membrane as a continuous surface is applicable as long as membrane deformations are significantly smaller than the membrane width. This study encountered membrane dynamics leading to the formation of constricted neck regions, yet additional terms and physical effects should be included in further research. Consequently, another possible extension of the models proposed in this dissertation is to include such mechanical effects arising in the onset of membrane scission.

In a model where recruitment of proteins from the bulk is one of the main driving mechanisms of membrane dynamics, it could be relevant to consider the effect the of bulk fluid flow induced by the membrane deformation. This flow in the vicinity of the budding region might contribute to the redistribution of bulk proteins, and influence the protein distribution on the membrane. The model presented in this study assumed that the bulk density of proteins was constant, but protein bulk dynamics could also be included in future studies, together with the coupling between the membrane interface deformation and bulk flow.

This minimal model of protein recruitment could serve as a starting point towards more complex integral modelling of biological membranes involving,

among other processes, protein recruitment and diffusive dynamics. The progressive inclusion of additional physical effects into membrane models has the potential of guiding future perspectives of membrane dynamics deformation in the years to come.

Papers

Paper I

Diffusion on membrane domes, tubes and pearling structures

I

Rojas Molina Rossana, Liese Susanne, Carlson Andreas

Published in *bioRxiv*, currently in review. 2020, DOI: 10.1101/2020.10.08.331629.

Paper II

Diffuso-kinetic membrane budding dynamics

Rojas Molina Rossana, Liese Susanne, Alimohamadi Haleh, Rangamani Padmini, Carlson Andreas

Accepted in *Soft Matter* (2020) DOI: 10.1039/D0SM01028F.

II

Soft Matter

Accepted Manuscript

This article can be cited before page numbers have been issued, to do this please use: R. Rojas Molina, S. Liese, H. Alimohamadi, P. Rangamani and A. Carlson, *Soft Matter*, 2020, DOI: 10.1039/D0SM01028F.

ROYAL SOCIETY OF CHEMISTRY

rsc.li/soft-matter-journal

View Article Online
DOI: 10.1039/D0SM01028F

Soft Matter

ARTICLE TYPE

Cite this: DOI: 00.0000/xxxxxxxxxx

Diffuso-kinetic membrane budding dynamics

Rossana Rojas Molina,[a†] Susanne Liese,[a] Haleh Alimohamadi,[b] Padmini Rangamani,[b] and Andreas Carlson [a*]

Received Date
Accepted Date

DOI: 00.0000/xxxxxxxxxx

A wide range of proteins are known to create shape transformations of biological membranes, where the remodelling is a coupling between the energetic costs from deforming the membrane, the recruitment of proteins that induce a local spontaneous curvature C_0 and the diffusion of proteins along the membrane. We propose a minimal mathematical model that accounts for these processes to describe the diffuso-kinetic dynamics of membrane budding processes. By deploying numerical simulations we map out the membrane shapes, the time for vesicle formation and the vesicle size as a function of the dimensionless kinetic recruitment parameter K_1 and the proteins sensitivity to mean curvature. We derive a time for scission that follows a power law $\sim K_1^{-2/3}$, a consequence of the interplay between the spreading of proteins by diffusion and the kinetic-limited increase of the protein density on the membrane. We also find a scaling law for the vesicle size $\sim 1/(\bar{\sigma}_{av}C_0)$, with $\bar{\sigma}_{av}$ the average protein density in the vesicle, which is confirmed in the numerical simulations. Rescaling all the membrane profiles at the time of vesicle formation highlights that the membrane adopts a self-similar shape.

1 Introduction

In a wide range of cellular processes, membrane shape remodeling due to the association and dissociation of proteins plays a fundamental role, *e.g.*, endo- and exocytosis[1], virus assembly[2] and the formation of intracellular compartments[3]. The presence of proteins on the membrane leads to changes in biomechanical properties such as bending rigidity[4], diffusion coefficient of proteins[5,6] and membrane curvature. The molecular machinery associated with curvature-inducing processes is often complex[7,8] and while some involve active motor proteins[9–11], there is a multitude of proteins that are able to passively induce membrane shape transformations[8,12]. The biophysical mechanisms that induce membrane curvature include the insertion of amphipathic helixes into the bilayer[13], producing an area difference between the inner and outer membrane leaflet through the binding of large proteins to one membrane side[14,15] or protein crowding[16,17]. Thus, the net effect of any asymmetry between the leaflets of the bilayer due to anchoring inclusions or steric pressure can be represented by the spontaneous curvature[18].

Reconstituted and synthetic vesicles are essential model systems that help to reveal the fundamental biophysical mechanisms by which proteins are able to induce membrane shape transformations[16–21]. For instance, experiments have demonstrated that the formation of tubular structures is directly correlated with the protein density on the membrane[16] and that protein crowding correlates with the formation and abscission of vesicles[17]. Moreover, it has been shown experimentally that the local membrane curvature and the resulting membrane shape is coupled to the concentration of curvature-inducing macromolecules. For example, tubular structures that are formed by anchoring polymers, shrink as diffusion reduces the local polymer density[21].

A typical membrane remodeling process starts from a flat surface and develops into a deformed membrane with the shape of a bud, vesicle or tubule[22,23] as proteins are locally recruited to the membrane surface and induce a spontaneous curvature[24,25]. Membrane deformation is thus driven by a gradual recruitment and accumulation of membrane-associated proteins and changes in physical properties over time[8], suggesting that in order to derive a theoretical description of the dynamic evolution of a membrane shape we must include the recruitment of curvature-inducing proteins.

Over the years, numerous theoretical studies have been dedicated to describe a wide range of mechanisms that play a vital role in various cellular processes, *i.e.* diffusion of transmembrane proteins[26], protein crowding[27–29] and spontaneous curvature induced by macromolecules such as polymers and proteins[18,21,30–32]. More complex theoretical models also include the viscous dissipation generated as the proteins move on the lipid bilayer[33,34], as well as non-local hydrodynamics where the entire

[a] *Mechanics Division, Department of Mathematics, University of Oslo, 0316 Oslo, Norway.*
[b] *Department of Mechanical and Aerospace Engineering, University of California, San Diego, CA 92093, USA.*
[*] *Email: acarlson@math.uio.no*

† Electronic Supplementary Material (ESM) available: See DOI: 10.1039/cXsm00000x/

View Article Online
DOI: 10.1039/D0SM01028F

flow field is resolved[35–37].

Since the thickness of a lipid bilayer is much smaller than the typical length scale of membrane deformations, it is common to treat biomembranes as elastic thin sheets[38–41]. Similarly, the size of an individual protein is at least an order of magnitude smaller than the extension of a membrane bud or vesicle, which justifies the proteins as a continuous field. Previous theoretical studies have investigated various aspects of membrane deformation generated by concentration-dependent spontaneous curvature, considering either a static protein distribution on the membrane[42–45] or including diffusion dynamics[26,30,34]. In addition, a theoretical framework based on the Onsager variational principles has been developed, where the dynamics are given by the balance between dissipative and driving forces[33,46,47]. This framework gives a compact mathematical description of adsorption and desorption of proteins from the bulk and its diffusive dynamic on a fixed membrane shape.

Compared to the diffusive protein dynamics on membranes, far less is known about the dynamic interplay between diffusion, local protein kinetics and membrane shape changes, where a theoretical model considering all three processes has not yet been explicitly established. In this study, we develop such model with a focus on finding temporal relationships between the kinetics of protein recruitment and the timescales of bud formation.

To study the spatio-temporal budding process of a membrane, we develop a minimal mathematical model for the diffuso-kinetics of membrane associated proteins. We treat the concentration of proteins as a continuous field following a diffusion equation with an adsorption term, describing the protein recruitment from a reservoir *i.e.* the cytosol or the extracellular space, and a detachment term representing the protein turnover. Additionally, our model incorporates that the protein concentration induces an effective local spontaneous curvature on the membrane, which drives the membrane shape evolution. Finally, to characterize the dynamic of membrane deformation over time, we spanned the phase space by varying the kinetic parameters and the protein sensitivity for the detection of membrane curvature to uncover scaling relationships between time for scission and kinetic recruitment parameters of proteins onto the membrane.

2 Theoretical model

2.1 Energy functional

To study how proteins that are bound to biological membranes influences the membrane shape evolution, we begin by defining the membrane energy per unit area W, which includes the bending energy, surface tension and entropic effects due to membrane-protein interactions given by[41,46,48]:

$$W = B(H - C_0\bar{\sigma})^2 + \lambda + \frac{k_b T}{a_p}\bar{\sigma}(\log\bar{\sigma} - 1) \tag{1}$$

The first term is the Helfrich energy[26,38], where H is the mean curvature and B is the bending rigidity. The Helfrich model is suitable to describe cases where the radii of membrane curvatures are much larger than the thickness of the bilayer[40], allowing us to treat the lipid bilayer as a thin elastic shell. Here, we assume that the induced spontaneous curvature $C = C_0\bar{\sigma}$ due to membrane-protein interactions depends linearly on the protein density[26,48,49], where C_0 is a proportionality constant associated to the spontaneous curvature induced by one protein and $\bar{\sigma}$ is the protein density on the membrane scaled by the saturation density[49]. The proteins are mobile on the membrane, hence the density $\bar{\sigma}$ varies in time and space.

The second term in Eq. 1 is the surface tension. We describe the membrane as an infinite surface, where the far-field acts as a lipid reservoir. In this case, a constant surface tension λ acts long the entire membrane. The third term accounts for entropic effects. When the protein density in the membrane surface is small and the available binding sites for the proteins are not bounded, the entropy term is well approximated by the mixing entropy of an ideal gas[46,50,51]. This model is simpler than the general Langmuir absorption model[52,53], where k_b is the Boltzmann constant, T is the temperature and a_p is the area occupied by one protein.

Additional terms may be included in W (Eq. 1), such as interaction terms between proteins $\sim\bar{\sigma}^2$ and the energy cost arising from density gradients $\sim(\nabla\bar{\sigma})^2$ [48,54]. Both terms scale with the magnitude of the protein-protein interaction. Since the non-specific interaction between proteins is weak compared to the bending and entropic energy, the interaction and gradient terms can be neglected. In the Supplementary Material (SM, section 8), we estimate the contribution to the energy functional by the interaction between proteins and the density gradients, to illustrate that the mixing entropy is the leading contribution to the energy, thus simplifying its description. To keep the mathematical model minimal, we assume that both the Gaussian bending modulus and the bending rigidity B are constant, *i.e*, they do not depend on the local protein density, which also implies that the Gaussian bending energy is a constant, since we do not consider topological changes such as membrane scission[30,55].

2.2 Membrane shape equations

The axially symmetric membrane is described in the arc-length parametrization with the radial and vertical components $r = r(s)$ and $z = z(s)$ and the tangent angle $\phi = \phi(s)$, where s is the arc-length. A schematic representation of the system and the coordinates are shown in Fig. 1.

The mean curvature H in the arc-length parametrization is given by[56]:

$$H = \frac{1}{2}\left(\frac{\sin\phi}{r} + \phi'\right) \tag{2}$$

The operator $()' \equiv \frac{d}{ds}()$ represents the derivative with respect to the arc-length s.

The arc-length parametrization allows to express the coordinates r, z and the area of the membrane, A, in the following way:

$$r' = \cos\phi \tag{3}$$

$$z' = \sin\phi \tag{4}$$

$$A' = 2\pi r \tag{5}$$

The shape of the membrane for a given protein distribution $\bar{\sigma}$ is

View Article Online
DOI: 10.1039/D0SM01028F

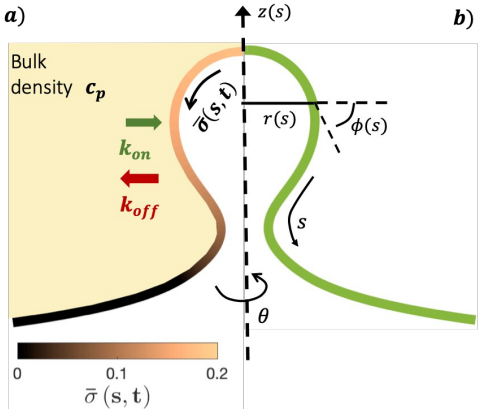

Fig. 1 a) The proteins in the bulk have a constant volume density c_p, represented by a uniform light yellow color. The proteins attach to the membrane at a rate k_{on} and detach from it at a rate k_{off}. The attached proteins on the membrane can diffuse on the surface of the membrane and also induce a spontaneous curvature proportional to the protein concentration $\bar{\sigma}(s,t)$ represented as a color gradient, which evolves in time according to a diffusion process coupled with kinetic recruitment and detachment leading to an inhomogeneous protein distribution on the membrane. b) A description of the membrane surface parametrization in axisymmetric coordinates. Here s is the arc-length measured along the membrane, $r(s)$ is the radial coordinate, $\phi(s)$ is the angle that the curved membrane forms with respect to the horizontal r-axis and z is the height of the membrane. The angle θ is the rotation around the symmetry axis.

such that it must minimize the total energy, given by the integral of Eq. 1 over the total area of the membrane, $W_{tot} = 2\pi \int W r ds$.

To derive the energy minimizing shape, we define $\mathscr{L}$

$$\mathscr{L} = r\left[\lambda + \frac{k_b T}{a_p}\bar{\sigma}(\log\bar{\sigma} - 1)\right] + rB\left[\frac{1}{2}\left(\frac{\sin\phi}{r} + \phi'\right) - C_0\bar{\sigma}\right]^2 + \Gamma(r' - \cos\phi) \quad (6)$$

which is equivalent to a Lagrange functional in analytical mechanics[57]. A Lagrange multiplier, Γ, is introduced in Eq. 6 to satisfy Eq. 3. We assume that far away from the budding region the membrane is not deformed and is modeled as a flat sheet of infinite size. In this case there is no constraint in the total area of the membrane, A, nor on the volume V enclosed by it.

The bending moment of the membrane, M, is given by[58]:

$$M = B(H - C) = B\left[\frac{1}{2}\left(\frac{\sin\phi}{r} + \phi'\right) - C_0\bar{\sigma}\right] \quad (7)$$

From eq. 7 we obtain the differential equation for the angle ϕ as:

$$\phi' = \frac{2M}{B} - \frac{\sin\phi}{r} + 2C_0\bar{\sigma} \quad (8)$$

Finally, following the Euler-Lagrange formalism, we obtain (see the Supplementary Material (SM) for details):

$$M' = U\sin\phi \equiv -Q \quad (9)$$

$$U' = \frac{M}{r}\left(\frac{2M}{B} + 2C_0\bar{\sigma} - \frac{2\sin\phi}{r}\right) \quad (10)$$

The boundary conditions implemented to solve the set of 6 equations given by Eq. 3-5 and Eq. 8-10), which enforce a transition into a flat membrane at the outer boundary, are described in detail in the SM.

2.3 Spatio-temporal dynamics of the protein concentration

At cell membranes proteins are recruited and disassociated in kinetic binding and unbinding processes[7,8,59] while they diffuse along the membrane[5,6]. Hence, the dynamics of the protein density $\bar{\sigma}(s,t)$ is described by a diffuso-kinetic equation with two contributions: the diffusive part, $\mathscr{E}_{diff}$, and the recruitment/turnover part, $\mathscr{E}_{source}$. The two terms have to fulfill $\mathscr{E}_{diff} = \mathscr{E}_{source}$, implying that the flux of proteins along the membrane arises from a protein source/sink. The general form of $\mathscr{E}_{diff}$ is written as:

$$\mathscr{E}_{diff} = \frac{\partial\bar{\sigma}}{\partial t} + \frac{1}{r}(rJ)' \quad (11)$$

where the first term is the time derivative of $\bar{\sigma}$ and the second term is the surface divergence of the protein flux J in axially symmetric coordinates.

In general, the protein flux is given in terms of the chemical potential derived from the energy functional in Eq. 1, $J = -\Lambda\bar{\sigma}\nabla\left(\frac{\delta W}{\delta\bar{\sigma}}\right)$,[46,60]. Λ is the protein mobility and $\frac{\delta W}{\delta\bar{\sigma}}$ is the functional derivative of the energy functional W with respect to the protein density. In the absence of gradient terms in the energy, the functional derivative reduces to $\frac{\delta W}{\delta\bar{\sigma}} = \frac{\partial W}{\partial\bar{\sigma}}$ [61]. Hence, the non-vanishing component of the flux, J, is given by:

$$J = -\Lambda\left(\frac{k_b T}{a_p}\bar{\sigma}' + 2C_0\bar{\sigma}Q\right) \equiv -D\bar{\sigma}' - 2\Lambda C_0\bar{\sigma}Q \quad (12)$$

where $D \equiv \Lambda\frac{k_b T}{a_p}$ is the diffusion coefficient and Q is defined in Eq. 9. Eq. 12 recovers a diffusive flux on a flat surface, in the limit, $C_0 \approx 0$, which implies that the membrane is flat in this limit, as the proteins have no influence in the membrane shape. However, in the general case the flux has a non-negligible contribution arising from the curvature of the membrane, via the function Q. Finally, the explicit form of $\mathscr{E}_{diff}$ is:

$$\mathscr{E}_{diff} = \frac{\partial\bar{\sigma}}{\partial t} - \frac{1}{r}(r(D\bar{\sigma}' + 2\Lambda\bar{\sigma}C_0Q))' \quad (13)$$

To model the protein recruitment, we make four assumptions: First, the recruitment is modeled following the linear adsorption-diffusion model[46], in which it is assumed that the protein density is small, and that the available binding sites for the proteins are not bounded, as in the more general Langmuir absorption model. Second, we assume that the protein density in the bulk is constant. Third, protein recruitment is triggered when the membrane curvature exceeds a threshold value H_0. This assumption is inspired by experimental observations, which found that certain proteins are enriched in curved regions of the membrane[62,63] with the ability to also induce a curvature[64]. Theoretical studies based on molecular dynamics simulations[65] and Monte Carlo simulations[66] have shown that various biophysical mechanisms can cause curvature sensing, where proteins adsorb to a membrane in a step-like manner with respect to the membrane cur-

View Article Online
DOI: 10.1039/D0SM01028F

vature. We incorporate this key characteristics in a phenomenological curvature sensing model by multiplying the on-rate by a Heaviside function $\Theta(H-H_0)$ and show in the SM (section 7) that regularizing the Heaviside function does not affect the prediction as long as the jump is sufficiently steep. Lastly, we consider the diffuso-kinetic dynamics i.e. out equilibrium, which is further illustrated below by our numerical simulations. We acknowledge that a more complex relation between the recruitment kinetics and the membrane curvature might be proposed[67], which requires a more elaborated theoretical treatment also satisfying detailed balance at equilibrium. To the best of our knowledge, a universal model for curvature-sensitive recruitment dynamics is still a topical question in the field.

In light of these assumptions, the mathematical form of $\mathscr{E}_{source}$ can be written as:

$$\mathscr{E}_{source} = c_p k_{on}\Theta(H-H_0) - k_{off}\bar{\sigma} \tag{14}$$

where c_p is the constant bulk density of proteins, k_{on} measures the recruitment rate of proteins, Θ is the Heaviside function, H_0 is the curvature above which the recruitment is triggered and k_{off} is the turnover rate. Biologically relevant values for the parameters that appear in the mathematical model are listed in Table 1.

Table 1 The parameters present in the evolution equation of the protein concentration σ.

Parameter	Typical value
Membrane thickness h	5nm[68]
Membrane viscosity η_m	$(10^{-9}-10^{-7})$Ns/m[33,69,70]
Cytosol viscosity η_c	$(1-4)\times10^{-2}$Ns/m^2[71,72]
Spontaneous curvature of one protein C_0	$(0.075-0.2)$nm^{-1}[73,74]
Area of one protein a_p	$(16-70)$nm^2[17,19,74]
Bulk concentration of proteins c_p	$(0.1-50)\mu$M[17,59]
Dissociation constant K_D	$(0.1-5)\mu$M[59]
Diffusion coefficient D	$(0.01-1)\mu$m^2/s[75,76]
Bending rigidity B	$(20-40)$k$_B$T[43,74]
Surface tension λ	$(0.003-0.3)\times10^{-3}$N/m[74,77]

To understand which process sets the time scale of the membrane dynamics, we perform a scaling analysis. The rate of change of the bending energy can be dissipated by membrane viscosity, *i.e*, $\frac{\partial E_b}{\partial t} \sim \eta_m(\nabla_s u)^2$, where $E_b = B(H-C_0\bar{\sigma})^2$ is the bending energy, η_m is the membrane viscosity and u is the membrane velocity. The bending energy scales as $E_b \sim B/L^2$, $u \sim L/\tau_v$, where τ_v is the viscous time scale and $\nabla \sim 1/L$, giving $B/\tau_v \sim \eta_m L^2/\tau_v^2$. We can then write $\tau_v \sim \eta_m L^2/B$. On the other hand, the diffusive time scale is given by $\tau_D \sim L^2/D$, where the diffusion coefficient D is related to the membrane viscosity η_m through the Saffman-Delbruck theory[78], where $D \sim \frac{k_BT}{4\pi\eta_m}\ln\left(\frac{\eta_c}{r_p\eta_c}\right)$. Here, η_c is the viscosity of the cytosol and $r_p \sim 5$nm is the typical radius of one protein. With the typical values of the membrane and cytosol viscosity in Table 1, the diffusion coefficient $D \sim \frac{6k_BT}{4\pi\eta_m}$. The ratio between these to time scales becomes $\frac{\tau_D}{\tau_v} \sim \frac{2B\pi}{3k_BT}$. With $B \sim 20k_BT$, we obtain that $\frac{\tau_D}{\tau_v} \sim 13\pi$, that is, the diffusive time scale can be more than one order of magnitude larger than the viscous time scale, supporting our assumption that the mechanical relaxation of the membrane is fast compared to its diffusive transport of proteins.

The equation governing the time evolution of $\bar{\sigma}$, $\mathscr{E}_{diff} = \mathscr{E}_{source}$ in non-dimensional form is written as (see the SM for details):

$$\frac{\partial\bar{\sigma}}{\partial\bar{t}} - \frac{1}{\bar{r}}\left(\bar{r}\left(\bar{\sigma}' + 2\bar{\Lambda}\bar{C}_0\bar{\sigma}\bar{Q}\right)\right)' = K_1\Theta(\bar{H}-\bar{H}_0) - K_2\bar{\sigma} \tag{15}$$

where we have scaled all lengths with $L = 1/(C_0\bar{\sigma}_{eq})$, *i.e*, the length scale given by the spontaneous curvature C_0 induced by the recruited proteins and the equilibrium density of proteins, $\bar{\sigma}_{eq} = K_1/K_2$, obtained as all gradients vanish in Eq. 15. Time has been scaled with τ_D. The energy has been scaled with the bending rigidity B. Introducing the scaling into the governing equations gives us the scaled variables, $\bar{Q} = \frac{QL^2}{B}$, $\bar{s} = \frac{s}{L}$, $\bar{r} = \frac{r}{L}$, $\bar{H} = HL$, $\bar{t} = \frac{tD}{L^2}$ and the dimensionless numbers, $\bar{\Lambda} = \frac{B}{k_bT}\frac{a_p}{L^2}$, $\bar{C}_0 = C_0L$ and $\bar{H}_0 = H_0L$, $K_1 = c_pk_{on}L^2/D$, $K_2 = k_{off}L^2/D$. To ease the notation, we drop all the bars from Eq. 15 and for simplicity we keep $()' \equiv \frac{d}{d\bar{s}}$.

The non-dimensional number $K_1 = c_pk_{on}L^2/D$ is the ratio between the diffusive time scale and the kinetic recruitment time scale and $K_2 = k_{off}L^2/D$ is the ratio between the diffusive time scale and the protein turnover time scale. $\Lambda = \frac{B}{k_bT}\frac{a_p}{L^2}$ is the ratio of the bending energy and the thermal energy. In addition, we set the surface tension λ to be zero, but the influence of $\lambda > 0$ is further discussed in the SM. The ratio between K_1 and K_2 can be written in terms of the dissociation constant K_D as $\frac{K_1}{K_2} = \frac{c_p}{K_D}$. Since we assume the protein density is small as compared to the saturation density, K_1 and K_2 must be chosen in such a way that the equilibrium density of proteins in the membrane is small. To reduce the number of parameters influencing the dynamics we set $K_1/K_2 = 1/5$ in all the numerical simulations, which for $\bar{\sigma}_t = \bar{\sigma}' = 0 = K_1 - K_2\bar{\sigma}$ gives $\bar{\sigma} = 1/5 < 1$, consistent with a system where the recruitment is slower that the turnover of proteins. We have chosen $B = 20k_BT$, $C_0 = 0.1$nm^{-1}, and $a_p = 27$nm^2, which gives $C_0 = 5$ and $\Lambda = 0.22$ in Eq. 15 and point out that Eq. 8 and 10 are the only shape equations that have a non-dimensional parameter in them, which is C_0. The rest of the shape equations, Eq. 3-5 and 9 are parameter-free. The non-dimensional numbers K_1 and H_0 form the basis of a parameter space that will allow us to determine the dependence of the membrane shape respect to the coupling between diffusion and kinetics.

As we span the phase space of $H_0 \in [0.0015-0.15]$ and $K_1 \in [0.2-9]$ we observe formation of thin membrane necks with respect to the rotational axis $r = 0$. Since the mathematical model is no longer valid if the neck width is comparable in size with the membrane thickness, we consider the numerical results up to the point when the neck width is equal to the membrane thickness h, that in non-dimensional form has the value $h = 0.1$ and corresponds to the membrane thickness h reported on Table 1. We define the scission time as t_{cut}. The range of H_0 corresponds to a radius of curvature of about 300 nm to 30 μm, covering the typical size range of cells ($\approx 6\mu$m), membrane-bound vesicles (≈ 500nm) and giant unilaminar vesicles (up to 200μm)[22,79].

3 Results:

We begin by illustrating the dynamic formation of two characteristic membrane shapes obtained using numerical simulations based on Eqs. 3-5, 8-10 and Eq. 15 for $H_0 = 0.0015$ (Fig. 2) and

View Article Online
DOI: 10.1039/D0SM01028F

$H_0 = 0.15$ (Fig. 3). Initially the membrane is flat with a small initial protein density near the axis of symmetry $r = 0$, which we model as a Gaussian profile with small amplitude and width $\bar{\sigma}(s,t=0) = 0.1e^{-(s/0.3)^2}$. The initial amplitude of the protein density on the membrane plays a minor role in the budding dynamics, as the scission time t_{cut} is insensitive to the initial amplitude of the Gaussian profile (see SM, section 6). This initial protein density induces a change in the spontaneous curvature and generates a small membrane deformation. The proteins start to be recruited and redistributed on the membrane, inducing a deformation that goes through a set of different shapes: Bump (Figs. 2a and 3a), U-shape (Figs. 2b and 3b), Ω- shape (Figs. 2c and 3c) and at the final stage a pearl, when $H_0 = 0.0015$ (Fig. 2d) or a single bud, when $H_0 = 0.15$ (Fig. 3d). These structures are also found for non-vanishing, but small surface tension, as shown in the SM (Section 9). From Figs. 2 and 3 we see that the parameter H_0, i.e. the proteins sensitivity to mean curvature, plays an important role in determining the final shapes of the membrane. If H_0 is small, pearled structures can be observed, whereas if H_0 is larger ($H_0 \gg 0.0015$), the formation of smaller, single buds is favored. A low value of H_0 ($H_0 = 0.0015$) leads to recruitment to a large area of the membrane and it adopts a pearl-like structure. In contrast, when H_0 is larger ($H_0 = 0.15$), an almost spherically shaped membrane emerges from the initially flat membrane, caused by the recruitment of proteins to a smaller area of the membrane, as compared to a smaller H_0. There are also some other noteworthy features we would like to highlight: Despite the fact that K_1 is identical for the two simulations, the proteins are distributed over a different area. Besides the obvious differences in shape, it appears that also H_0 will determine the continuation of the process for $t > t_{cut}$. If a vesicle is shed from the membrane at $t = t_{cut}$ in Fig. 2d the rest of the membrane will still have a significant portion covered by curvature inducing proteins and it appears that another vesicle will form from the Ω shape. When H_0 is larger a single vesicle forms (Fig. 3d), which contain almost all the proteins. In this case, after scission the membrane may return to its undeformed state stalling the dynamics.

To see the details of the protein distribution on the membrane in Figs. 2 and 3, we plot in Fig. 4 the protein density $\bar{\sigma}$ as a function of the membrane area A. In order to clearly illustrate the influence of H_0 on the protein distribution over the membrane we extract $\bar{\sigma}$ at the same snapshots in time as in Figs. 2 and 3 using the time for membrane scission t_{cut} as a point of reference: $t = 0.2t_{cut}, 0.5t_{cut}, 0.8t_{cut}$ and t_{cut} where $[H_0 = 0.0015,\ t_{cut} = 0.1]$ and $[H_0 = 0.15,\ t_{cut} = 0.38]$. A general feature is that the protein density is distributed over a larger area on the membrane when H_0 is small and it has a smaller gradient as we move from the axis of symmetry to the undeformed membrane. In contrast, when H_0 is larger the proteins are limited to a much smaller region of the membrane with a steep decay in $\bar{\sigma}$. By inspecting Figs. 4a-4d we can notice the growth rate of the area covered by proteins is much faster when H_0 is small. To see this, we can roughly estimate the rate of change of covered area ΔA in the time interval $\Delta t = (0.5 - 0.2)t_{cut}$, which for $H_0 = 0.0015$ is $\Delta A/\Delta t \sim 600$

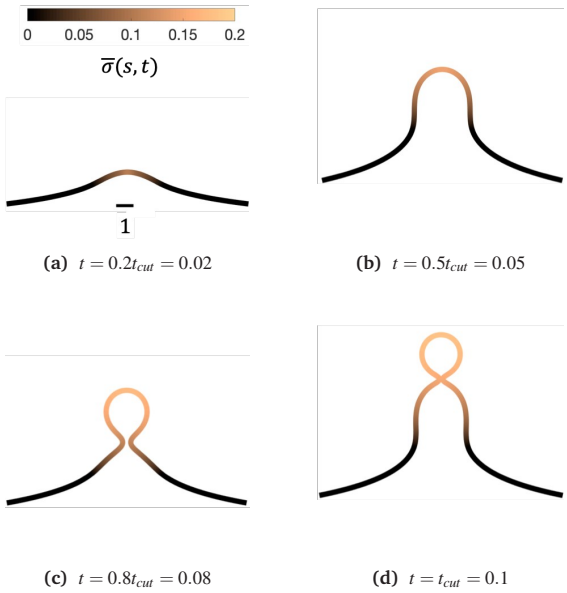

(a) $t = 0.2t_{cut} = 0.02$ **(b)** $t = 0.5t_{cut} = 0.05$

(c) $t = 0.8t_{cut} = 0.08$ **(d)** $t = t_{cut} = 0.1$

Fig. 2 Characteristic membrane shapes at four different snapshots in time when the dimensionless rate coefficient is $K_1 = 4.5$ and the threshold for protein recruitment is $H_0 = 0.0015$. As we march forward in time the membrane deforms from a nearly flat membrane (not shown) into a pit-shape (a), an U-shape (b), an Ω-shape (c) and finally into a pearl-like membrane shape (d). The color bar represents the protein density $\bar{\sigma}(s,t)$. In Figs. 2c and 2d the protein density is almost uniform on the vesicle at the top of the budding structure and decays gradually along the rest of the deformed membrane. The scale bar is the dimensionless unit length of the system, equivalent to $L = 50$nm.

contrasting the same calculation $\Delta A/\Delta t \sim 50$ when $H_0 = 0.15$. During the last stages of the membrane deformation (Figs. 4b - 4d) the area covered by proteins increases much slower once an Ω-shape is formed (see Figs. 2b-2d and Figs. 3b-3d) and at the last stage (Figs. 4c and 4d) this area barely increases and just an increment on the protein density is observed on the membrane for both values of H_0. Thus, the geometry of the membrane may also play a role in the dynamic growth process. H_0 appears to be a critical parameter, because it determines bot only the overall size of the budding structures, but also determine in part how proteins are distributed on the membrane. Fig. 4d also shows that as a single vesicle forms ($H_0 = 0.15$) the recruited proteins leaves the membrane and stalls the dynamics, contrary to when proteins are almost insensitive to the mean curvature and covers a much larger membrane area ($H_0 = 0.0015$).

To further characterize qualitatively the membrane dynamics we extract the height of the membrane, z_{max}, along the symmetry axis $r = 0$ for $K_1 = 4.5$ when $H_0 = 0.0015$ (Fig. 5a) and $H_0 = 0.15$ (Fig. 5b). Initially, we can observe that z_{max} increases as the membrane bud grows in size, but as the membrane starts to form an Ω-shape its height starts to decrease as the neck constricts. The features of z_{max} also allows us to identify the pit-, U- and Ω-shape of the membrane already shown in Figs. 2 and 3. When

View Article Online
DOI: 10.1039/D0SM01028F

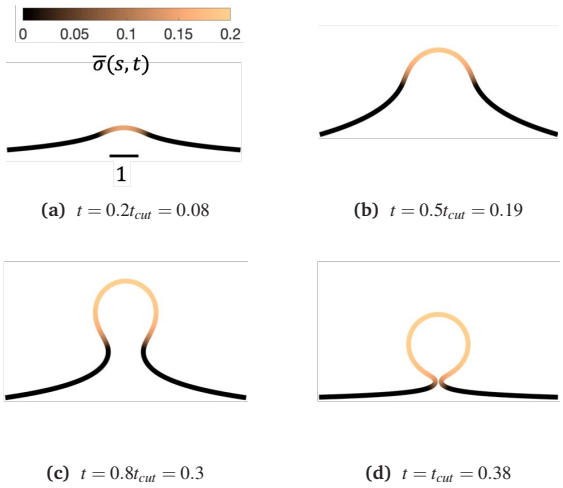

(a) $t = 0.2t_{cut} = 0.08$ **(b)** $t = 0.5t_{cut} = 0.19$

(c) $t = 0.8t_{cut} = 0.3$ **(d)** $t = t_{cut} = 0.38$

Fig. 3 Characteristic membrane shapes at four different snapshots in time when the dimensionless rate coefficient is $K_1 = 4.5$ and the threshold for protein recruitment is $H_0 = 0.15$. Similarly to the intermediate shapes shown in Figs. 2a - 2c), we observe that here the membrane shape exhibits a pit-shape (a), U-shape (b) and Ω-shape (c), but at $t = t_{cut}$ a single bud with a constricted neck is formed (d) instead of a pearl, as in Fig. 2d. The color bar represents the protein density $\bar{\sigma}(s,t)$. In Figs. 3c and 3d we also observe and almost constant protein density on the vesicle, but it rapidly decays outside of the neck. The scale bar is the dimensionless unit length of the system, equivalent to $L = 50$nm

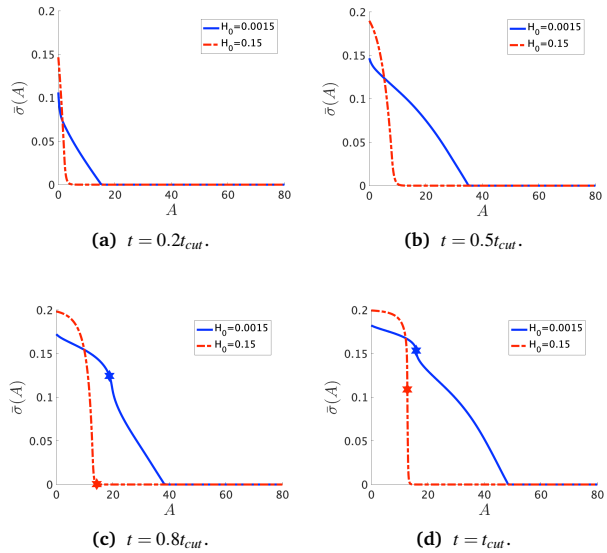

(a) $t = 0.2t_{cut}$. **(b)** $t = 0.5t_{cut}$.

(c) $t = 0.8t_{cut}$. **(d)** $t = t_{cut}$.

Fig. 4 Characteristic protein density at four different snapshots in time when the dimensionless rate coefficient is $K_1 = 4.5$ and the threshold for protein recruitment is $H_0 = 0.0015$ and $H_0 = 0.15$. At first ((a) and (b)) $\bar{\sigma}(A,t)$ decays nearly linearly with A from the maximum at the symmetry axis $r = 0$, but once an Ω-shape is formed (c) $\bar{\sigma}(A,t)$ in the vesicle is more uniform whereas the steepest decay in $\bar{\sigma}$ occurs from the membrane neck to the undeformed membrane, specially when $H_0 = 0.15$. In (c) we observe that there are proteins distributed in the region beyond the vesicle neck when $H_0 = 0.0015$ but there are no protein outside the vesicle when $H_0 = 0.15$. (d) At $t = t_{cut}$ we observe that the protein density in the membrane neck does not vanish. The star shaped markers in (c) and (d) represent the position of the neck (smallest radius at that given point in time).

the membrane forms a pearl-like shape, the bud growth and neck constriction happens several times. The insets in Fig. 5a show the shapes corresponding to the first maximum and the first minimum of z_{max} as well as the final shape at $t = t_{cut}$. In the time interval between the first maximum and first minimum in $z_{max}(t)$, the membrane shows a gradual transition between a pit-, U- and Ω-shape. As the neck size in the Ω-shape corresponding to the first minimum of z_{max} in Fig 5a is larger than the typical width h of the membrane bilayer, its height starts to increase again forming a vesicle at the top of the newly formed Ω-shape as we march forward in time. The oscillatory behaviour of z_{max} is not observed when $H_0 = 0.15$ (Fig. 5b) but z_{max} has a similar growth and decay when the Ω-shaped membrane is formed.

Next, we turn to map out the membrane shapes predicted by the mathematical model at the scission time, i.e. $t = t_{cut}$, by systematically varying $K_1 \in [0.2 - 9]$ and $H_0 \in [0.0015 - 0.15]$, see Fig. 6. As we go through the parameter space we see how the values of the non-dimensional numbers K_1 and H_0 determines if a vesicle buds directly from the membrane or on a deformed foundation as a pit, U or Ω-shape. The phase space in membrane shapes also suggests that we can distinguish membrane deformations that are likely to form only a single vesicle ($H_0 = 0.15$) and those that appear to continuously form vesicles by budding from a pit-shape ($H_0 = 0.015, K_1 = 1.4, 4.5, 9$ and $H_0 = 0.0015, K_1 = 9$), U-shape ($H_0 = 0.0015, K_1 = 4.5$) and Ω-shape ($H_0 = 0.0015, K_1 = 1.4$). Qualitatively we can understand the effect of H_0 by associating this parameter with the membrane region where recruitment of protein occurs: The inverse of H_0 sets a length scale that becomes large for small H_0, then proteins are recruited into a larger portion of the membrane, leading to larger budding structures such as pearls (see Fig. 6), while for larger H_0 this length scale will become smaller and in this case smaller budding structures would be expected.

The exploration of the phase space spanned by the parameters K_1 and H_0 also allows us to determine how they affect the dynamics of the membrane deformation. One quantity that helps to illustrate the time scale of the budding process is t_{cut}. The scission time is measured as the neck size reaches $h = 0.1$ in the radial direction, see Fig. 7a. In Fig. 7b we present the dependence of t_{cut} with respect to K_1 in logarithmic axis. Interestingly, we find a universal behavior: $t_{cut} \sim K_1^{-2/3}$ despite that we vary K_1 over two orders of magnitude and changing H_0 only affects the pre-factor of the scaling relation and not the power law. The universal behavior suggests that the same mechanisms are present across different simulations, where there is a complex interplay between the membrane geometry, diffusion and the area limited for protein recruitment.

To rationalise the power-law dependence we turn to look at the different mechanisms at play. First, we notice that t_{cut} effectively measures the time required for the proteins to cover an area that scales with the typical length of the bud $\sim L^2$. We notice that the growth of this area in time must involve diffusion as it helps

View Article Online
DOI: 10.1039/D0SM01028F

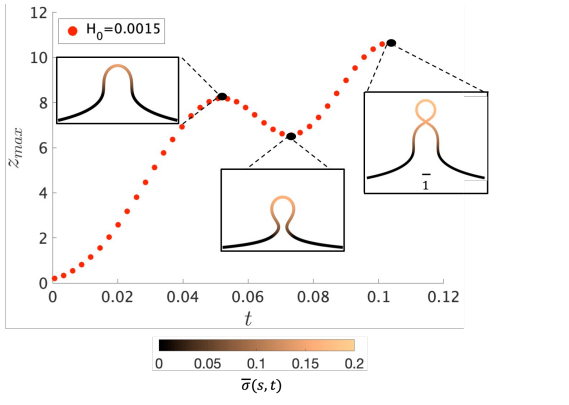

(a)

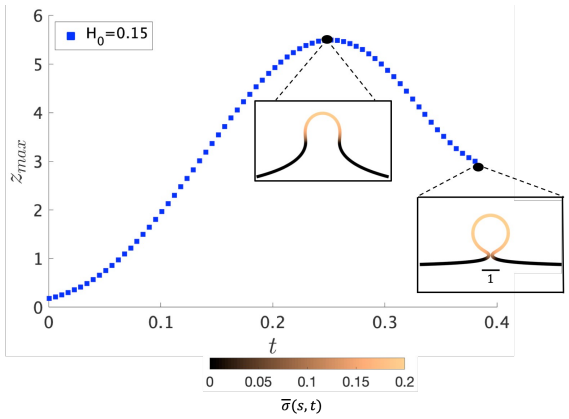

(b)

Fig. 5 The maximum height of the membrane respect to its symmetry axis, z_{max}, as a function of time, for $K_1 = 4.5$ and different values of H_0. In (a) it is shown that z_{max} oscillates. Once a pit shape is formed and z_{max} starts to decrease (first maximum of z_{max}), an Ω-shape starts to emerge. During the decrease of z_{max}, up to the first minimum of z_{max} in (a) the construction of the bud neck proceeds. As at this stage the neck radius is larger than the membrane thickness, the membrane shape evolution leads to a pearl structure at a later time ($t = t_{cut}$). In contrast, a higher value of H_0 prevents oscillation on z_{max}, as shown in (b). The color bar represents the protein density along as a function of the arc-length s and time t, $\bar{\sigma}(s,t)$.

increase the area on the membrane in which $H > H_0$. Such a diffusive motion scales by a balance between the two terms on the left hand side of the evolution equation for $\bar{\sigma}$, Eq. 15, which indicates that $\frac{1}{t_{cut}} \sim \frac{1}{L^2}$, or equivalently $t_{cut} \sim L^2$. On the other hand, within the region where $H > H_0$, the increase of the protein density is kinetically limited and the characteristic length scale is given by $L \sim (C_0\bar{\sigma})^{-1}$. Since we have for the region with $H > H_0$ that $\frac{\bar{\sigma}}{t_{cut}} \sim K_1$, or, $\bar{\sigma} \sim t_{cut}K_1$ and then $L \sim (C_0K_1t_{cut})^{-1}$. By combining these relations between t_{cut} and K_1, *i.e*, $t_{cut} \sim L^2 \sim (C_0K_1t_{cut})^{-2}$, we obtain $t_{cut} \sim K_1^{-2/3}$ as predicted by our numerical simulations. Thus, the time scale associated with bud formation, t_{cut}, is a combination of a diffusive front spreading the proteins and the kinetically-limited recruitment process responsible for the local increase of the protein density on the membrane.

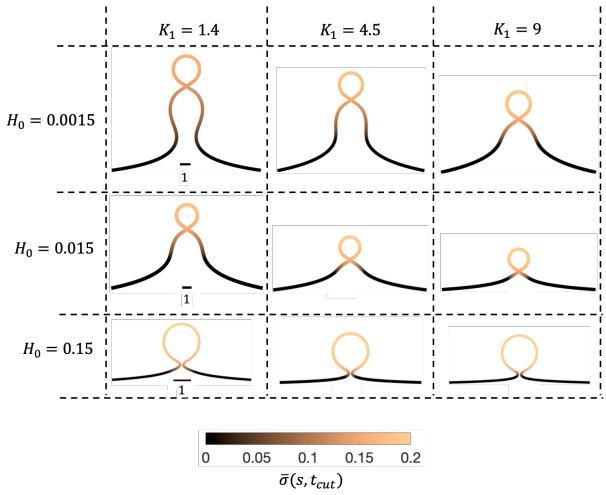

Fig. 6 The membrane shapes at $t = t_{cut}$ for $K_1 \in [0.2-9]$ and $H_0 \in [0.0015-0.15]$. The color bar represents the protein concentration as function of the arc-length at $t = t_{cut}$, $\bar{\sigma}(s,t_{cut})$.

At the defined scission time we are now in place to measure the size, r_{bud}, of the vesicle that forms. Fig. 8a reveals that also r_{bud} is a function of K_1 and H_0. We find that when H_0 is small, the bud radius is sensitive to the parameter K_1, but as H_0 increases, the bud radius becomes insensitive to K_1 where the formed vesicles have nearly the same size. To understand what sets r_{bud} we turn to the mechanism that drives the dynamics, i.e., the spontaneous curvature induced by the protein density on the membrane. A length scale that appears in our system is $1/(C_0\bar{\sigma}_{av})$, with $\bar{\sigma}_{av} = \frac{1}{A_{bud}}\int_{A_{bud}} \bar{\sigma} dA$ is the mean protein density on the bud, *i.e*. in the region above the membrane neck, and A_{bud} is the area of the membrane comprised between $s = 0$ and the membrane neck. The vesicle size is now predicted to scale as $r_{bud} \sim 1/(C_0\bar{\sigma}_{av})$. To test our scaling prediction we scale the bud radius r_{bud} with $C_0\bar{\sigma}_{av}$, which collapses the data onto a single line. To further illustrate the self-similar dynamics in the budding process, we rescale all lengths with the predicted bud size $\sim 1/(C_0\bar{\sigma}_{av})$ at the time t_{cut} and shift the profiles so they all start at the same z_{max} at $r = 0$, see Fig. 8c-8e. The upper part of the vesicle all follow the same spherical cap as we would expect from Fig. 8b, but interestingly the profiles map onto a universal shape also in the neck region (inner region) although the far field (outer region) is very different as it takes an Ω, pearl and flat shape. We zoom into the shedding vesicle and plot all the obtained membrane profiles together, which collapses onto a universal shape, shown in Fig. 8f. It is interesting to place this in the context of models for neck closure, where it was recently shown that there are optimal angles formed by the membrane depending on the outer membrane shape with a shape of a dome or a cone[80]. In the model developed here neck constriction is achieved despite that there is no assembly of specialised scission proteins, but still reveal an optimal angle shared among all shapes Fig. 8f for all the rescaled data $K_1 \in [1.35-9]$, $H_0 \in [0.0015-0.15]$.

View Article Online
DOI: 10.1039/D0SM01028F

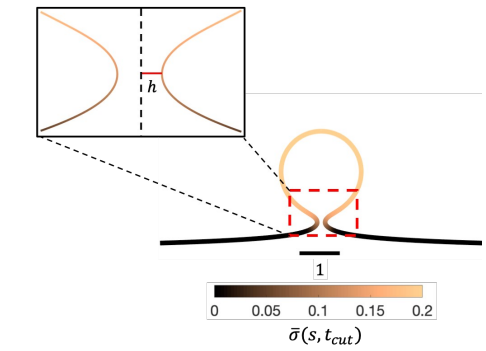

(a) The neck region of a vesicle.

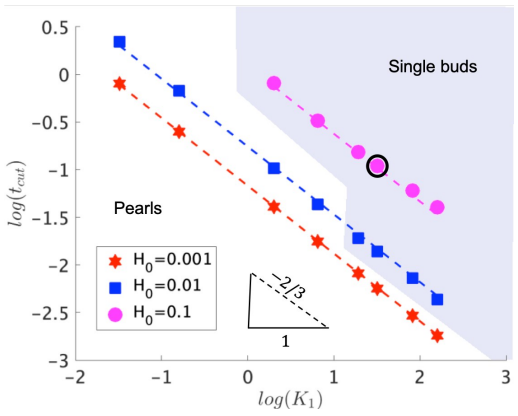

(b) The time t_{cut} as function of K_1 for different values of H_0, in logarithmic scale.

Fig. 7 (a) The membrane shape at time t_{cut} for $K_1 = 4.5$ and $H_0 = 0.15$ (point of the phase space highlighted in a black circle on Fig. 7b). The inset shows a zoom of the membrane neck region. The color bar represents the protein density $\bar{\sigma}(s, t = t_{cut})$ along the membrane. (b) The dependence of the scission time t_{cut} as a function of K_1 for different values of H_0 in logarithmic axis, showing that t_{cut} follows a power law respect to K_1. The scission time follows a power law $t_{cut} \sim K_1^{\alpha}$, with $\alpha \approx -2/3$ for all values of H_0. The dashed lines in each of the curves is a fit respect to the average value of the slopes obtained for each value of H_0. The two regions in Fig. 7b represent the parts of the phase space where single buds (blue) or pearls (white) are formed. When H_0 is small, the formation of pearls is observed across all the values of K_1. When $H_0 = 0.015$, the formation of pearls is observed only for small values of K_1 and as K_1 increases pearls are no longer observed. When $H_0 = 0.15$ pearl formation is prevented and only single buds are formed, up to $K_1 = 1.35$. For smaller K_1 we predict no budding structures.

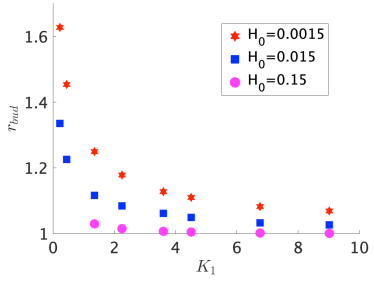

(a)

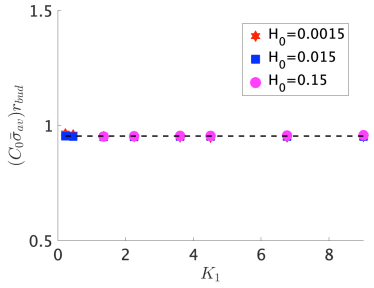

(b)

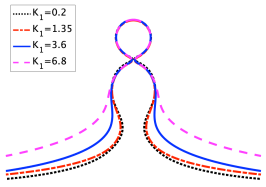

(c) $H_0 = 0.0015$.

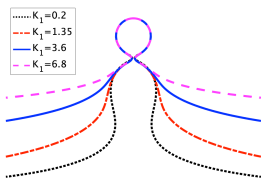

(d) $H_0 = 0.015$.

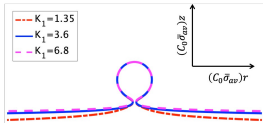

(e) $H_0 = 0.15$.

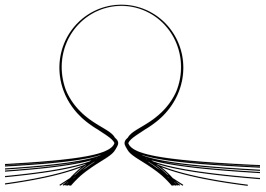

(f) $K_1 \in [0.2 - 9]$ and $H_0 \in [0.0015 - 0.15]$.

Fig. 8 (a) The bud radius r_{bud} as a function of K_1. For small values of H_0, the vesicle size depends on the parameter K_1: As K_1 is smaller the vesicles have larger sizes, but as H_0 increases this dependence becomes less significant, as it happens when $H_0 = 0.15$. In this case, all the vesicles formed have nearly the same size, independent of K_1. (b) We approximate the bud size as the inverse of the spontaneous curvature induced by the average concentration of proteins on the bud $\sim \frac{1}{C_0\bar{\sigma}_{av}}$. The average protein density on the bud is computed as $\bar{\sigma}_{av} = \frac{1}{A_{bud}} \int_{A_{bud}} \bar{\sigma} dA$. It is observed that all vesicle sizes shown in (a) collapse onto a single curve. The dashed straight line illustrates the average ratio $(C_0\bar{\sigma}_{av})r_{bud}$. In Fig. (c)-(e) we plot the rescaled shapes at $t = t_{cut}$ for selected values of K_1, when (c) $H_0 = 0.0015$, (d) $H_0 = 0.015$ and (e) $H_0 = 0.15$. The radial coordinate r and the height z have been scaled with $1/(\bar{\sigma}_{av}C_0)$ for each of the values of K_1 and H_0 considered. Fig. (c)-(e) show that the upper part of the budding structures are very similar despite being connected to a membrane with very different shape (Ω, pearl, flat). In (f) we zoom into the vesicle and plot together all the obtained shapes at t_{cut}. This reveals that in addition to the vesicle radius, the vesicle neck has almost the same shape regardless of K_1 and H_0.

View Article Online
DOI: 10.1039/D0SM01028F

4 Conclusions

We proposed a minimal mathematical model to describe the diffuso-kinetic membrane dynamics as curvature inducing proteins are recruited to a membrane and diffuse along its surface. The ratio of the diffusive and the kinetic time scale (K_1) and the proteins sensitivity to mean curvature (H_0) are systematically changed in our numerical simulations, which predicts a continuous formation of vesicles from a pearl-like membrane structure to the formation of a single vesicle from a nearly flat membrane. The coupled mechanism between diffusion and kinetic recruitment of protein in the membrane leads to the formation of vesicles with narrow necks at the last stages of the membrane deformation, without the action of additional mechanisms or protein complexes that might be responsible for constriction of membrane vesicle necks. The budding time is found to follow a power-law $t_{cut} \sim K_1^{-2/3}$, despite varying the parameter H_0 over few orders of magnitude and of going from diffusion ($K_1 < 1$) dominated to recruitment dominated ($K_1 > 1$) dynamics.

We derive a scaling law $t_{cut} \sim K_1^{-2/3}$ based on considering the interplay between the time scale associated with the diffusive spreading of the area allowing protein recruitment and the kinetically limited recruitment process associated with the increase of the local protein density in this area of the membrane. We extract the predicted vesicle size r_{bud} that is a function of both K_1 and H_0, but asymptotes towards a constant vesicle size for $K_1 > 9$ where it becomes insensitive to H_0. We propose a scaling law for the vesicle size $r_{bud} \sim 1/(C_0\bar{\sigma}_{av})$ based on the spontaneous curvature induced by the recruited proteins ($C_0\bar{\sigma}_{av}$) where $\bar{\sigma}_{av}$ is the mean protein density in the vesicle. By rescaling the numerical prediction for r_{bud} with this scaling law collapses the data onto a single curve, further highlighting the self-similar budding dynamics.

The membrane shapes predicted by our minimal model can be found in a wide range of biological processes as well as induced by polymers and nanoparticle on lipid vesicles[18,81]. The mathematical model couples the energy of the membrane to the diffuso-kinetics of the recruited proteins, providing a minimal description of the dynamics. Since the kinetic models describing protein recruitment are phenomenological, as details about the precise binding mechanisms of proteins are, to a large extent, missing in the field, we hope future work can closer couple these and incorporate the statistical mechanics properties as well as viscous flow effects in the recruitment dynamics of curvature sensing proteins. The model proposed here may form a basis for further characterizing how additional biophysical effects e.g., line tension, non-homogeneous bending rigidity and diffusion coefficient and direct protein-protein interactions influence the membrane dynamics.

Conflicts of interest

There are no conflicts to declare.

Notes and references

1 L.-G. Wu, E. Hamid, W. Shin and H.-C. Chiang, *Annual Review of Physiology*, 2014, **76**, 301–331.
2 W. Weissenhorn, E. Poudevigne, G. Effantin and P. Bassereau, *Current Opinion In Virology*, 2013, **3**, 159–167.
3 J. H. Hurley and P. I. Hanson, *Nature Reviews Molecular Cell Biology*, 2010, **11**, 556–566.
4 A. F. Loftus, V. L. Hsieh and R. Parthasarathy, *Biochemical and Biophysical Research Communications*, 2012, **426**, 585–589.
5 J. A. Dix and A. Verkman, *Annual Review of Biophysics*, 2008, **37**, 247–263.
6 A. Kenworthy, B. Nichols, C. Remmert, G. Hendrix, M. Kumar, J. Zimmerberg and J. Lippincott-Schwartz, *Journal Of Cell Biology*, 2004, **165**, 735–746.
7 N. Jouvenet, M. Zhadina, P. D. Bieniasz and S. M. Simon, *Nature Cell Biology*, 2011, **13**, 394–U124.
8 E. M. Wenzel, S. W. Schultz, K. O. Schink, N. M. Pedersen, V. Nahse, A. Carlson, A. Brech, H. Stenmark and C. Raiborg, *Nature Communications*, 2018, **9**, 2932.
9 T. Itoh, K. S. Erdmann, A. Roux, B. Habermann, H. Werner and P. de Camilli, *Developmental Cell*, 2005, **9**, 791–804.
10 S. Boulant, C. Kural, J.-C. Zeeh, F. Ubelmann and T. Kirchhausen, *Nature Cell Biology*, 2011, **13**, 1124–U158.
11 L. Lanzetti, *Current Opinion in Cell Biology*, 2007, **19**, 453–458.
12 S. Liese, E. M. Wenzel, R. V. Rojas Molina, S. W. Schultz, H. Stenmark, C. Raiborg and A. Carlson, *bioRxiv*, 2019.
13 M. G. Ford, I. G. Mills, B. J. Peter, Y. Vallis, G. J. Praefcke, P. R. Evans and H. T. McMahon, *Nature*, 2002, **419**, 361–366.
14 F. Campelo, H. T. McMahon and M. M. Kozlov, *Biophysical Journal*, 2008, **95**, 2325–2339.
15 P. D. Blood, R. D. Swenson and G. A. Voth, *Biophysical Journal*, 2008, **95**, 1866–1876.
16 J. C. Stachowiak, C. C. Hayden and D. Y. Sasaki, *Proceedings Of The National Academy Of Sciences Of The United States Of America*, 2010, **107**, 7781–7786.
17 W. T. Snead, C. C. Hayden, A. K. Gadok, C. Zhao, E. M. Lafer, P. Rangamani and J. C. Stachowiak, *Proceedings Of The National Academy Of Sciences Of The United States Of America*, 2017, **114**, E3258–E3267.
18 I. Tsafrir, D. Sagi, T. Arzi, M. Guedeau-Boudeville, V. Frette, D. Kandel and J. Stavans, *Physical Review Letters*, 2001, **86**, 1138–1141.
19 J. C. Stachowiak, E. M. Schmid, C. J. Ryan, H. S. Ann, D. Y. Sasaki, M. B. Sherman, P. L. Geissler, D. A. Fletcher and C. C. Hayden, *Nature Cell Biology*, 2012, **14**, 944+.
20 R. Dimova, *Advances In Colloid And Interface Science*, 2014, **208**, 225–234.
21 I. Tsafrir, Y. Caspi, M.-A. Guedeau-Boudeville, T. Arzi and J. Stavans, *Phys. Rev. Lett.*, 2003, **91**, 138102.
22 O. Avinoam, M. Schorb, C. J. Beese, J. A. G. Briggs and M. Kaksonen, *Science*, 2015, **348**, 1369–1372.
23 H. McMahon and J. Gallop, *Nature*, 2005, **438**, 590–596.
24 M. Kaksonen, C. Toret and D. Drubin, *Cell*, 2005, **123**, 305–320.

View Article Online
DOI: 10.1039/D0SM01028F

25 M. Rosendale and D. Perrais, *International Journal Of Biochemistry & Cell Biology*, 2017, **93**, 41–45.

26 A. Agrawal and D. J. Steigmann, *Zeitschrift Fur Angewandte Mathematik Und Physik*, 2011, **62**, 549–563.

27 J. Derganc, B. Antonny and A. Copic, *Trends In Biochemical Sciences*, 2013, **38**, 576–584.

28 G. Guigas and M. Weiss, *Biochimica Et Biophysica Acta-Biomembranes*, 2016, **1858**, 2441–2450.

29 J. Derganc and A. Copic, *Biochimica Et Biophysica Acta-Biomembranes*, 2016, **1858**, 1152–1159.

30 W. T. Gozdz, *Journal Of Chemical Physics*, 2011, **134**, 024110.

31 R. Lipowsky, *Faraday Discussions*, 2013, **161**, 305.

32 P. Rangamani, K. K. Mandadap and G. Oster, *Biophysical Journal*, 2014, **107**, 751–762.

33 C. Tozzi, N. Walani and M. Arroyo, *New Journal Of Physics*, 2019, **21**, 093004.

34 A. Mahapatra, D. Saintillan and P. Rangamani, *bioRxiv*, 2020.

35 J. S. Sohn, Y.-H. Tseng, S. Li, A. Voigt and J. S. Lowengrub, *Journal of Computational Physics*, 2010, **229**, 119 –144.

36 J. Lowengrub, J. Allard and S. Aland, *Journal of Computational Physics*, 2016, **309**, 112–128.

37 K. E. Teigen, X. Li, J. Lowengrub, F. Wang and A. Voigt, *Communications In Mathematical Sciences*, 2009, **7**, 1009–1037.

38 W. Helfrich, *Zeitschrift fur Naturforschung c-a Journal of Biosciences*, 1973, **C 28**, 693–703.

39 P. B. Canham, *Journal Of Theoretical Biology*, 1970, **26**, 61–81.

40 H. Deuling and W. Helfrich, *Biophysical Journal*, 1976, **16**, 861–868.

41 H. Alimohamadi and P. Rangamani, *Biomolecules*, 2018, **8**, 120.

42 D. Schley, R. J. Whittaker and B. W. Neuman, *Journal Of The Royal Society Interface*, 2013, **10**, 20130403.

43 S. Dmitrieff and F. Nedelec, *PLOS Computational Biology*, 2015, **11**, 1–15.

44 L. Foret, *The European Physical Journal E*, 2014, **37**, 42.

45 H. Alimohamadi, B. Ovryn and P. Rangamani, *Scientific Reports*, 2020, **10**, 1–15.

46 M. Arroyo, N. Walani, A. Torres-Sánchez and D. Kaurin, *Onsager's Variational Principle in Soft Matter: Introduction and Application to the Dynamics of Adsorption of Proteins onto Fluid Membranes. In: Steigmann D. (eds) The Role of Mechanics in the Study of Lipid Bilayers. CISM International Centre for Mechanical Sciences (Courses and Lectures)*, Springer, Cham, 2018.

47 A. Torres-Sanchez, D. Millan and M. Arroyo, *Journal Of Fluid Mechanics*, 2019, **872**, 218–271.

48 N. S. Gov, *Philosophical Transactions of the Royal Society B: Biological Sciences*, 2018, **373**, 20170115.

49 A. Veksler and N. S. Gov, *Biophysical Journal*, 2007, **93**, 3798–3810.

50 R. Lipowsky, *Faraday Discussions*, 2013, **161**, 305–331.

51 R. Lipowsky, *Advances In Colloid And Interface Science*, 2014, **208**, 14–24.

52 C.-H. Chang and E. I. Franses, *Colloids and Surfaces A: Physicochemical and Engineering Aspects*, 1995, **100**, 1–45.

53 K. Foo and B. Hameed, *Chemical Engineering Journal*, 2010, **156**, 2–10.

54 s. Leibler, *Journal De Physique*, 1986, **47**, 507–516.

55 H. Jian-Guo and O.-Y. Zhong-Can, *Phys. Rev. E*, 1993, **47**, 461–467.

56 M. Deserno, *Notes on differential geometry*, 2004.

57 U. Seifert, K. Berndl and R. Lipowsky, *Physical Review A*, 1991, **44**, 1182–1202.

58 S. P. Preston, O. E. Jensen and G. Richardson, *Quarterly Journal Of Mechanics And Applied Mathematics*, 2008, **61**, 1–24.

59 E. M. Smith, J. Hennen, Y. Chen and J. D. Mueller, *Biophysical Journal*, 2015, **108**, 2648–2657.

60 Chaikin, P. M. and Lubensky, T. C., *Principles of condensed matter physics*, Cambridge University Press, 1995.

61 George B. Arfken and Hans J. Weber and Frank E. Harris, *Mathematical methods for physicists*, Academic Press, Seventh Edition edn, 2013.

62 T. Masuda, H. Hirose, K. Baba, A. Walrant, S. Sagan, N. Inagaki, T. Fujimoto and S. Futaki, *Bioconjugate Chemistry*, 2020, **31**, 1611–1615.

63 J. B. Larsen, M. B. Jensen, V. K. Bhatia, S. L. Pedersen, T. Bjornholm, L. Iversen, M. J. Uline, I. Szleifer, K. J. Jensen, N. S. Hatzakis and D. Stamou, *Nature Chemical Biology*, 2015, **11**, 192–U176.

64 W. Zhao, L. Hanson, H.-Y. Lou, M. Akamatsu, P. D. Chowdary, F. Santoro, J. R. Marks, A. Grassart, D. G. Drubin, Y. Cui and B. Cui, *Nature Nanotechnology*, 2017, **12**, 750+.

65 C. Florentsen, A. Kamp-Sonne, G. Moreno-Pescador, W. Pezeshkian, A. A. H. Zanjani, H. Khandelia, J. Nylandsted and P. M. Bendix, *Soft Matter*, 2020.

66 T. V. S. Krishnan, S. L. Das and P. B. S. Kumar, *Soft Matter*, 2019, **15**, 2071–2080.

67 J. Liu, Y. Sun, D. G. Drubin and G. F. Oster, *PLOS Biology*, 2009, **7**, 1–16.

68 P. A. Janmey and P. K. J. Kinnunen, *Trends In Cell Biology*, 2006, **16**, 538–546.

69 P. Cicuta, S. L. Keller and S. L. Veatch, *The Journal of Physical Chemistry B*, 2007, **111**, 3328–3331.

70 P. Sens, *Physical Review Letters*, 2004, **93**, 108103.

71 A. Carlson and L. Mahadevan, *PLOS Computational Biology*, 2015, **11**, 1–16.

72 D. Wirtz, *Annual Review of Biophysics*, 2009, **38**, 301–326.

73 J. Liu, R. Tourdot, V. Ramanan, N. J. Agrawal and R. Radhakrishanan, *Molecular Physics*, 2012, **110**, 1127–1137.

74 Z. Shi and T. Baumgart, *Nature Communications*, 2015, **6**, 5974.

75 D. Thalmeier, J. Halatek and E. Frey, *Proceedings Of The National Academy Of Sciences Of The United States Of America*, 2016, **113**, 548–553.

76 J. Liu, Y. Sun, G. F. Oster and D. G. Drubin, *Current Opinion In Cell Biology*, 2010, **22**, 36–43.

View Article Online
DOI: 10.1039/D0SM01028F

77 M. M. Kozlov and L. V. Chernomordik, *Current Opinion In Structural Biology*, 2015, **33**, 61–67.

78 P. G. Saffman and M. Delbrück, *Proceedings of the National Academy of Sciences*, 1975, **72**, 3111–3113.

79 P. Bassereau, R. Jin, T. Baumgart, M. Deserno, R. Dimova, V. A. Frolov, P. V. Bashkirov, H. Grubmueller, R. Jahn, H. J. Risselada, L. Johannes, M. M. Kozlov, R. Lipowsky, T. J. Pucadyil, W. F. Zeno, J. C. Stachowiak, D. Stamou, A. Breuer, L. Lauritsen, C. Simon, C. Sykes, G. A. Voth and T. R. Weikl, *Journal Of Physics D-Applied Physics*, 2018, **51**, 343001.

80 J. Agudo-Canalejo and R. Lipowsky, *PLOS Computational Biology*, 2018, **14**, 1–21.

81 Y. Yu and S. Granick, *Journal Of The American Chemical Society*, 2009, **131**, 14158+.

Diffuso-kinetic membrane budding dynamics: Electronic Supplementary Material (ESM)

Rossana Rojas Molina[1], Susanne Liese[1], Haleh Alimohamadi[2], Padmini Rangamani[2], and Andreas Carlson[1*]

[1]Mechanics Division, Department of Mathematics, University of Oslo, 0316 Oslo, Norway.
[2]Department of Mechanical and Aerospace Engineering, University of California, San Diego, CA 92093, USA
[*]Email: acarlson@math.uio.no

1 Derivation of the shape equations

The energy functional that describes the membrane is given by:

$$W = B(H - C_0\bar{\sigma})^2 + \lambda + \frac{k_bT}{a_p}\bar{\sigma}(\log\bar{\sigma} - 1) \tag{1}$$

To derive the energy minimizing shape, we define the Lagrangian functional $\mathcal{L}$ as:

$$\mathcal{L} = r\left[\lambda + \frac{k_bT}{a_p}\bar{\sigma}(\log\bar{\sigma} - 1)\right] + rB\left[\frac{1}{2}\left(\frac{\sin\phi}{r} + \phi'\right) - C_0\bar{\sigma}\right]^2 + \Gamma(r' - \cos\phi) \tag{2}$$

The equations that describe the membrane shape are derived from the minimization of a Lagrange functional $\mathcal{L}$ given by Eq. 2 with respect to the functions r and ϕ. These functions are parametrized by the arc-length s. The Euler-Lagrange equations for these functions read:

$$\frac{\partial\mathcal{L}}{\partial r} - \frac{d}{ds}\left(\frac{\partial\mathcal{L}}{\partial r'}\right) = 0 \rightarrow \frac{d\Gamma}{ds} = \lambda + \frac{k_bT}{a_p}\bar{\sigma}(\log\bar{\sigma} - 1) + \frac{M^2}{B} - \frac{M\sin\phi}{r} \tag{3}$$

$$\frac{\partial\mathcal{L}}{\partial\phi} - \frac{d}{ds}\left(\frac{\partial\mathcal{L}}{\partial\phi'}\right) = 0 \rightarrow \frac{dM}{ds} = \frac{\Gamma\sin\phi}{r} \tag{4}$$

We derive a Hamiltonian from the Lagrangian functional in Eq. 2. The total energy of the membrane depends on its area, which is an implicit function of the arc-length s. This implies that the Lagrangian depends on the spatial coordinate s *implicitely* as well. In order to specify the domain where the shape equations are to be solved, the protein concentration $\bar{\sigma}$ must be evaluated on the membrane area. This can be done as the relation $A' = 2\pi r$ provides a one-to-one correspondence between the area A and the arc-length s. Moreover, as the size of the upper limit of the coordinate s is not fixed the following relations are obtained:

$$\frac{\partial\mathcal{L}}{\partial s} = -\frac{d\mathcal{H}}{ds} = 0 \tag{5}$$

$$\mathcal{H}(s_{max}) = 0 \rightarrow \mathcal{H}(s) = 0 \tag{6}$$

The Hamiltonean is given by:

$$\mathcal{H} = -\mathcal{L} + r'\frac{\partial\mathcal{L}}{\partial r'} + \phi'\frac{\partial\mathcal{L}}{\partial\phi'} = 0 \tag{7}$$

Explicitly:

$$\mathcal{H} = r\left[-\left(\lambda + \frac{k_bT}{a_p}\bar{\sigma}(\log\bar{\sigma} - 1)\right) - \frac{M^2}{B} + \frac{\Gamma\cos\phi}{r} + \phi' M\right] = 0 \tag{8}$$

The expression inside the brackets in Eq. 8 vanishes and then we express the terms inside the parenthesis as function of M^2, Γ, r and ϕ. Inserting the resulting expression into Eq. 3 we obtain:

$$\frac{d\Gamma}{ds} = \frac{\Gamma \cos\phi}{r} - \frac{2M \sin\phi}{r} + M\left(\frac{2M}{B} + 2C_0\bar{\sigma}\right) \tag{9}$$

Next, we write Eq. 3 and Eq. 4 as a function of two new variables Q and T:

$$Q \equiv -\frac{\Gamma \sin\phi}{r} \tag{10}$$

$$T \equiv \frac{\Gamma \cos\phi}{r} \tag{11}$$

Using Eq. 9 these new variables fulfill the following differential equations:

$$\frac{dQ}{ds} = -\frac{M \sin\phi}{r}\left(\frac{2M}{B} - \frac{2\sin\phi}{r} + 2C_0\bar{\sigma}\right) - \phi' T \tag{12}$$

$$\frac{dT}{ds} = \frac{M \cos\phi}{r}\left(\frac{2M}{B} - \frac{2\sin\phi}{r} + 2C_0\bar{\sigma}\right) + \phi' Q \tag{13}$$

A solution to Eq. 12 and Eq. 13 is given by the following ansatz:

$$Q = -U \sin\phi \tag{14}$$

$$T = U \cos\phi \tag{15}$$

where U satisfies

$$\frac{dU}{ds} = \frac{M}{r}\left(\frac{2M}{B} - \frac{2\sin\phi}{r} + 2C_0\bar{\sigma}\right) \tag{16}$$

Finally, the equations that determine the shape of the membrane are given by the ones obtained of the geometry described in Fig. 1 of the Main Text together with Eq. 4 and Eq. 16:

$$\phi' = \frac{2M}{B} - \frac{\sin\phi}{r} + 2C_0\bar{\sigma} \tag{17}$$

$$r' = \cos\phi \tag{18}$$

$$z' = \sin\phi \tag{19}$$

$$A' = 2\pi r \tag{20}$$

$$M' = U \sin\phi \tag{21}$$

$$U' = \frac{M}{r}\left(\frac{2M}{B} - \frac{2\sin\phi}{r} + 2C_0\bar{\sigma}\right) \tag{22}$$

We notice that the shape equations do not depend on the parameter $k_b T$.

2 Boundary conditions

From the geometry used to describe the shape of the membrane, shown in Fig. 1 of the Main Text the following boundary conditions can be extracted:

$$r(s=0) = 0 \tag{23}$$

$$\phi(s=0) = 0 \tag{24}$$

$$A(s=0) = 0 \tag{25}$$

and we define the origin of the z coordinate to be located at $s = 0$:

$$z(s=0) = 0 \tag{26}$$

However, given the form of the shape equations and its divergent behaviour at $s = 0$ these boundary conditions need to be regularized by doing a Taylor expansion around $s = 0$. Then, we define the boundary condition at $s = \epsilon$ instead of $s = 0$, where $\epsilon \ll 1$:

$$r(\epsilon) \approx r(0) + \epsilon r'(0) = \epsilon \tag{27}$$

$$\phi(\epsilon) \approx \phi(0) + \epsilon\phi'(0) \equiv \epsilon c_1 \tag{28}$$

$$A(\epsilon) \approx A(0) + \epsilon A'(0) + \frac{\epsilon^2}{2} A''(0) = \pi\epsilon^2 \tag{29}$$

$$z(\epsilon) \approx z(0) + \epsilon z'(0) + \frac{\epsilon^2}{2} z''(0) = \frac{c_1}{2}\epsilon^2 \tag{30}$$

$$M(\epsilon) \approx B(c_1 - C_0\bar{\sigma}(\epsilon)) \tag{31}$$

where c_1 is defined as the mean curvature at $s = \epsilon$ and results from solution of the ODEs. Additionally, we impose that at the far boundary s_{max} the membrane is nearly flat which implies:

$$\phi(s_{max}) = 0 \tag{32}$$

To find a boundary condition for the function U, we use the expression for the Hamiltonean in Eq. 8. This equation holds identically assuming that $r(s = 0) = 0$, and it holds for $s = s_{max}$ only if the term in brackets vanishes. The equation 32 allow us to assume that the mean curvature and the bending moment M vanish at the far boundary. With these assumptions, we can find a relation for $U(s_{max})$:

$$U(s_{max}) = \lambda + \frac{k_b T}{a_p}\bar{\sigma}(\log\bar{\sigma} - 1) \approx \lambda \tag{33}$$

where $\bar{\sigma}$ is evaluated at s_{max}. As we are considering a large spacial domain, the protein concentration at the far boundary satisfies $\bar{\sigma}(s_{max}) \approx 0$, and then $U(s_{max})$ can be written as in eq. 33. In this way, we have a system of 6 coupled ordinary differential with the boundary conditions in Eq. 27-33 and the parameter c_1.

3 Non-dimensional analysis

Assuming that the characteristic length of the system, L, is given by the typical vesicle size, we can non-dimensionalize the shape equations and the evolution equation for the protein concentration σ as follows:

$$\bar{s} = \frac{s}{L}, \qquad \bar{r} = \frac{r}{L}, \qquad \bar{z} = \frac{z}{L}, \qquad \bar{M} = \frac{ML}{B}, \qquad \bar{C_0} = C_0 L$$

$$\bar{U} = \frac{UL^2}{B}, \qquad \bar{Q} = \frac{QL^2}{B}, \qquad \bar{\lambda} = \frac{\lambda L^2}{B}, \qquad \bar{\sigma} = \frac{\sigma}{\sigma_m}$$

$$\bar{t} \equiv \frac{t}{\tau_D} = \frac{tD}{L^2}, \qquad \bar{\Lambda} = \frac{\Lambda B}{L^2 D} = \frac{B}{k_b T}\frac{a_p}{L^2}$$

Substituting the dimensional quantities in terms of the non-dimensional variables and then dropping all the bars, the evolution equation can be written in dimensionless form as

$$\bar{\sigma_t} - \frac{1}{r}(r(\sigma' + 2\bar{C_0}\bar{\Lambda}\bar{\sigma}\bar{Q}))' = \frac{\tau_D}{\tau_{on}}\Theta(H - H_0) - \frac{\tau_D}{\tau_{off}}\bar{\sigma} \tag{34}$$

where τ_{on} and τ_{off} define the time scales of recruitment and detachment, respectively, and are given by:

$$\tau_{on} = \frac{1}{c_p k_{on}}, \qquad \tau_{off} = \frac{1}{k_{off}}$$

where c_p is the typical protein concentration on the bulk surrounding the membrane and k_{on} is the affinity between the proteins and the membrane. Further, we define the ratio between the time scales as:

$$K_1 \equiv \frac{\tau_D}{\tau_{on}} \qquad K_2 \equiv \frac{\tau_D}{\tau_{off}}$$

where $\tau_D = \frac{L^2}{D}$ is the typical diffusive time scale on a biological membrane. With these definitions we recover Eq. 15 of the Main Text.

4 Numerical implementation

To solve numerically the shape equations we used the solver bvp4c in Matlab and the evolution equation of the protein concentration was solved using a finite difference discretization in time and space, where the spatial derivatives where computed by a centered-difference scheme and the time derivative by a backward scheme. The steps to solve the coupled equations are summarised as follows:

1. Give an initial protein concentration $\bar{\sigma}_0$, for example a Gaussian profile, with small amplitude.
2. Solve the associated shape equations using bvp4c in Matlab.
3. With the geometry given by the solution of the shape equations, solve the difusso-kinetic equation to obtain the protein concentration at a later time step, namely, $\bar{\sigma}$, using as initial density $\bar{\sigma}_0$.
4. Solve the shape equations with the new protein concentration $\bar{\sigma}$.
5. Update the initial protein concentration, $\bar{\sigma} \to \bar{\sigma}_0$
6. Iterate over the steps 3 to 5, until the formation of a bud neck with almost vanishing width is reached. In this case the shape equations and the evolution equation for $\bar{\sigma}$ becomes singular and the numerical solver cannot provide a valid numerical solution. As explained in the main text, we will consider the evolution of the membrane shape until the time t_{cut}, at which the membrane neck has a small but finite width, equal to the membrane thickness.

5 Validity of the solutions given by the shape equations.

To show that the shapes obtained as a result of the integration of the shape equations, Eq. 17-22 do correspond to a minimized energy we consider the case of zero surface tension, namely $\lambda = 0$ in the energy functional given by Eq. 1. In this case, the bending moment M given in Eq. 21 should vanish, which implies that the mean curvature of the membrane follows the spontaneous curvature imposed by the proteins. Hence, a simplified set of equations can be obtained by setting $M = 0$. As a consequence, $U = 0$. These equations are:

$$\phi' = -\frac{\sin\phi}{r} + 2C_0\bar{\sigma} \tag{35}$$

$$r' = \cos\phi \tag{36}$$

$$z' = \sin\phi \tag{37}$$

$$A' = 2\pi r \tag{38}$$

with the following boundary conditions:

$$r(\epsilon) = \epsilon$$
$$\phi(\epsilon) = C_0\bar{\sigma}(A=0)\epsilon$$
$$A(\epsilon) = \pi\epsilon^2$$
$$z(\epsilon) = \frac{C_0\bar{\sigma}(A=0)}{2}\epsilon^2$$

In Fig. 1a we compare the shapes obtained at $t = t_{cut}$ by solving the full set of equations, Eq. 17-22 (set of equations 1), and the simpler equations given by Eq. 35-38 (set of equations 2) for $K_1 = 2.25$ and $H_0 = 0.015$. The shapes obtained are very similar, indicating that the assumption of vanishing bending moment, $M = 0$, when the surface tension vanishes is correct. In addition, in Fig. 1b we show that by solving the set of equations 1, the bending moment is zero.

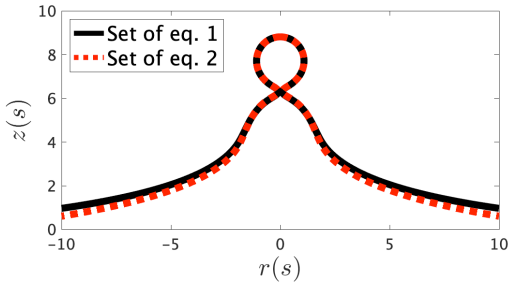

(a) Comparison between the shapes obtained by solving the set of equations 1 and 2.

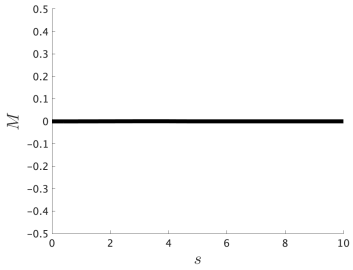

(b) The bending moment $M(s)$ obtained by solving the set of equations 1.

Figure 1: Verification of the validity of the solutions given by the shape equations (set 1), for the particular case of vanishing surface tension, $\lambda = 0$. The shape obtained agrees well with the solution given by the simplified equations (set 2). The bending moment $M(s)$ obtained as a solution of the shape equations vanishes, as shown in fig. 1b.

6 Effect of the initial protein density

In all the simulations, we have assumed that the initial protein density is given by a Gaussian profile, $\bar{\sigma}(s, t = 0) = \sigma_0 e^{-(s/0.3)^2}$, where σ_0 measures the amplitude of the initial density. In all the results presented in the main text we have chosen $\sigma_0 = 0.1$. Given that the recruitment term depends on the mean curvature via a cutoff function, the membrane should have initially a small but finite deformation to trigger the recruitment. Then it is expected that if the initial protein density is too small, the membrane will not evolve into a budded shape. To see the effect of the parameter σ_0 on the membrane shape dynamics, we chose $K_1 = 9$ and $H_0 = 0.15$ and varied the amplitude of the initial density. If $\sigma_0 = 0.03$, *i.e*, almost one order of magnitude smaller than the one we have considered, the membrane remains flat, as shown in Fig. 2a. However, with an initial amplitude of $\sigma_0 > 0.03$ the membrane evolves into a budded shape, similar to the one obtained when $\sigma_0 = 0.1$. In Fig. 2b we show the dependence between the time at which the neck width equals the membrane thickness, t_{cut}, and the amplitude of the initial protein density, σ_0, where it is observed that the initial amplitude σ_0 has a small effect on t_{cut}. Hence, the parameter σ_0 plays a minor role in the budding dynamics.

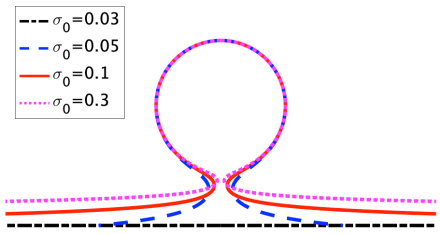

(a) Shapes at $t = t_{cut}$.

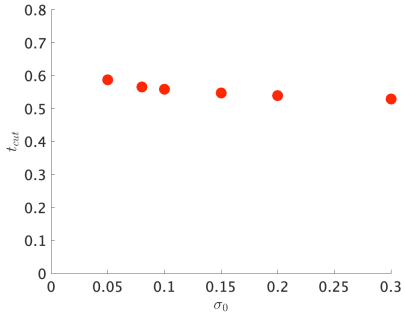

(b) t_{cut} as function of σ_0.

Figure 2: (a) Comparison of the shapes obtained at $t = t_{cut}$ for $K_1 = 9$ and $H_0 = 0.15$, when $\sigma_0 = 0.1$. The amplitude of the initial protein density does not have a strong influence in the final membrane shape, provided $\sigma_0 > 0.03$. If $\sigma_0 < 0.03$ the membrane shape does not evolve into a budded structure. (b) The scission time t_{cut} as a function of the initial density amplitude, σ_0, showing that indeed t_{cut} is only slightly modified by the parameter σ_0. Then, this parameter does not play a key role in the membrane budding dynamics.

7 Influence of other recruitment models:

In the main text we have assumed that the protein recruitment depends on the membrane curvature via a cut-off or Heaviside function that is piece-wise constant, giving a finite and constant on and off rates when the membrane mean curvature exceeds a threshold, $H > H_0$, and vanishing rates when $H < H_0$. The Heaviside function is discontinuous, but can be regularized with an hyperbolic tangent function, *i.e*, $\Theta(H - H_0) \to 0.5(1 + \tanh a(H - H_0))$, where a determines the steepness of the tanh function. To mimic the Heaviside, a should be large enough, to ensure that if $H < H_0$ the recruitment vanishes. This cut-off model is restrictive, as it assumes that recruitment is only possible in a very restricted membrane region. However, the parameters K_1 and K_2 have a clear physical interpretation, as on and off rates. Other models for protein recruitment could be considered. For example, one could assume that the recruitment term is proportional to the mean curvature, $\sim \beta H$, where β is a constant of proportionality. Nevertheless, β might not have a straightforward physical interpretation, and to address the general effect of changing the recruitment model is beyond the scope of this work. In Fig. 3a we show the comparison between the shapes obtained for the Heaviside and tanh, for $K_1 = 2.25$ and $H_0 = 0.015$, corresponding to $t = t_{cut}$. We observe that the Heaviside and tanh model give similar shapes, provided that a is large. If $a < 300$ the shapes differ considerably. In Fig. 3b we show the protein profiles $\bar{\sigma}$ as a function of the area A. The profiles look similar compared to the Heaviside models, but start to differ if $a < 300$. However, regularizing the recruitment model do not affect the results.

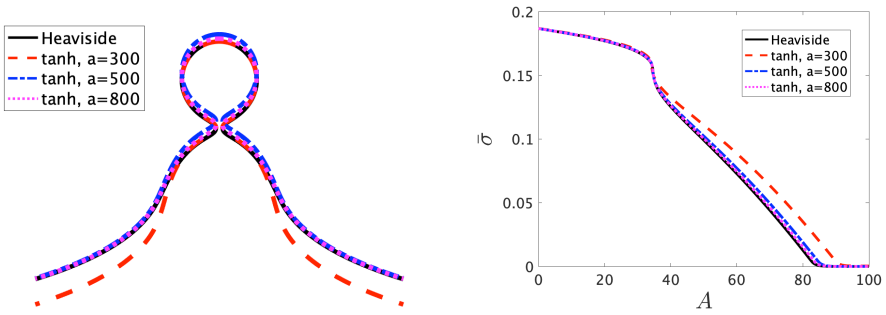

(a) Shapes at $t = t_{cut}$ for $K_1 = 2.25$ and $H_0 = 0.015$.

(b) $\bar{\sigma}(A)$ for the shapes in Fig. 3a.

Figure 3: (a) Shapes obtained with the Heaviside model and its regularized version $\sim 0.5(1 + \tanh a(H - H_0))$ at $t = t_{cut}$ for $H_0 = 0.015$ and $K_1 = 2.25$. The shapes are similar, provided that the tanh is steep enough. If $a < 300$ the shapes differ. (b) The protein density $\bar{\sigma}$ as a function of the area A, associated to the shapes in Fig. 3a. If the tanh function is not steep enough ($a < 300$), the density $\bar{\sigma}$ start to differ, as the recruitment term does not capture the same features of the Heaviside function.

8 Estimation of the interaction and gradient terms in the energy functional

According to Eq. 1, we are considering an energy functional where interaction terms $\sim b\bar{\sigma}^2$ and gradient terms $\sim b(\nabla\bar{\sigma})^2$ are absent, as we have assumed that the interaction between proteins b is weak. This choice a priori is arbitrary, as in general these terms should be present. However, it is illustrative to estimate the relative importance of these terms respect to the bending energy and the entropy. In order to do this, for simplicity we will assume that $\lambda = 0$. Following the result of the previous section, if the surface tension vanishes the bending moment and hence the bending energy vanishes for any given protein concentration profile (see Fig. 1b). We will assume that the protein concentration is one of the solutions obtained from the numerical simulations at a given time step, for $K_1 = 2.25$ and $H_0 = 0.015$, shown in Fig. 4a.

It has been estimated theoretically and experimentally that the interaction potential is of the order of $2k_bT$ (1; 2), which in practice is considerably smaller than the typical bending energy of the membrane. Then the interaction potential should satisfy $b \ll B$. In Fig. 4b we plot the adimensional entropic term $\frac{k_bT}{B}\frac{L^2}{a_p}\bar{\sigma}(\log(\sigma) - 1)$, the interaction term $-\frac{b}{B}\frac{L^2}{a_p}\bar{\sigma}^2$ and the gradient term $\frac{b}{B}(\nabla\bar{\sigma})^2$ assuming that the ratio $\frac{b}{B} = \frac{1}{10}$. We can observe that in this case the entropy dominates over the interaction and the gradient terms. Hence, it is reasonable to neglect these terms in the

energy functional.

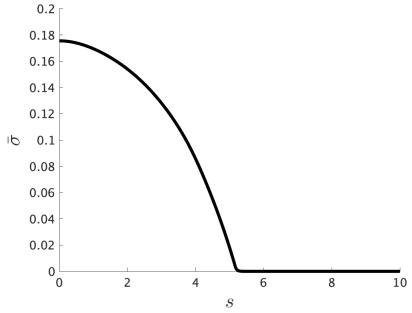

(a) A protein profile obtained from numerical simulations, for $K_1 = 2.25$ and $H_0 = 0.015$.

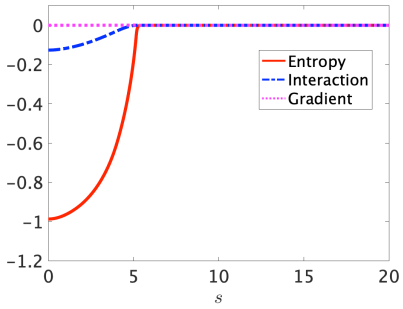

(b) Comparison between the entropy and the interaction term for the protein profile in fig. 4a

Figure 4: Estimation of the contributions to the energy arising from the entropy and interaction between proteins. Assuming that the ratio $\frac{b}{B} = \frac{1}{20}$, the interaction and gradient terms have a small contribution to the energy.

9 The effect of surface tension in the membrane shape evolution

The surface tension influences the budding time and the shape of the forming vesicle. In order to establish the effect of the surface tension in the membrane dynamics we fix the parameters K_1 and H_0 and change the the parameter λ. As λ increases, the numerical calculations become challenging and exploring the effect of the surface tension on the membrane shape evolution is limited to very small values of λ. The dependence of z_{max} with respect to time is shown in Fig. 5a for some values of λ. One of the effects of having surface tension in the system is that the variable z_{max} defined in the main text ceases to have an oscillatory behaviour after a certain value of λ, which implies that the formation of pearl structures is prevented in general. The budding time t_{bud} is defined respect to the local minimum of $z_{max}(t)$, which, following the discussion presented in the main text, correspond to the formation of an Ω-shape. The budding time t_{bud} as a function of λ is shown in Fig. 5b, where it can be observed that the surface tension delays the formation of the bud, as t_{bud} increases if the surface tension becomes larger.

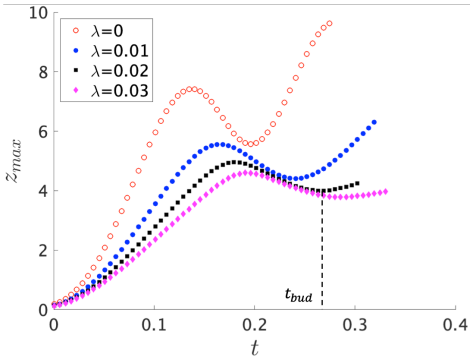

(a) $z_{max}(t)$ for different values of λ.

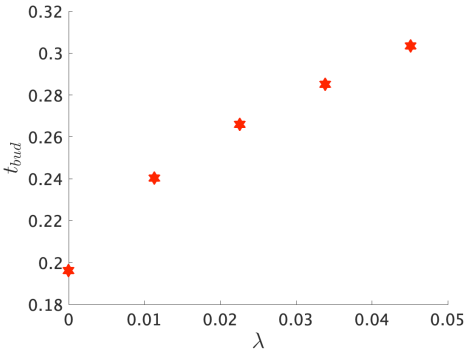

(b) t_{bud} as a function of λ.

Figure 5: The effect of the membrane tension in its shape evolution. Fig. 5a shows the evolution in time of the height of the budding structure z_{max}. This function does not exhibit oscillations in general, as in the case where $\lambda = 0$. Hence, the formation of pearls is prevented in most cases. In Fig. 5b the budding time, t_{bud} is plotted as function of the tension λ. The budding time corresponds to the first local minimum of z_{max}. t_{bud} increases as the surface tension becomes larger. This indicates that the surface tension delays the budding process. In all simulations $K_1 = 2.25$ and $H_0 = 0.015$.

To further characterise the effect of surface tension on the membrane shape, we compare the shapes obtained when

$\lambda = 0.04$ and the ones corresponding to $\lambda = 0$, at given times. This comparison is shown in Fig. 6, where is shown that at the scission time $t = t_{cut}$ corresponding to vanishing surface tension, $\lambda = 0$, $H_0 = 0.015$ and $K_1 = 2.25$, the membrane under the effect of surface tension exhibits quite different shapes. In general, the surface tension favors the formation of budding structures with small height, as compared with the shapes when $\lambda = 0$.

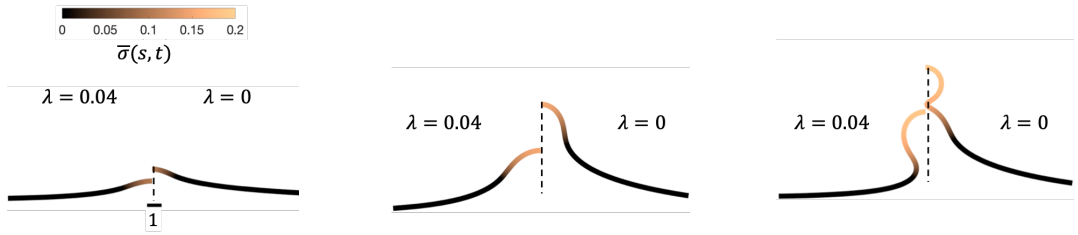

(a) $t = 0.2t_{cut} = 0.05$. **(b)** $t = 0.5t_{cut} = 0.13$. **(c)** $t = t_{cut} = 0.25$.

Figure 6: Comparison between the shapes obtained when the surface tension is zero, $\lambda = 0$ and $\lambda = 0.04$ at three different snapshots in time defined respect to t_{cut} discussed in the main text, when the dimensionless rate coefficient is $K_1 = 2.25$ and the threshold for protein recruitment is $H_0 = 0.015$. As we march forward in time the membrane deforms from a nearly flat membrane (not shown) into a pit-shape for both values of λ (a), but the shapes start to differ visibly at a later time ((b) and (c)) and at $t = t_{cut}$ a pearl structure is already formed when $\lambda = 0$ but only a single bud is formed when $\lambda = 0.04$ (c). The color bar represents the protein density $\bar{\sigma}(s,t)$. A finite but small value of λ has the overall effect of reducing the height of the budding structure and preventing the formation of pearls. The scale bar is the dimensionless unit length of the system, equivalent to $L = 50$nm.

References

[1] I. Casuso, P. Sens, F. Rico, and S. Scheuring, "Experimental Evidence for Membrane-Mediated Protein-Protein Interaction," *Biophysical Journal*, vol. 99, no. 7, pp. L47–L49, 2010.

[2] H. Zhou, "Enhancement of protein-protein association rate by interaction potential: Accuracy of prediction based on local Boltzmann factor," *Biophysical Journal*, vol. 73, no. 5, pp. 2441–2445, 1997.

Paper III

Protein crowding mediates membrane remodeling in upstream ESCRT-induced formation of intraluminal vesicles

Liese Susanne, Wenzel Eva Maria, Kjos Ingrid, Rojas Molina Rossana, Schultz Sebastian W., Brech Andreas, Stenmark Harald, Raiborg Camilla, Carlson Andreas

Accepted in *Proceedings of the National Academy of Sciences of the United States of America* (2020) DOI: 10.1101/834457.

III